STUDY OF DUST DEVILS

IN RELATION TO THE MARTIAN YELLOW CLOUDS

Third Interim Progress Report

1 February through 31 July 1968

J. A. Ryan
Principal Investigator
Space Sciences Department

McDonnell Douglas Astronautics Company

Santa Monica, California

Significant contributions to the writing of this report have been made by Dr. William Hildreth and Mr. John Carroll of this Department.

TABLE OF CONTENTS

ABSTRACT

Work during this reporting period consisted of obtaining additional field data on dust devils, and finishing the computer program for determining temperature lapse rates in the lowermost Martian atmosphere. Five days of good field data were obtained. These have provided several important clues concerning the mechanics of dust devil generation, and have served to verify previous assumptions. Computer runs have shown that the temperature lapse rates in the lowermost Martian atmosphere can become highly superadiabatic, a condition favorable to dust devil generation.

1.0 INTRODUCTION AND SUMMARY

This report presents a summary of work accomplished during the period February 1 through July 31, 1968 on a study of dust devils as related to the Martian yellow clouds. The objective of this study is to determine whether dust devils could occur on Mars and be responsible for the observed yellow clouds. Particular emphasis is being given to field studies of dust devils since relatively few good data are available concerning their structure and the conditions under which they form.

Five good days of field data were obtained during this reporting period. These data included, in addition to measurement of those quantities reported previously (e.g. temperature from the surface to 1540 meters altitude, environmental wind velocity and direction, tangential wind velocity inside the dust devils, dust devil frequency and size), measurement of local environmental vorticity, direction of dust devil rotation, and the vertical velocities in dust devils. The vorticity and direction of dust devil rotation measurements are considered to be important to establish whether direct connection indeed exists between the atmospheric angular momentum and the magnitude of the tangential wind velocities in dust devils (such a connection would be indicated if the direction of dust devil rotation, particularly for the larger devils, is found to be related to the local area atmospheric direction of rotation). The vertical wind velocity measurements inside dust devils are considered to be important since they should aid in the establishment of a dust devil model.

The major findings during this reporting period are (a) that the vertical wind velocities in dust devils increase as the temperature lapse rate increases, indicating the role of bouyancy in dust devil formation, (b) that the direction

of dust devil rotation appears correlated with the direction of atmospheric vorticity, and (c) that both lapse rates and atmospheric vorticity play important roles in dust devil generation. Additional findings are (a) that tangential wind velocities in dust devils decrease as background (environmental) wind velocity increases, an indication of the role of mechanical turbulence in hindering dust devil formation, (b) that dust devil tangential velocity increases as dust devil diameter increases, and (c) that the tangential velocity appears insensitive to lapse rate, indicating again the importance of atmospheric vorticity in generating the dust devil mode of heat transfer. These findings indicate that if dust devils are the causal agents of the Martian yellow clouds these clouds would be formed preferentially at times when superadiabatic temperature lapse rates are present in conjunction with appreciable atmospheric vorticity. Yellow clouds are known to form during times of maximum surface heating (conducive to the production of superadiabatic lapse rates) and most vigorous atmospheric circulation (conducive to the presence of considerable vorticity). Hence the data to date indicate dust devils could produce the yellow clouds. However, the data as yet cannot predict whether the wind velocities generated could be sufficiently large to raise granular material on Mars.

The computer program for determining temperature lapse rates in the lowermost portion of the Martian atmosphere, as a function of time and location, has been completed. The first runs indicate that highly superadiabatic lapse rates are generated close to the surface, in accordance with the findings of others.

2.0 INSTRUMENTATION AND PROCEDURES

Various changes to the instrumentation and measurement procedures were made during the reporting period. These changes and the reasons for which they were made are given in the following sections.

2.1 Balloon Measurements

During the early phases of the program a tethered balloon was used to obtain temperature measurements in the height range (30-150 meters) between that covered by the pole and the aircraft. The balloon was vee-shaped to provide aerodynamic lift and maintain itself over the pole in the presence of wind. It was found, however, that it was impossible to keep the balloon at anything like a constant altitude, and the altitude changes were extreme and rapid (at various times the balloon would rapidly drop a hundred meters or so, depositing the sensors on the ground). It appears that this behavior was caused by downward moving air currents whose velocity, though low, acted upon the large surface area of the balloon and hence could overcome the balloon lift. Two attempts to remove this problem, first flying two balloons in tandem, one 150 meters above the other, and second, providing means for ground control of the balloon pitch (means to point the balloon nose into the downdrafts when they occurred) were made. Neither approach was successful. Accordingly, it was decided to do away with the balloons and have the aircraft fly continuously. This approach has proven quite successful (to cover the gap left by the balloon's absence, aircraft measurements at 77 meters were added to the measurement set).

2.2 Pole Temperature Measurement Heights

During the earlier phases of the program, temperature sensors were mounted at

heights of 0, 1, 2, 5 and 9 meters. Analysis of the records indicated, however, that determination of the shape of the steep temperature lapse rate region within the first 10 or so meters above the ground would be enhanced by changing the sensor heights and adding an additional sensor. The poll sensor heights utilized during this reporting period were 0, 0.3, 1, 2, 4, 8 and 14 meters and this change has produced the desired result.

2.3 Two-Axis Hot Wire Anemometer

The theoretical studies underway, which were discussed in the previous report and are discussed futher in the present report, have indicated the desirability of measuring vertical wind velocities in dust devils. These measurements provide important information required for an understanding of dust devil generation mechanisms. Accordingly, we began to measure both tangential and vertical velocities with our single-axis hot wire. This, however, involved making two penetrations of each dust devil and it was found that with much forward motion of the devils this was impossible to do. A two-axis hot wire amemometer with recorders was therefore constructed and calibrated for both wind velocity magnitude and directional response characteristics. This instrument has been utilized through most of the present reporting period.

2.4 Background Wind Velocity and Direction

Recorders have been added to the instruments measuring background wind velocity and direction so that continuous records could be obtained. This was considered to be important since then it is possible to look for possible correlations between these quantities and dust devil activity.

2.5 Vorticity Meter and Dust Devil Rotation Counts

The source of the concentrated angular momentum of a dust devil is one of the major questions to be answered if the necessary conditions for dust devil

formation are to be established.

As discussed in Section 2 of the 2nd interim report, the intensity, size, sense of rotation and lifetime of a dust devil are probably related to the magnitude and sense of the available background vorticity (ζ_e) in the dust devil's environment. Therefore two additional observations were added to the field program to try to determine the scale and magnitude of ζ_e.

The first of these was the stationing of from 4 to 6 observers in a line perpendicular to the mean wind. Their assignment is to observe at close hand as many dust devils as possible; recording the time of observation, location, dust diameter, sense of rotation, and comments on the shape, degree of development, duration, etc. The object of these observations is to obtain statistics on the temporal and areal distribution of sense of rotation, size, and duration. These statistics can give a fair indication of the time and space scale of ζ_e.

Measurement of ζ_e directly is a difficult task using standard instrumentation. In view of this a new type of sensor was designed. This instrument consists of four 8 cm diameter styrofoam spheres mounted on the ends of two mutually perpendicular one meter rods. The intersection of these rods is mounted perpendicular to the shaft of a one turn, low-torque, continuous potentiometer wired as a voltage divider. The output voltage is continuously recorded. Each arm is balanced and the device mounted two meters above the ground with the plane of the arms level. Wind tunnel tests showed that the device is insensitive to changes in wind direction and speed (below 65 km hr^{-1}) and responds only to horizontal gradients in horizontal velocity, or rotary motion (ie ζ_e). The starting threshold of the device is not known but appears to be

very low. With this "vorticitv" meter, good indications of the sense and magnitude of the background rotation in the vicinity of the meter can be obtained.

3.0 FIELD DATA AND DISCUSSION

3.1 Basic Field Data

The basic field temperature data are given in Appendix A. These are for five days of operations during this reporting period and represent those days where meteorological conditions met study requirements. The first graph shown for each day presents the temperature data obtained by the aircraft at 77, 150, 300, 920 and 1540 meters altitude as a function of time. The following graphs for each day show the temperature profiles with height at sequential times during the day. Ground temperatures, though monitored, are not shown.

The wind velocity and direction data for each day are shown in Figures 2, 5, 8, 11, and 14. Dust devil frequency and size data as a function of time for each day are shown in Figures 1, 4, 7, 10 and 13. Figures 1-15 also show derived quantities which will be defined shortly. Data for dust devil wind velocities are presented in Table 1. Most column headings are self-explanatory. The quantities v_{max} and w_{max} respectively represent the maximum tangential and maximum vertical (upward) wind velocities in the devils; c refers to clockwise rotation looking toward the surface from above, and cc refers to counterclockwise rotation. The dust devil diameter given is that of the visible dust column.

The basic vorticity data are given in Figures 16-18. These figures show sense of vorticity meter rotation (2 minute intervals) and dust devil rotation directions as a function of time, for three days.

3.2 Discussion of Field Data

3.2.1 Temperature Profiles

The temperature profiles, Appendix A, when plotted on a linear scale show typically a steep temperature lapse rate region adjacent to the ground overlain by a layer

in which the lapse rate is still superadiabatic but much less so, and finally by a layer where the lapse rate is dry to sub-adiabatic. The height of the highly superadiabatic layer has, to date, always been about 10 meters. The height (h) to the top of the overlying superadiabatic layer ranges from a few tens of meters to several hundreds of meters. Both of these layers can be approximated well by linear temperature profiles. This approximation is utilized whenever applicable in the following discussions.

3.2.2 Dust Devil Frequencies and Sizes as a Function of Derived Temperature Profile Parameters

The pertinent data are shown in Figures 1-15. The quantity ΔT is simply the temperature difference between the sensor at 0.3 meters and the temperature at the height where the lapse rate is no longer superadiabatic. The quantity h is the height of the total superadiabatic layer. The quantity ΔT_s is the difference in temperature between the sensor at 0.3 meters and the temperature at the top of the highly superadiabatic layer (h_s) adjacent to the ground. Since the height of this layer has always been about 10 meters, ΔT_s is directly proportional to the lapse rate in this layer. The final quantity is dT/dZ. This is defined as the temperature difference between the top of the super layer adjacent to the ground ($\simeq$ 10 meters) and h, divided by h minus the height of the base layer. It directly represents the lapse rate in the rather thick layer between the stable atmosphere above and the extremely superadiabatic layer adjacent to the ground.

The search for correlations is best done by studying the results for given days.

Table 1A

Dust Devil Penetrations for 3/28/68

Time	Background Wind (Ave.) (km hr^{-1})	Diameter (meters)	v_{max} (km hr^{-1})	w_{max} (km hr^{-1})	Direction of Rotation
1224	< 5	10-15	19	No measurement	C
1235	7-8	6-8	11	No measurement	C
1426	6	30	25	No measurement	CC

Table 1B

Dust Devil Penetrations for 5/3/68

Time	Background Wind (Ave.) (km hr^{-1})	Diameter (meters)	v_{max} (km hr^{-1})	w_{max} (km hr^{-1}	Direction of Rotation
1325	< 5	<1	4.5	No Measurement	C
1336	12	6-8	32	No Measurement	C

Table 1C

Dust Devil Penetrations for 6/13/68

Time	Background Wind (Ave.) (km hr^{-1})	Diameter (meters)	v_{max} (km hr^{-1})	w_{max} (km hr^{-1})	Direction of Rotation
1308	25	3	4.6	2.6	Not Obtained

Table 1D

Dust Devil Penetrations for 6/26/68

Time	Background Wind (Ave.) (km hr^{-1})	Diameter (meters)	v_{max} (km hr^{-1})	w_{max} (km hr^{-1})	Direction of Rotation
1100	<5	<1	3.7	1.5	C
1110	<5	1	8.5	3.7	C
1128	<5	1	6.5	2.8	C
1137	5	1	4.6	3.3	C
1144	<5	<1	3.7	1.1	CC
1156	<5	2	7.4	1.5	CC
1213	<5	1	6.5	5.5	CC
1225	<5	<1	4.1	1.1	CC
1227	<5	<1	4.6	1.3	CC
1229	<5	3	9.2	6.9	C
1256	<5	1	6.5	6.5	C
1315	<5	1	7.4	4.4	C
1327	<5	3	12	3.7	C
1349	13	2	6.9	<0.6	CC

Table 1E

Dust Devil Penetrations for 6/27/68

Time	Background Wind (Ave.) (km hr^{-1})	Diameter (meters)	v_{max} (km hr^{-1})	w_{max} (km hr^{-1})	Direction of Rotation
1100	16	3-4	11	2.8	C
1113	21	6-9	10	1.9	CC
1216	13	2-3	10	2.8	CC
1223	16	6-9	12.5	< 0.7	C
1224	18	3	7.5	<0.7	C
1231	18	2-3	10	1.3	C
1239	18	3	12.5	1.3	CC
1241	15	4	7.5	1.3	CC
1248	17	10	12.5	3.1	C
1306	No Record	5	7.5	1.9	CC
1323	22	6-9	5.5	1.9	C
1352	23	10	7.5	1.9	C
1358	18	13-17	20	2.2	CC
1424	No Record	10-15	20	1.9	C

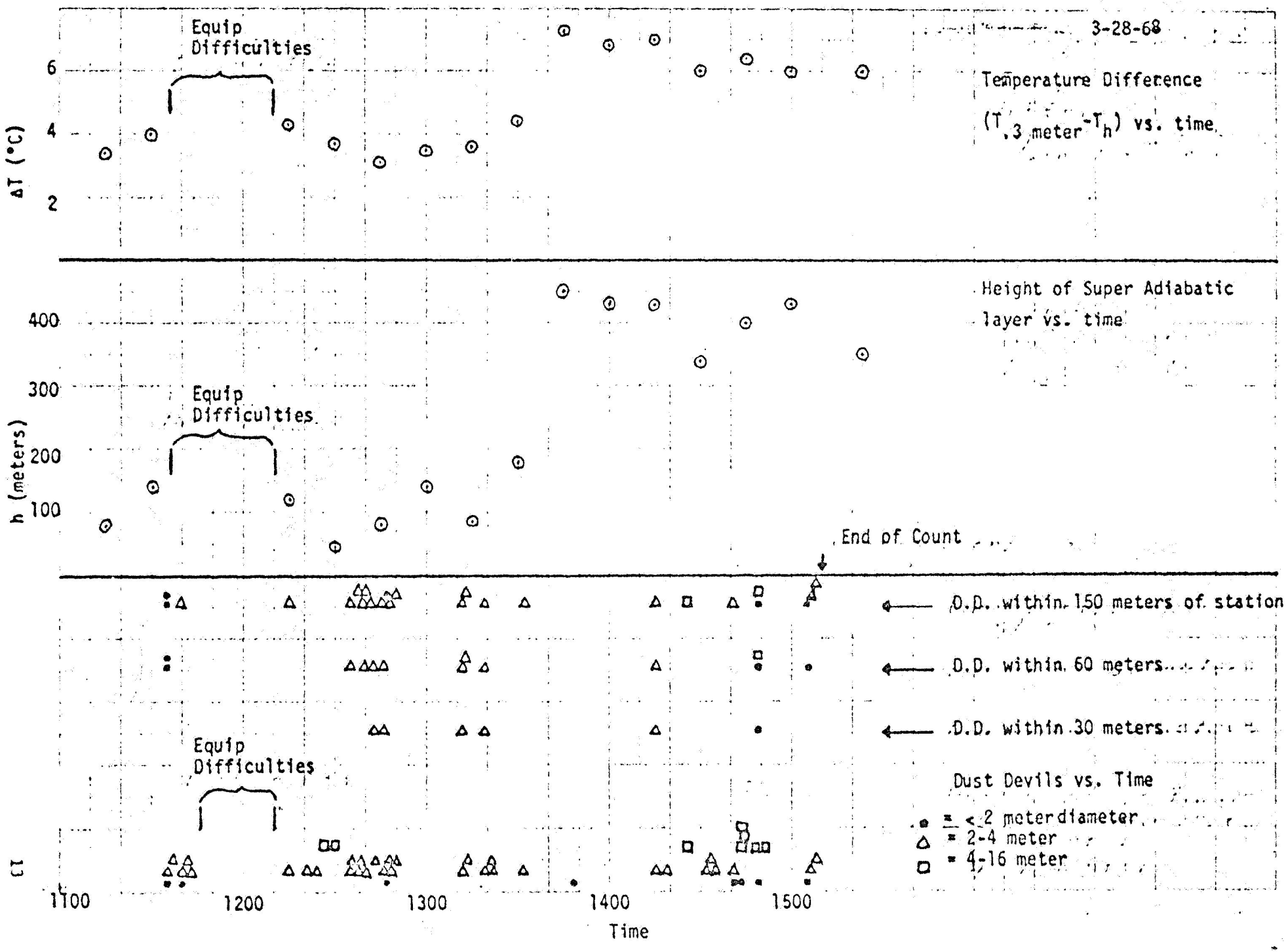
3-28-68
Temperature Difference
($T_{.3\ meter}$-T_h) vs. time
ΔT (°C)
6
4
2
Equip Difficulties
Height of Super Adiabatic layer vs. time
h (meters)
400
300
200
100
Equip Difficulties
End of Count
D.D. within 150 meters of station
D.D. within 60 meters
D.D. within 30 meters
Dust Devils vs. Time
• = < 2 meter diameter
△ = 2-4 meter
□ = 4-16 meter
Equip Difficulties
1100
1200
1300
1400
1500
Time

Figure 1

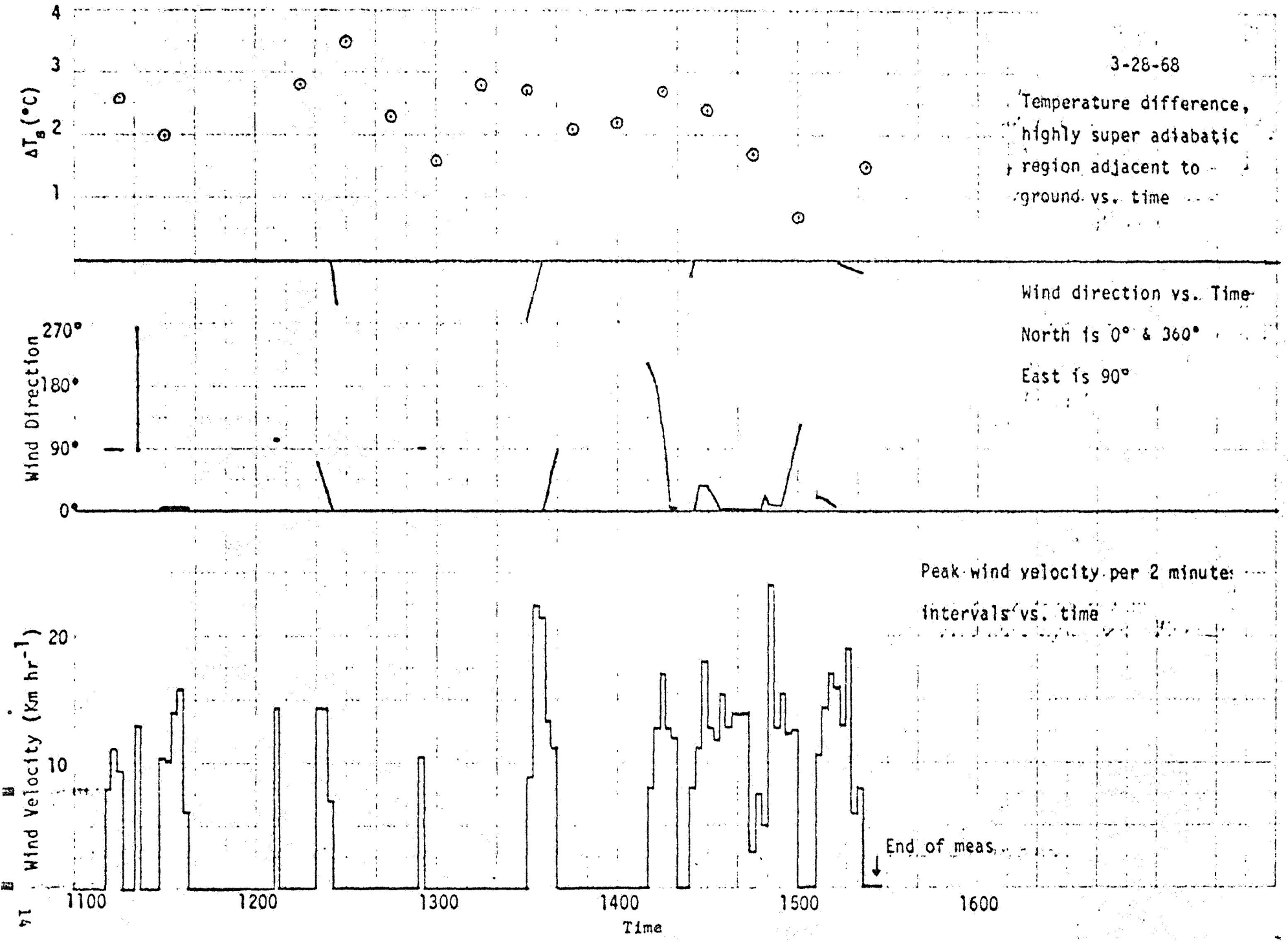
4
3
2
1
ΔT_s (°C)
3-28-68
Temperature difference, highly super adiabatic region adjacent to ground vs. time
Wind direction vs. Time
North is 0° & 360°
East is 90°
270°
180°
90°
0
Wind Direction
Peak wind velocity per 2 minute intervals vs. time
20
10
Wind Velocity (Km hr^{-1})
End of meas.
1100
1200
1300
1400
1500
1600
Time

Figure 2

Figure 3

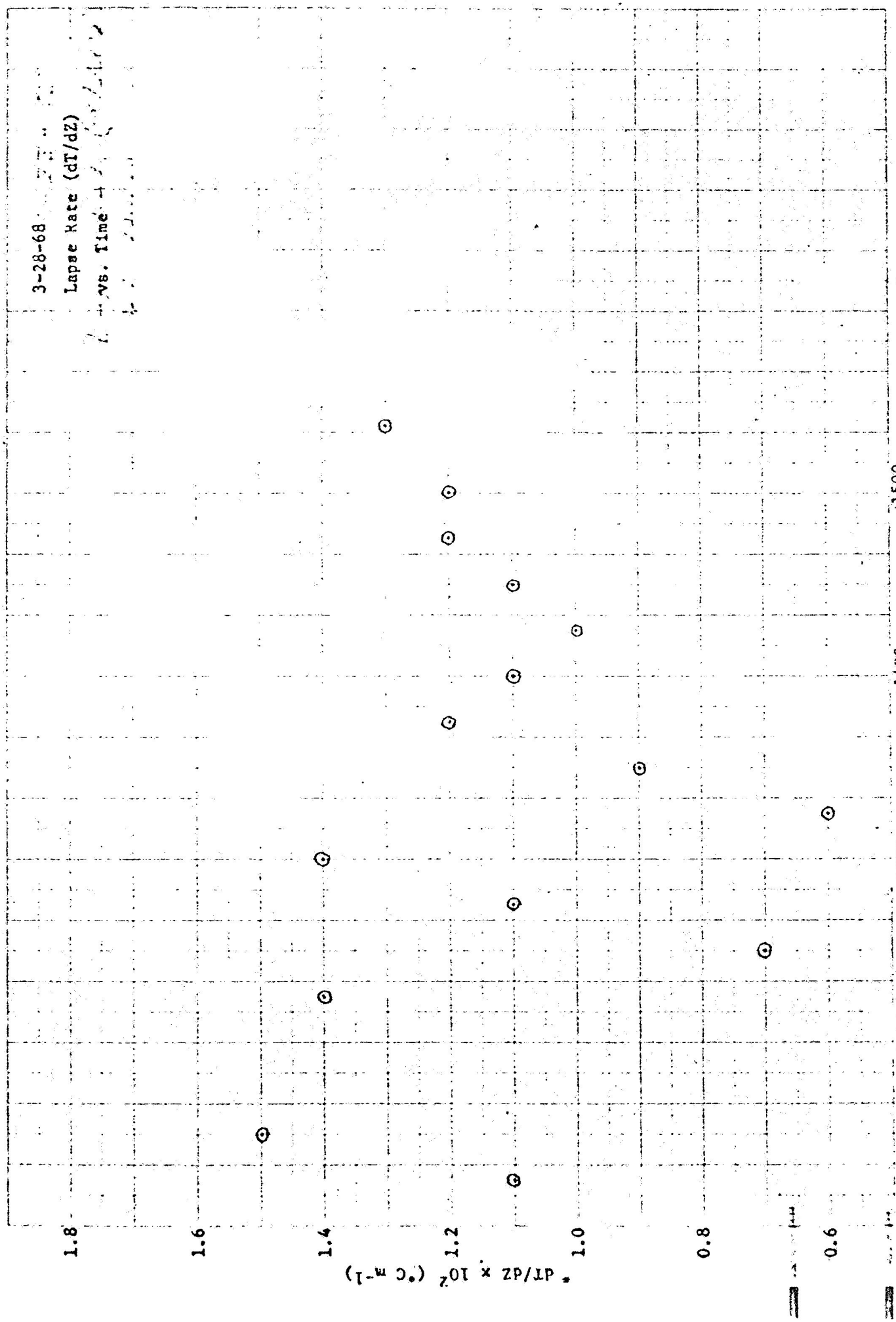
3-28-68
Lapse Rate (dT/dZ)
vs. Time
1.8
1.6
1.4
1.2
1.0
0.8
0.6
1100
1200
1300
1400
1500
Time
* dT/dZ x 10² (°C m⁻¹)

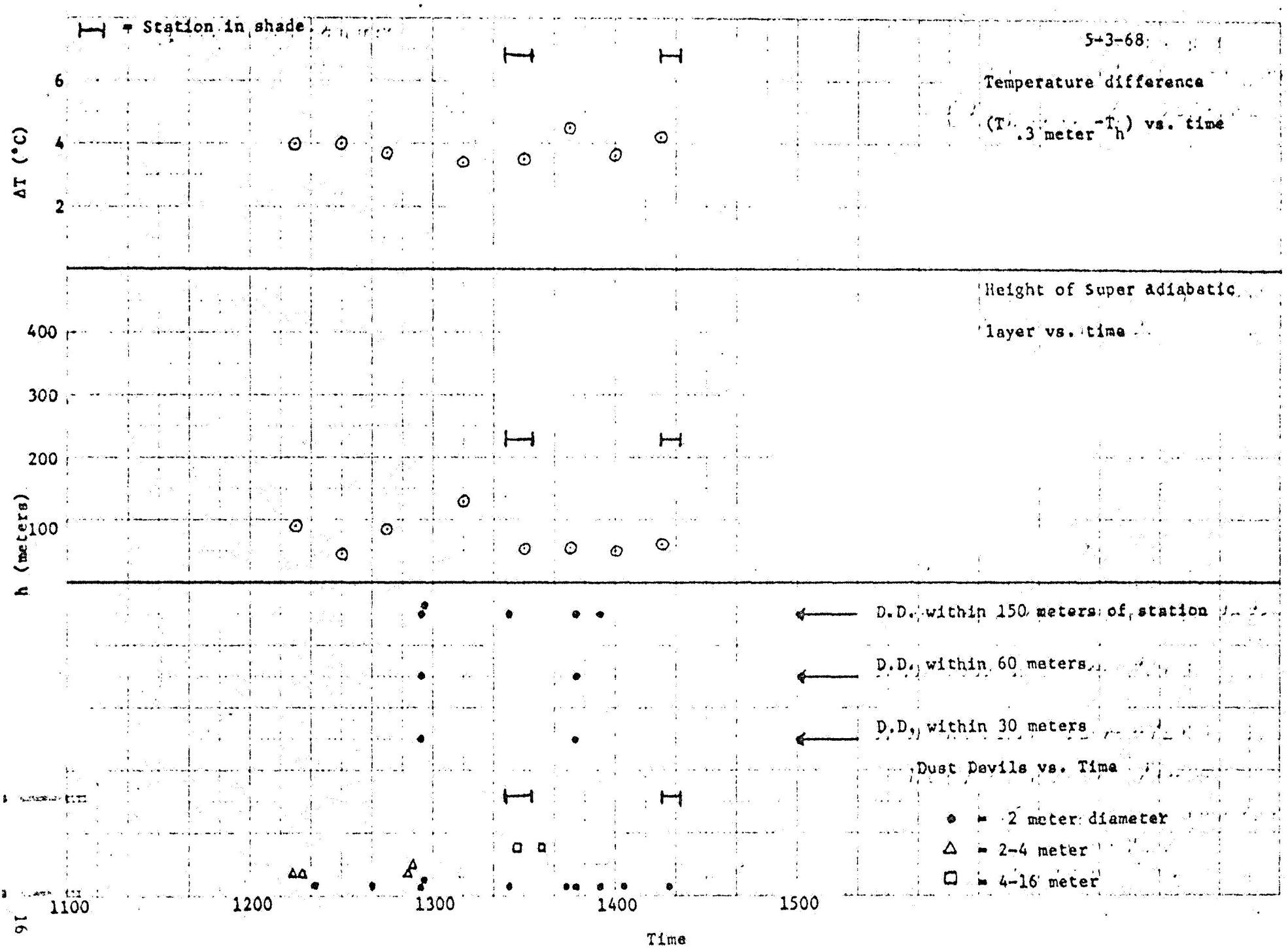
⊢ = Station in shade
5-3-68
Temperature difference
($T_{.3\ meter} - T_h$) vs. time
ΔT (°C)
6
4
2
Height of Super adiabatic
layer vs. time
h (meters)
400
300
200
100
D.D. within 150 meters of station
D.D. within 60 meters
D.D. within 30 meters
Dust Devils vs. Time
• = 2 meter diameter
△ = 2-4 meter
□ = 4-16 meter
1100
1200
1300
1400
1500
Time

Figure 4

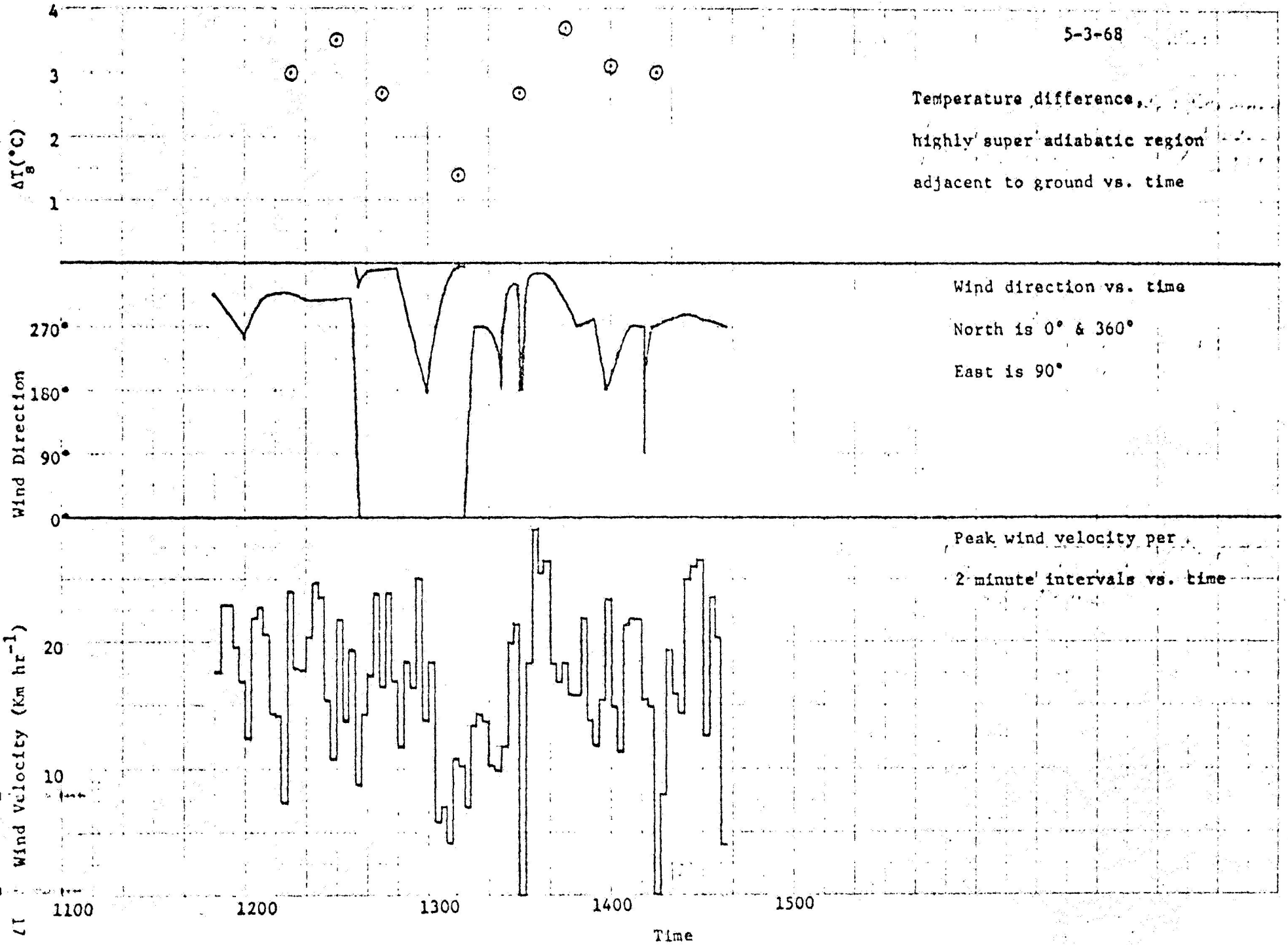
5-3-68
Temperature difference, highly super adiabatic region adjacent to ground vs. time
ΔT_g(°C)
4
3
2
1
Wind direction vs. time
North is 0° & 360°
East is 90°
Wind Direction
270°
180°
90°
0
Peak wind velocity per 2 minute intervals vs. time
Wind Velocity (Km hr^{-1})
20
10
1100
1200
1300
1400
1500
Time

Figure 5

Figure 6

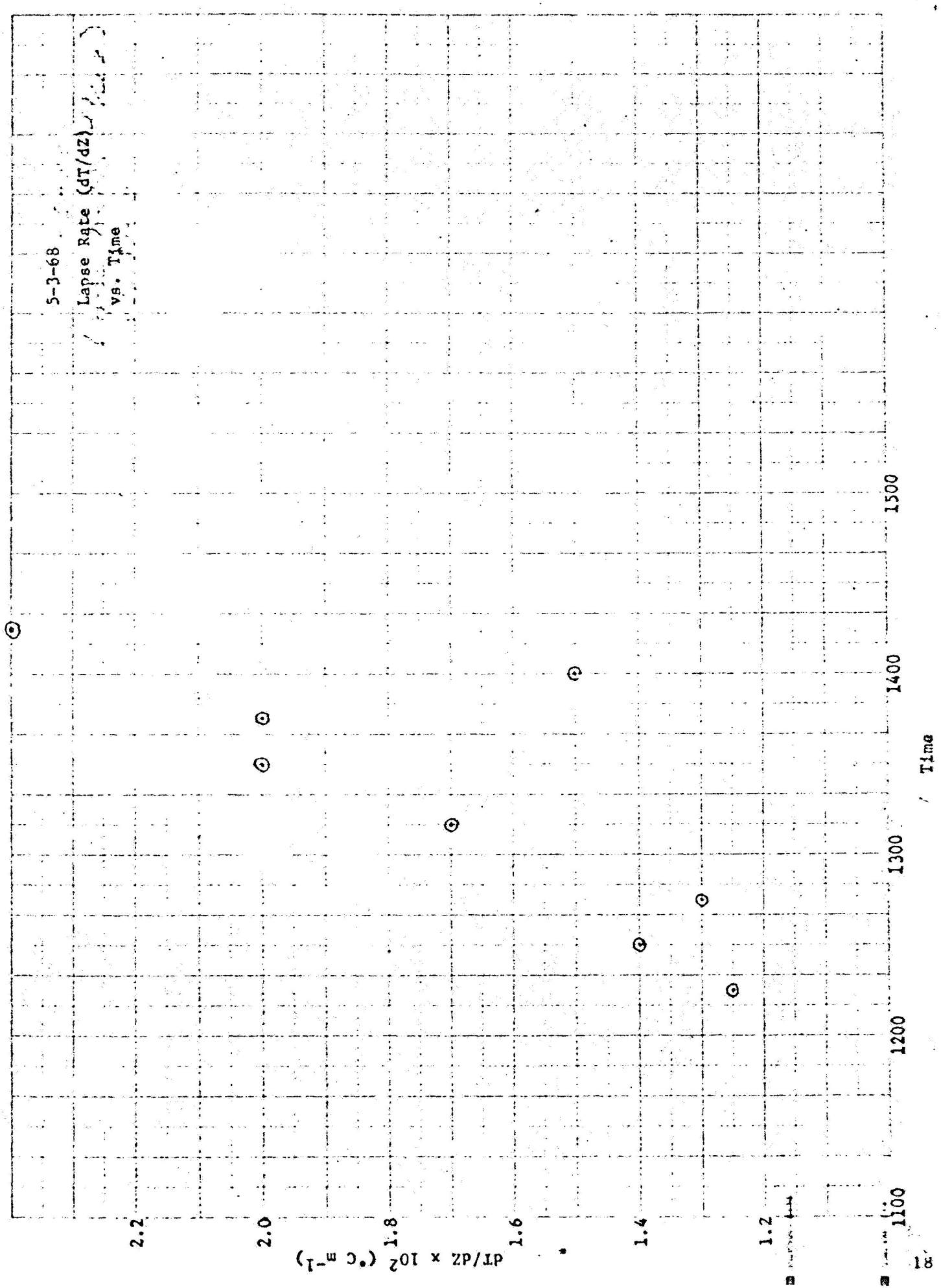
5-3-68
Lapse Rate (dT/dz)
vs. Time
dT/dz x 10² (°C m⁻¹)
2.2
2.0
1.8
1.6
1.4
1.2
1100
1200
1300
1400
1500
Time

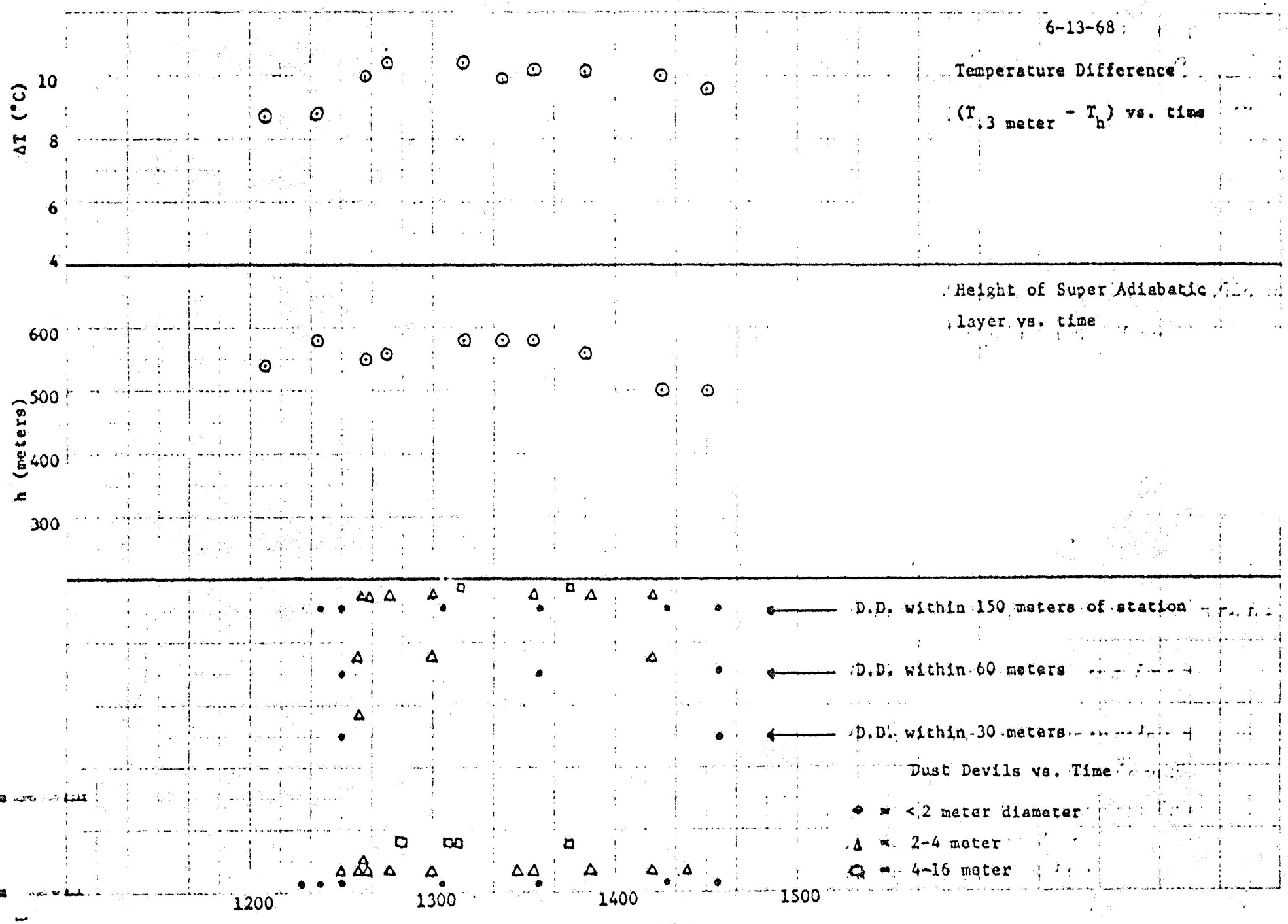
6-13-68
Temperature Difference
($T_{3\ meter} - T_h$) vs. time
ΔT (°C)
10
8
6
4
Height of Super Adiabatic layer vs. time
h (meters)
600
500
400
300
D.D. within 150 meters of station
D.D. within 60 meters
D.D. within 30 meters
Dust Devils vs. Time
◆ = <2 meter diameter
△ = 2-4 meter
Q = 4-16 meter
1200
1300
1400
1500
Time

Figure 7

Figure 8

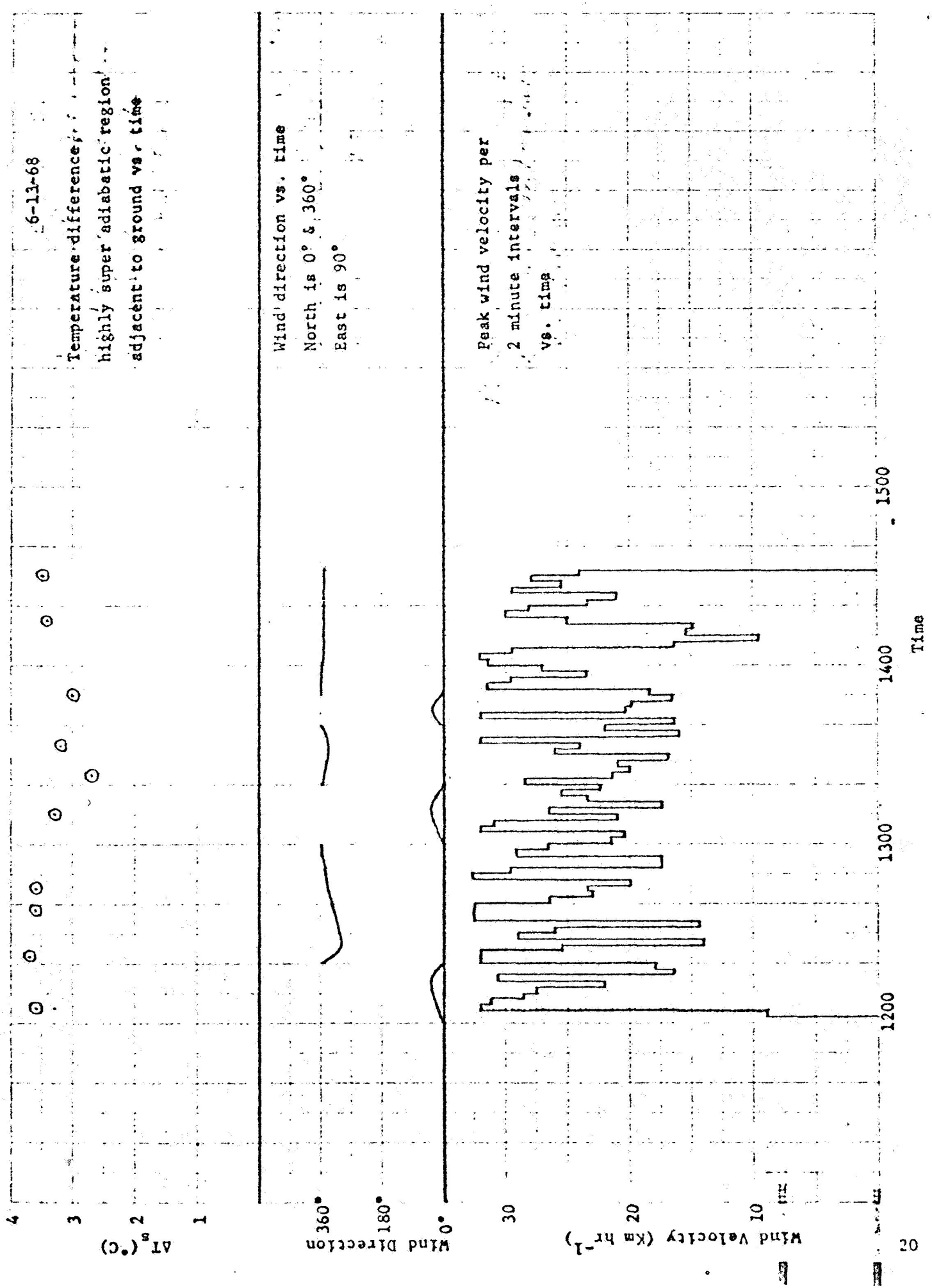
6-13-68
Temperature difference, highly super adiabatic region adjacent to ground vs. time
ΔT_s (°C)
4
3
2
1
Wind direction vs. time
North is 0° & 360°
East is 90°
Wind Direction
360°
180°
0°
Peak wind velocity per 2 minute intervals vs. time
Wind Velocity (km hr^{-1})
30
20
10
1200
1300
1400
1500
Time
20

Figure 9

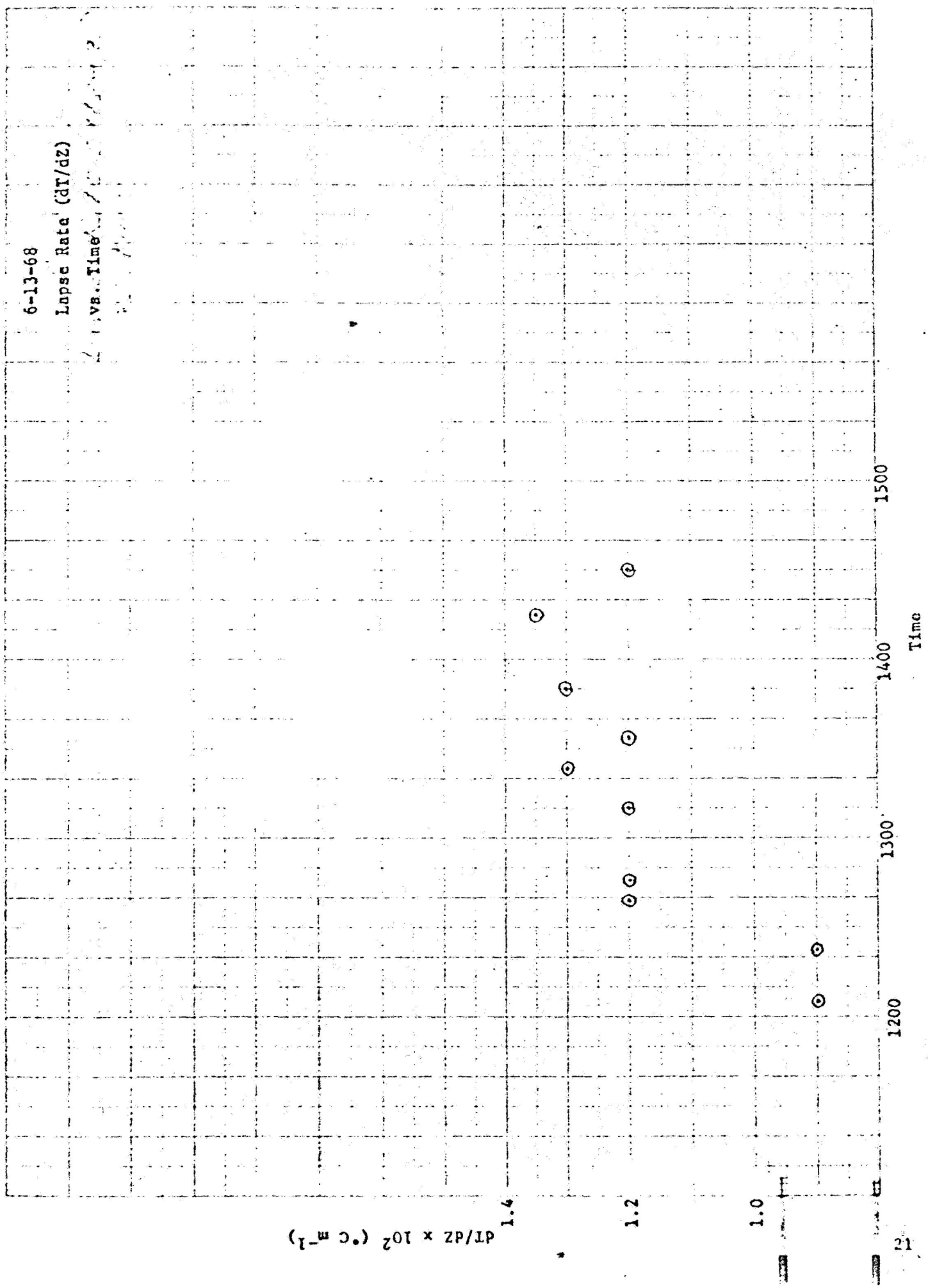
6-13-68
Lapse Rate (dT/dz)
vs. Time
dT/dz x 10² (°C m⁻¹)
1.4
1.2
1.0
1500
1400
1300
1200
Time

Figure 10

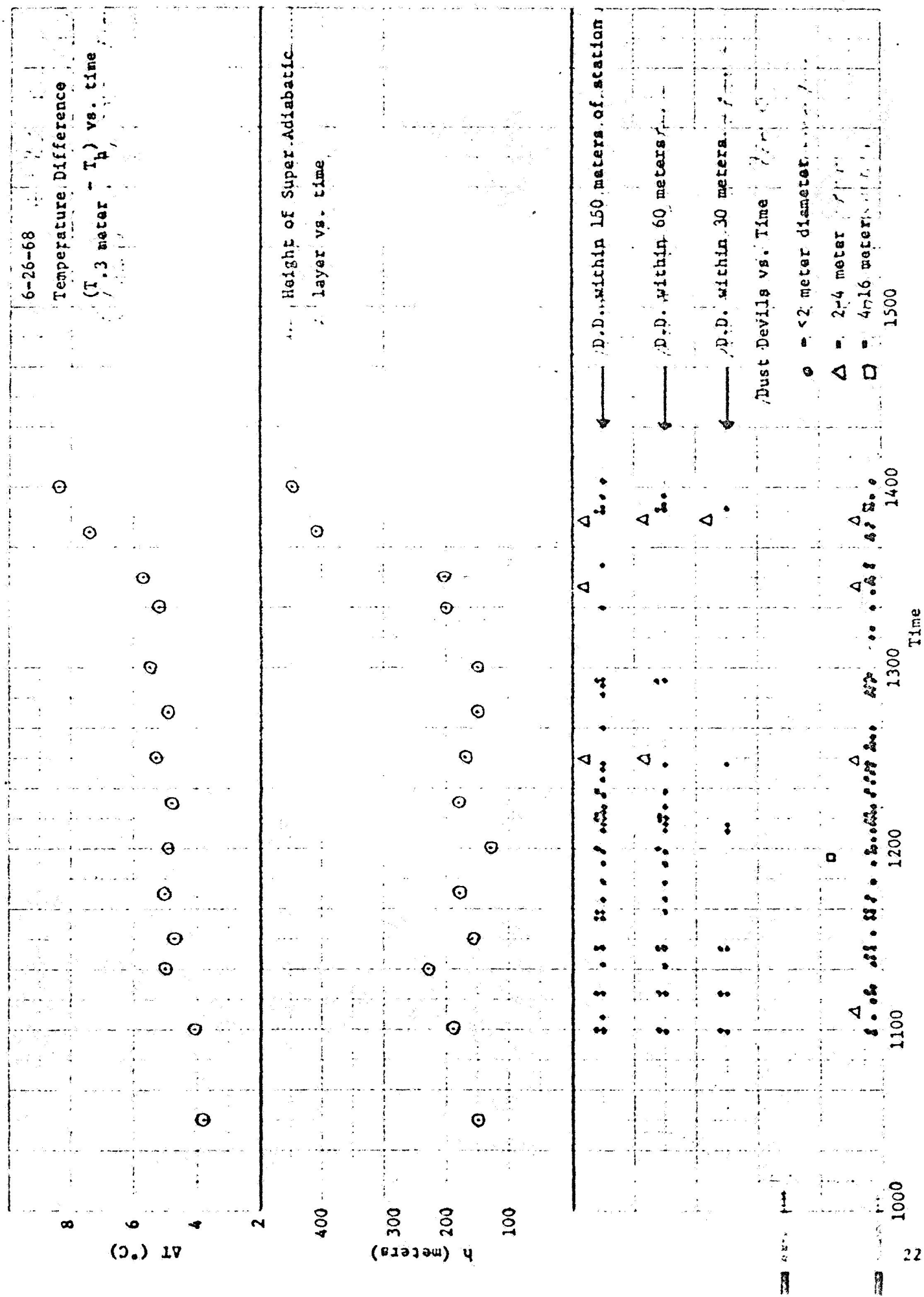
6-26-68
Temperature Difference
($T_{.3\ meter} - T_h$) vs. time
Height of Super Adiabatic
layer vs. time
D.D. within 150 meters of station
D.D. within 60 meters
D.D. within 30 meters
Dust Devils vs. Time
= <2 meter diameter
= 2-4 meter
= 4-16 meter
ΔT (°C)
h (meters)
Time
1000
1100
1200
1300
1400
1500
2
4
6
8
100
200
300
400

Figure 11

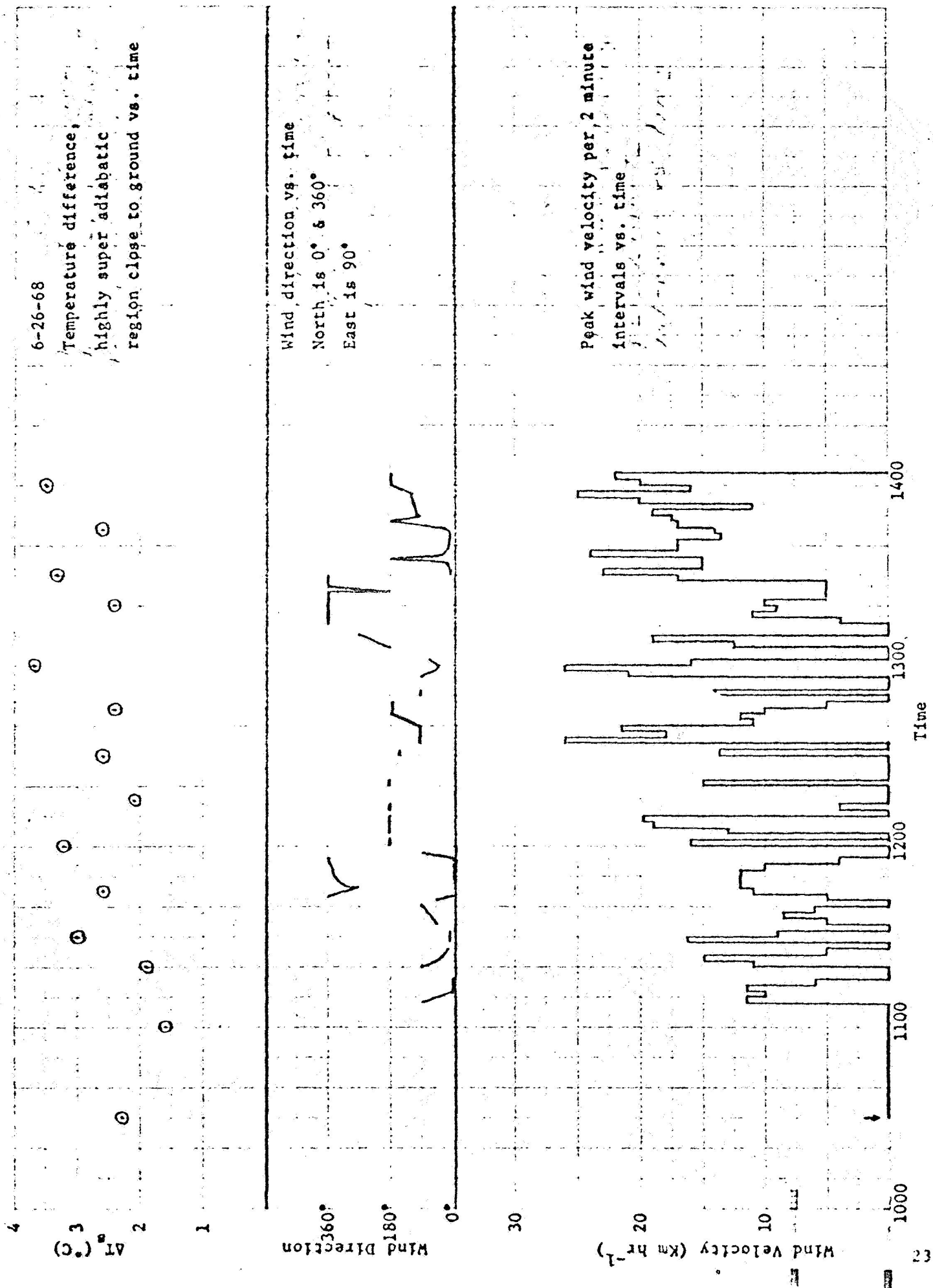
6-26-68
Temperature difference,
highly super adiabatic
region close to ground vs. time
ΔT_s (°C)
4
3
2
1
Wind direction vs. time
North is 0° & 360°
East is 90°
Wind Direction
360°
180°
0°
Peak wind velocity per 2 minute
intervals vs. time
Wind Velocity (Km hr^{-1})
30
20
10
1000
1100
1200
1300
1400
Time

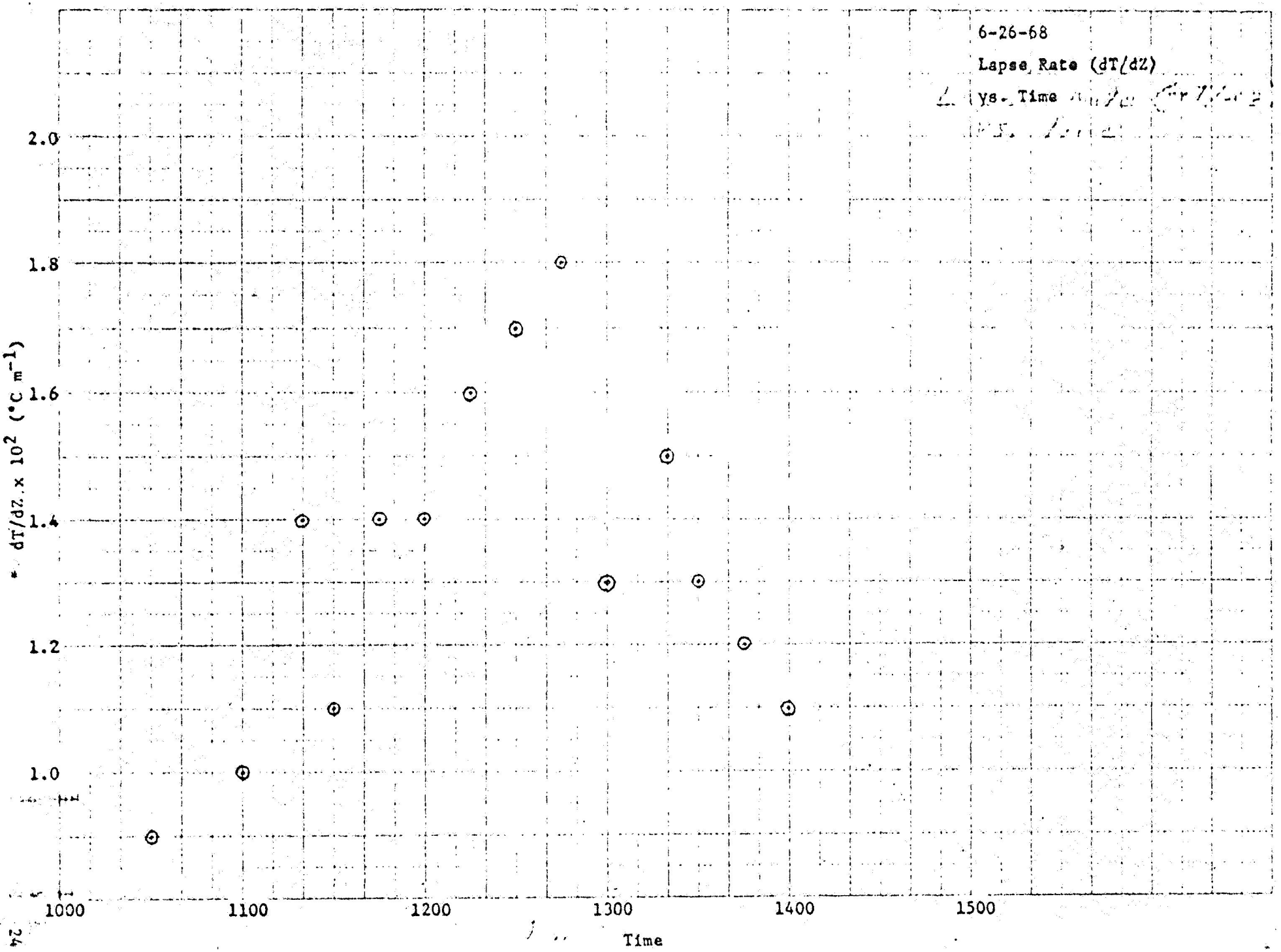

Figure 12

Figure 13

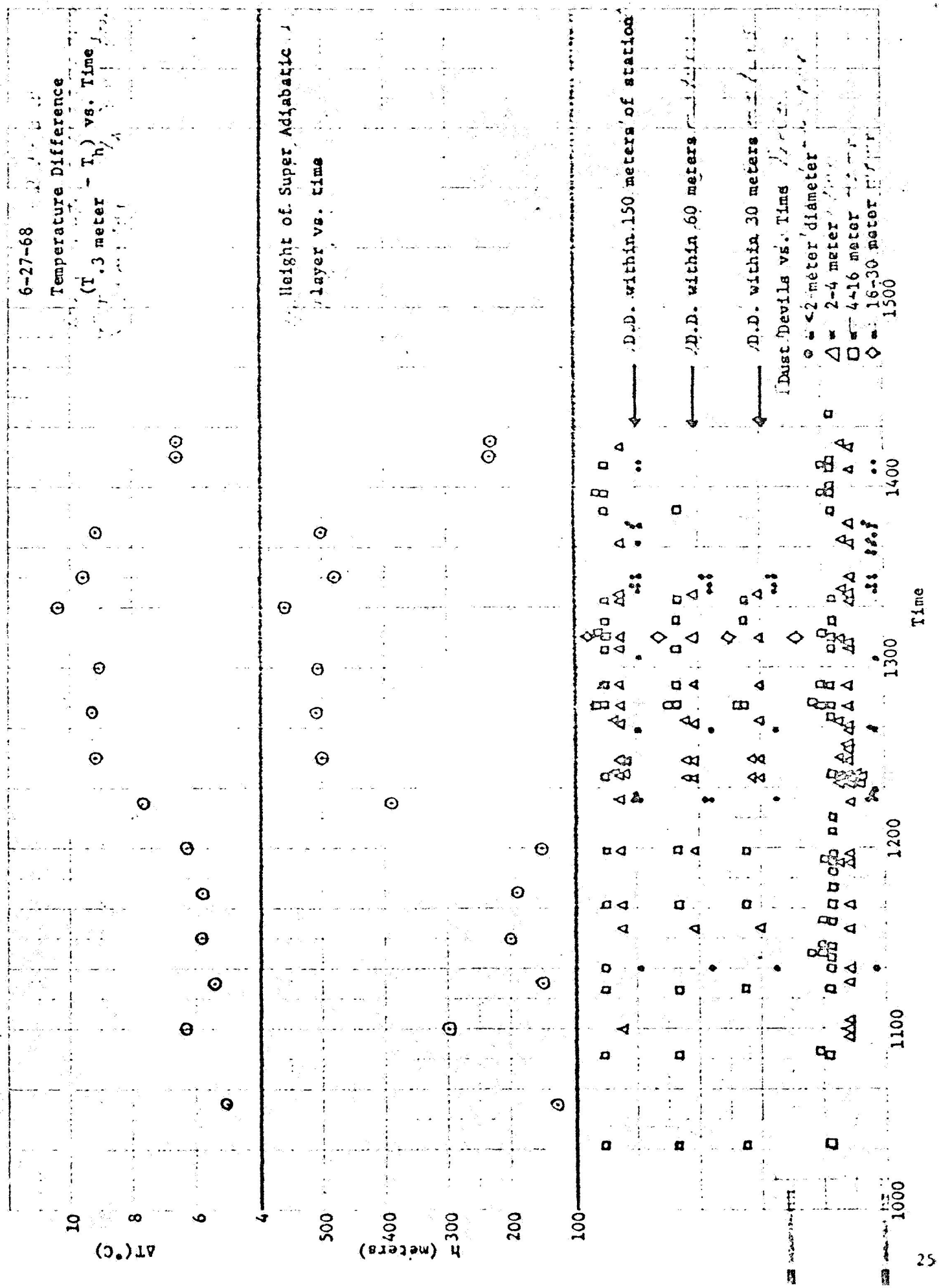
6-27-68
Temperature Difference
($T_{.3\ meter} - T_h$) vs. Time
Height of Super Adiabatic Layer vs. time
ΔT(°C)
π (meters)
Time
D.D. within 150 meters of station
D.D. within 60 meters
D.D. within 30 meters
Dust Devils vs. Time
○ = <2 meter diameter
△ = 2-4 meter
□ = 4-16 meter
◇ = 16-30 meter
1000
1100
1200
1300
1400
1500

Figure 14

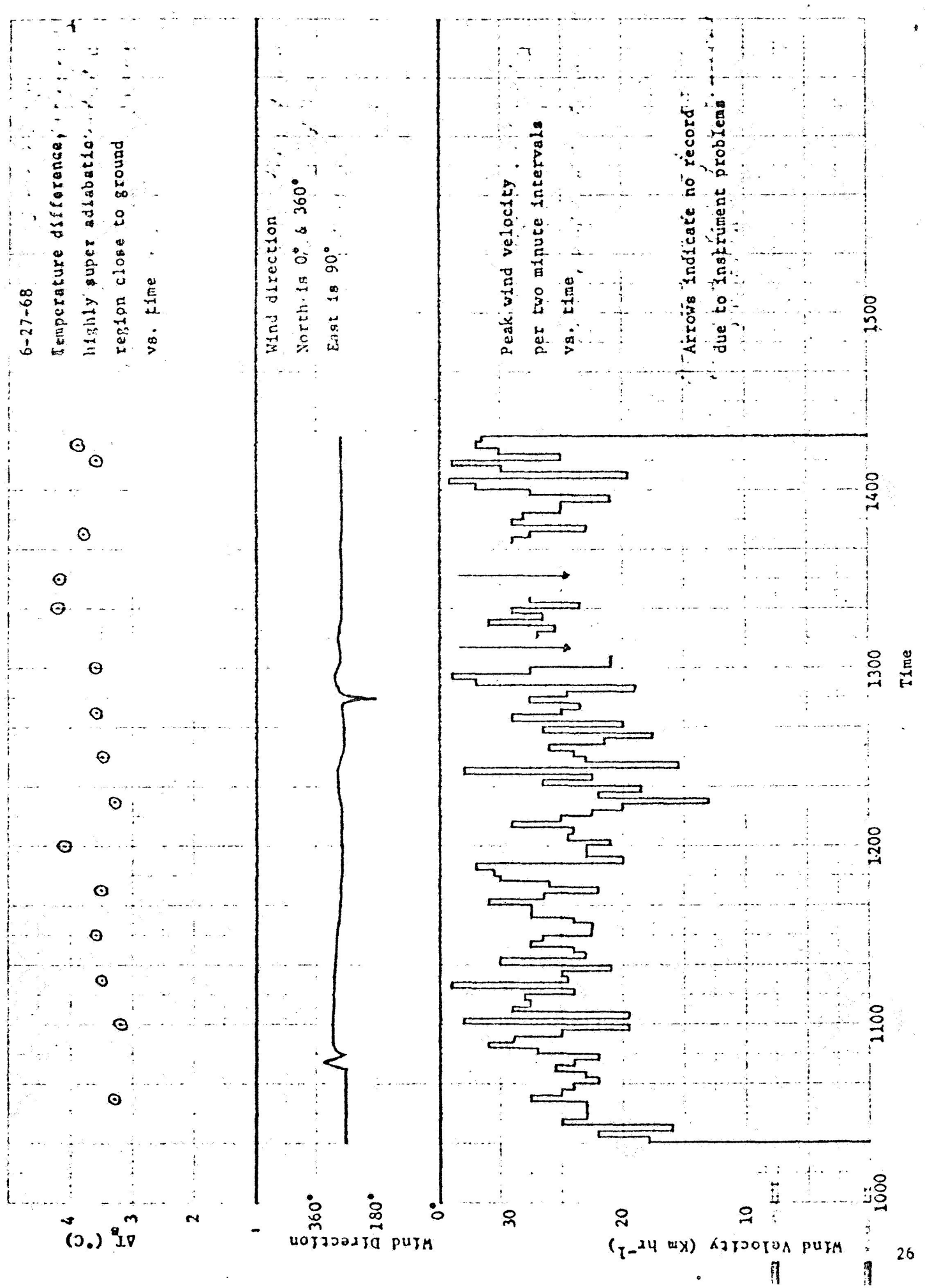
6-27-68
Temperature difference, highly super adiabatic region close to ground vs. time
Wind direction
North is 0° & 360°
East is 90°
Peak wind velocity per two minute intervals vs. time
Arrows indicate no record due to instrument problems
ΔT (°C)
Wind Direction
Wind Velocity (Km hr⁻¹)
Time
1000
1100
1200
1300
1400
1500
360°
180°
0°
30
20
10
4
3
2
1

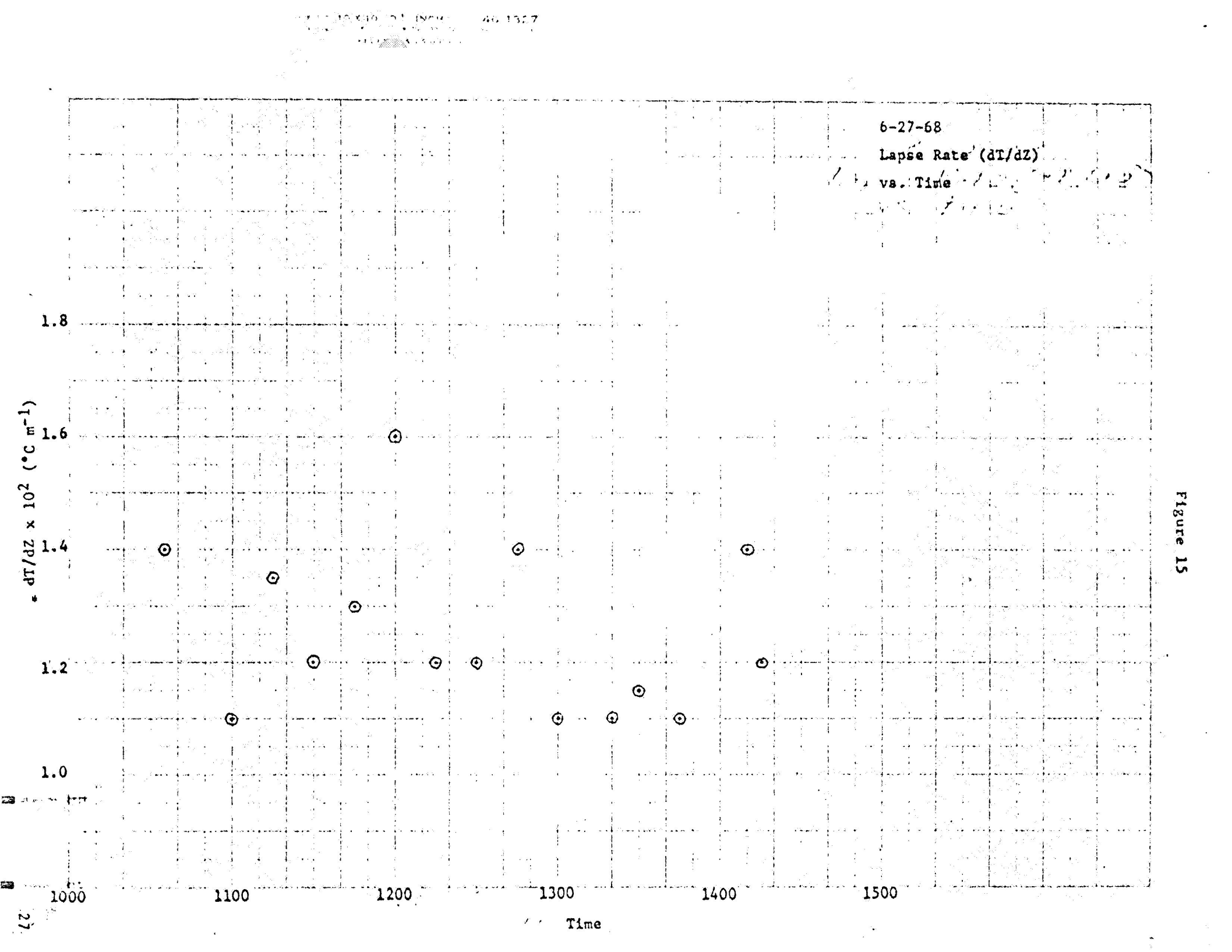
6-27-68
Lapse Rate (dT/dZ)
vs. Time
dT/dZ x 10² (°C m⁻¹)
1.8
1.6
1.4
1.2
1.0
1000
1100
1200
1300
1400
1500
Time

Figure 15

3-28-68

The applicable data are given in Figures 1-3. The day was clear with very little wind. What wind there was came mostly from the north. A total of 48 dust devils entered the counting area (≈ 600 x 200 meters). The dust devil frequency and size data are shown in Figure 1. They are plotted as total in counting area, and those within 150, 60, and 30 meters of the station (pole for temperature measurement). The type of mark used indicates dust devil diameter. It is seen that the devils cluster into two main groups (in time) with two subsidiary groups. Also note that the period around 1200 involved equipment (balloon) difficulties which involved the entire field crew so that counts are lacking and the subsidiary peak at 1140 may be part of the major peak at 1230.

The 1230 peak in frequency is preceeded by a gradual increase in ΔT, h and dT/dZ. It also occurs simultaneously with a peak in ΔT_s. Note the time lag, however, between the ΔT and h peaks and the frequency peak, ΔT and h reaching a maximum earlier. Note also that dT/dZ reaches a minimum coinciding with the frequency maximum. Following this frequency maximum, the activity diminishes and then abruptly ceases. This cessation occurs at a minimum for ΔT_s, shortly after a minimum in ΔT, but as dT/dZ is reaching a maximum. This oscillating behavior continued during the remainder of the day.

It appears from this that dust devil activity increases at ΔT_s increases, that is, as the layer adjacent to the ground becomes more unstable. Conversely, dT/dZ appears to behave inversely to dust devil activity. A possible explanation for this latter behavior is given at the end of this section.

5-3-68

The applicable data are given in Figures 4-6. The day was clear except for two brief intervals of shade. A total of only 16 dust devils entered the counting area. A fairly steady wind averaging between 10-20 km hr^{-1}, but highly variable in direction, was present all day. The dust devils fall into two basic activity groups, one between 1200-1300 and the other from 1330-1430. It is seen that both peaks correspond to maxima of ΔT_s, and that the quiet period corresponds to a ΔT_s minimum. There is some indication of the inverse behavior of dT/dZ noted previously, particularly with regards to those dust devils within 150 meters of the station.

6-13-68

The applicable data are given in Figures 7-9. The day was clear with a strong north wind of about 20-30 km hr^{-1} blowing the entire day. Only 22 dust devils appeared in the counting area. The quantity ΔT_s did not change much during the day, nor did dust devil frequency. There is, however, a small frequency maximum between 1220 and 1310 corresponding to a broad maximum of ΔT_s. There also is a brief frequency minimum at about 1330 corresponding to a ΔT_s minimum. No correlation between activity and dT/dZ is evident except for the initial rapid increase in dT/dZ at the beginning of the day.

6-26-68

The applicable data are given in Figures 10-12. The day was clear; also calm during the early morning. The wind, picking up about 1110, was highly variable in both velocity and direction with a general trend of increasing velocity with time. A total of 80 dust devils appeared in the counting area. Almost all of these were significantly less than 2 meters in diameter

(a possible factor in the large number of very small dust devils observed is that the counting area was scraped at the beginning of the day to produce loose dust, most of the previous dust having been blown away during windstorms the previous week). Dust devil activity was relatively constant after activity began. The larger dust devils, particularly within 150 meters of the station, did however show a tendency to increase in frequency in the afternoon. The quantity ΔT_s, though quite variable, also increased slowly with time. Considerable variation was noted for dT/dZ.

6-27-68

The applicable data are given in Figures 13-15. The day was clear. A steady wind of average velocity about 20 km hr^{-1} was present all day, blowing almost solely from the west. A total of 108 dust devils appeared in the counting area. Dust devil activity was relatively constant after 1100, but several small maxima and minima are evident. These correspond well with maxima and minima in ΔT_s. The quantity dT/dZ was highly variable, but it does show fairly clearly the inverse behavior, tending toward a maximum with decreasing activity and a minimum with increasing activity.

Summary

The data to date, for dust devil frequency as related to temperature profile characteristic indicate that

a. Dust devil frequency is correlated with ΔT_s, the temperature lapse in the highly superadiabatic layer adjacent to the surface, activity increasing as ΔT_s increases. This correlation holds best when little or no wind is present. It also holds fairly well when the wind is steady, but the correlation is not as definite when the wind is highly variable in velocity. For this latter condition the temperature

profiles undergo considerable variation and this is a possible cause for decreased definitiveness in the correlation (as will be noted in a subsequent section, dust devil frequency also appears to depend on atmospheric vorticity).

b. There appears to be an inverse correlation between dust devil frequency and dT/dZ (the temperature lapse rate in the superadiabatic layer above the highly super surface layer), dT/dZ reaching a minimum when activity is a maximum. This is particularly evident under light and steady wind conditions. A likely explanation for this is that the minimum is produced by heat transferred upward during dust devil activity, whereas the lapse rate in this layer recovers when activity ceases. The decrease in inverse correlation under variable and/or very strong wind conditions could be due to the increased mechanical turbulence and mixing produced.

Correlations of dust devil frequency have been made for given days. Correlations between days have not as yet been attempted because of (a) the variability of the general meteorological conditions, such as area vorticity, between days and (b) the variability in the amount of loose dust present at the surface.

3.2.3 Dust Devil Wind Velocity Correlations

A search has been made for possible correlations between dust devil wind velocities and (a) background (environmental) wind velocity, (b) $\Delta T_s/h_s$, (c) dT/dZ, and (d) dust devil diameter.

Background Wind

The quantity v_{max} (maximum tangential wind velocity in the dust devil) is

plotted versus background wind velocity in Figure 19. Dust devil diameter was held constant. It is seen that there is an apparent decrease in v_{max} as background wind increases. On the other hand w_{max} (the maximum vertical velocity in the dust devil) appears to be unaffected (Figure 20). These were then plotted again, but holding dT/dZ constant. This was done since the background wind could affect the lapse rate which could then affect the dust devil wind velocities (ideally one would like to hold lapse rate and diameter both constant but there are as yet insufficient data to do this). The results for v_{max} are shown in Figure 21. It is seen again that v_{max} decreases as the background wind velocity increases. On the other hand w_{max} (Figure 22) is unaffected. This is the type of behavior one would expect if the magnitude of w is determined principally by bouyancy while the magnitude of v depends largely upon the concentration of angular momentum, this concentration being impeded by the disruptive influence of the wind and associated turbulence. This could be one reason why it has been observed by many investigators that dust devil formation is inhibited with high background winds. (A second possible contributing mechanism is that, with turbulence, an increased amount of heat transfer is accomplished by turbulent mixing, with a decreasing necessity for operation of the dust devil and "thermal" modes).

$\Delta T_s/h_s$

No evident correlation was found between $\Delta T_s/h_s$, the temperature lapse rate in the highly superadiabatic layer adjacent to the ground, and v_{max} and w_{max}.

dT/dZ

The applicable data are shown in Table 2. In this table the dust devils are grouped by diameter. It is immediately seen that, with the exception of

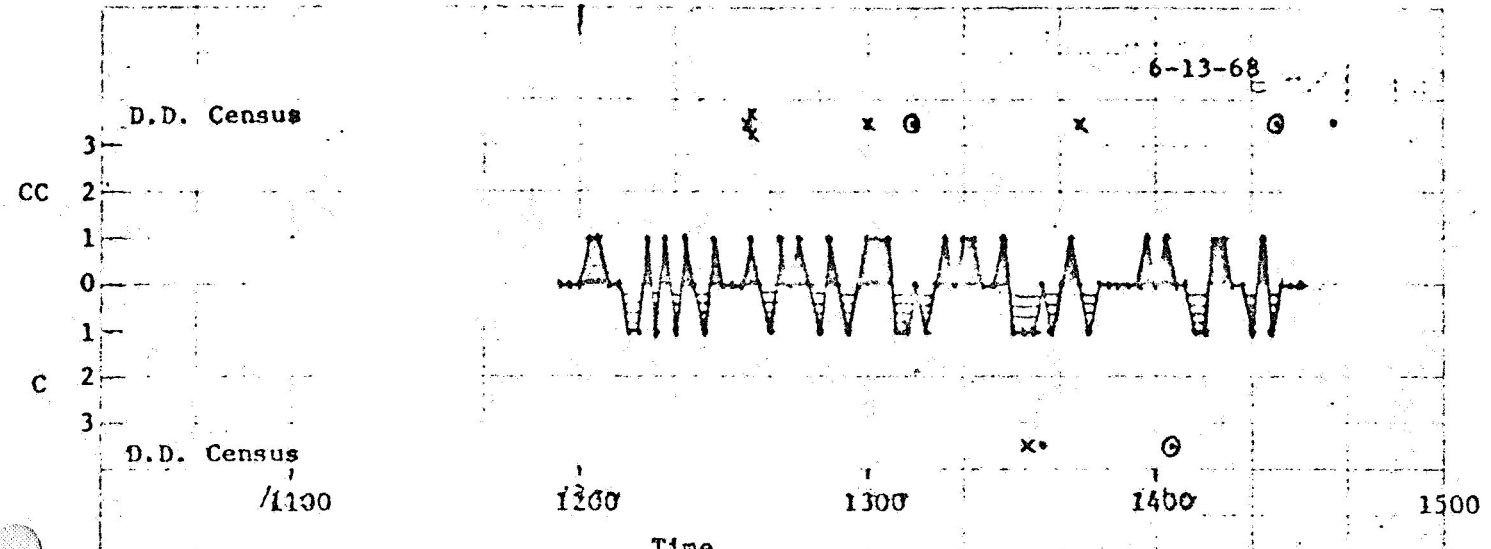

Figure 16

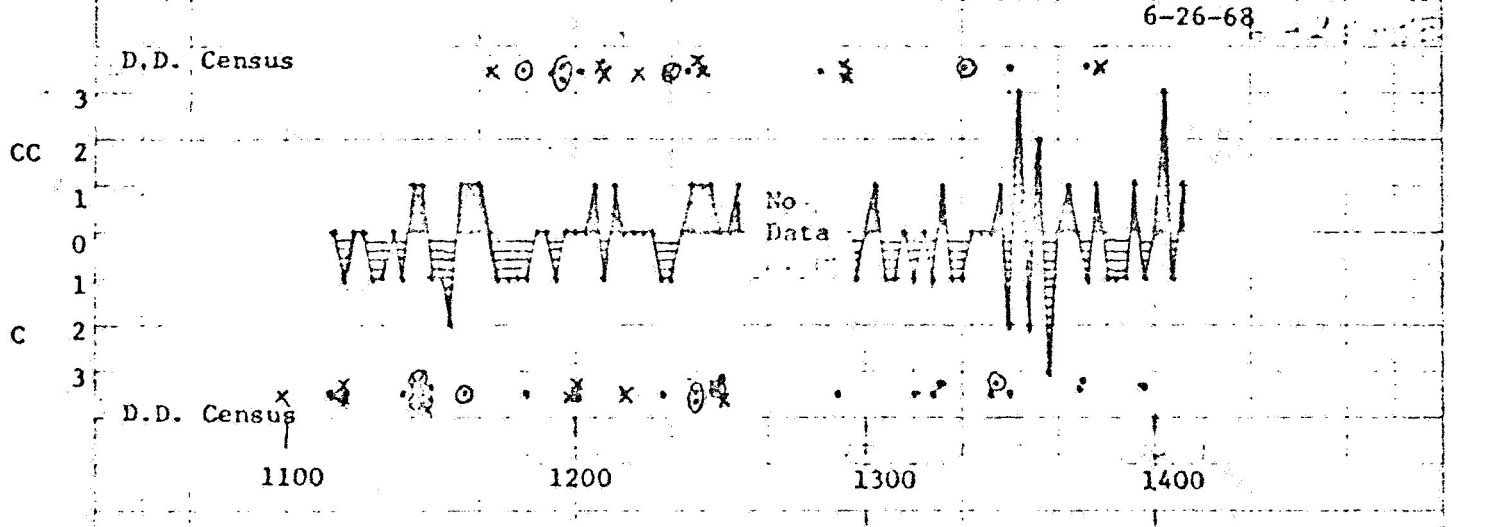

Figure 17

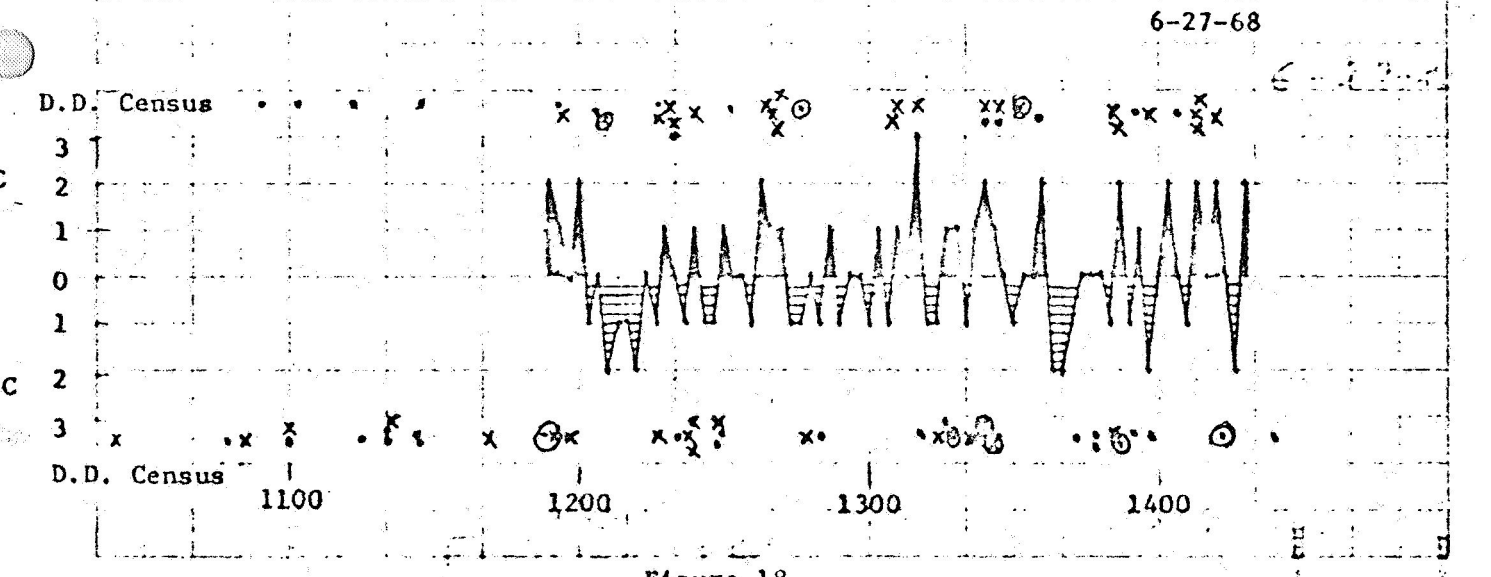

Figure 18

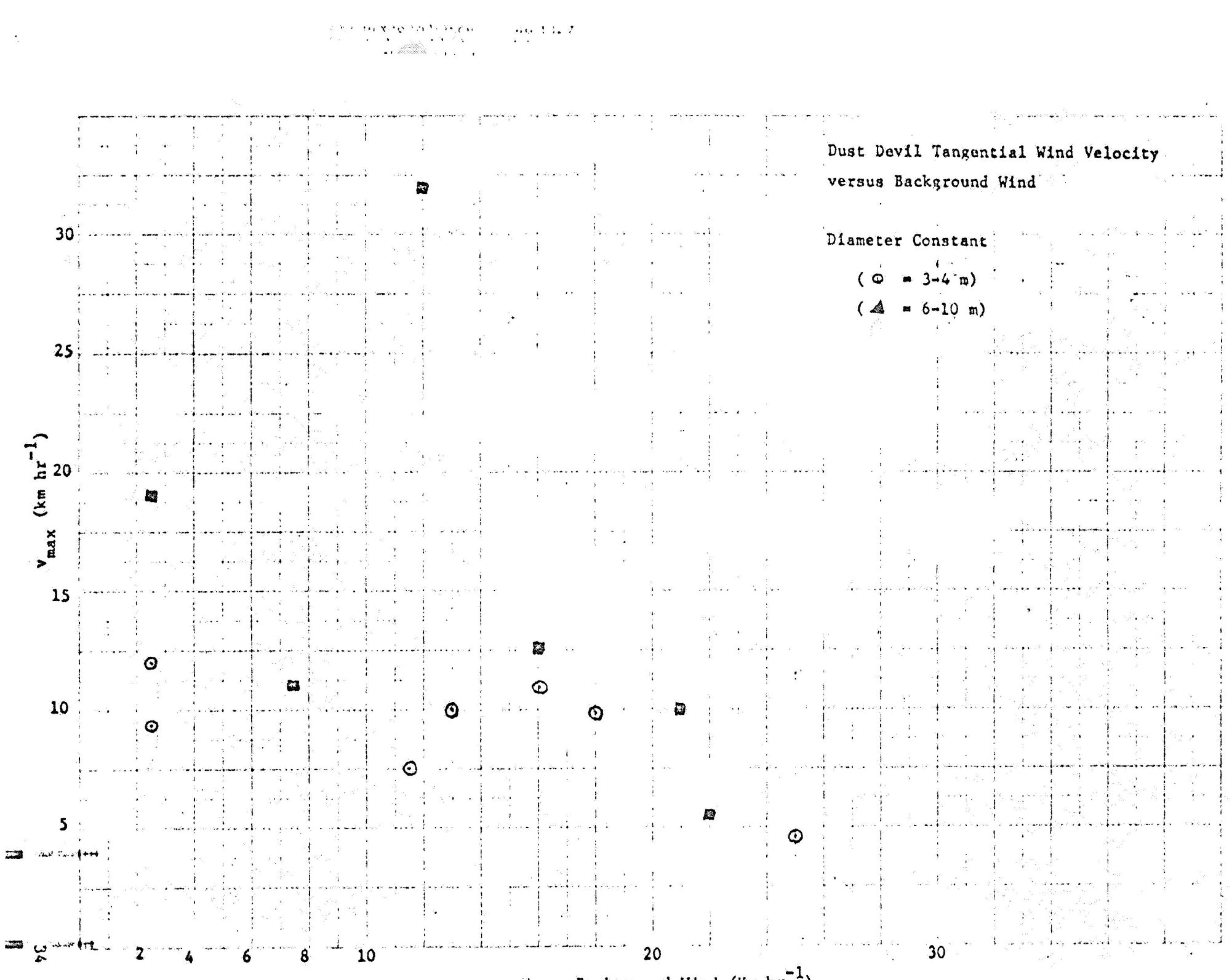
Dust Devil Tangential Wind Velocity
versus Background Wind
Diameter Constant
(⊙ = 3-4 m)
(◢ = 6-10 m)
v_{max} (km hr^{-1})
30
25
20
15
10
5
2
4
6
8
10
20
30
Background Wind (Km hr^{-1})

Figure 19

Figure 20

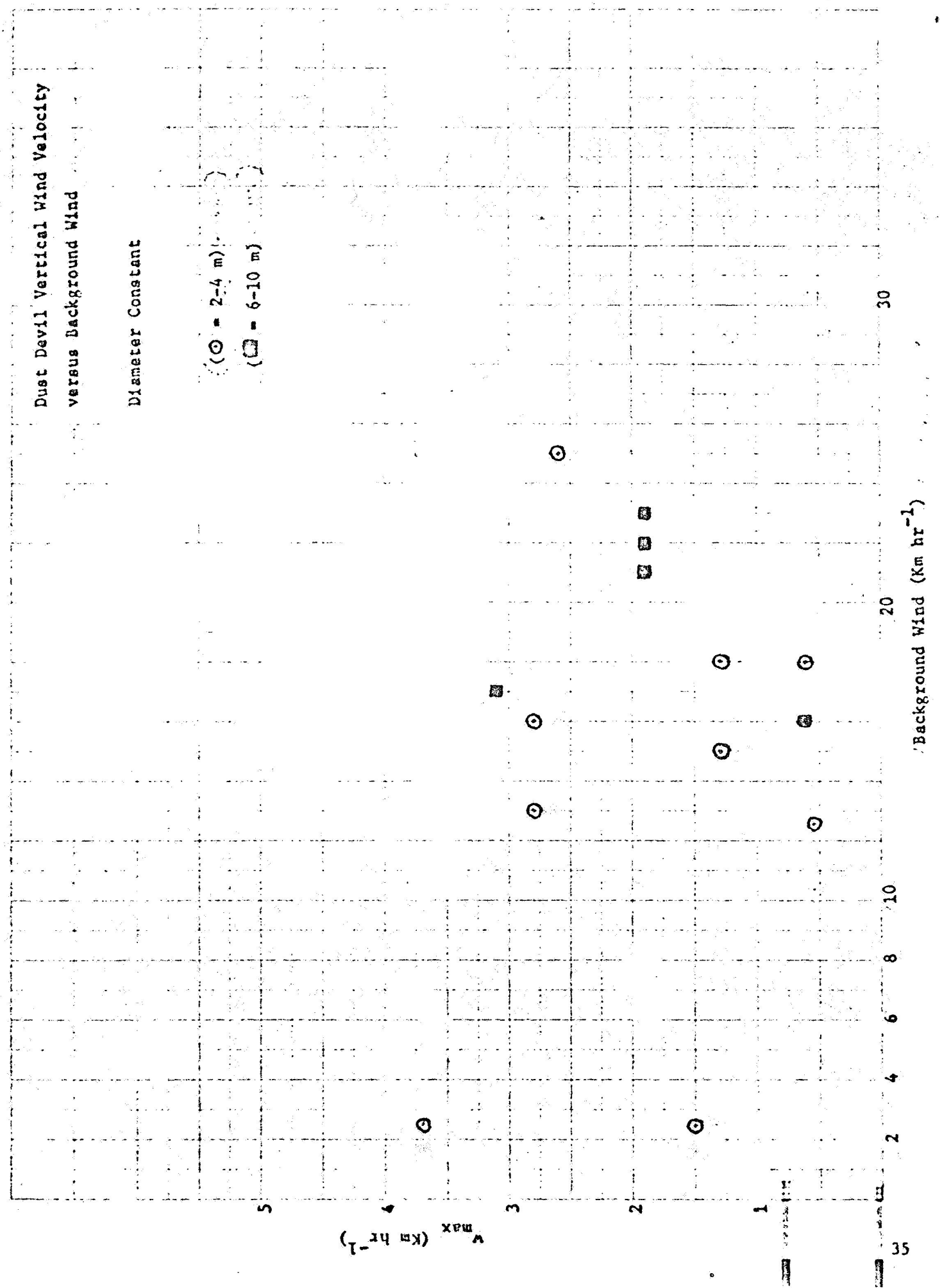
Dust Devil Vertical Wind Velocity
versus Background Wind
Diameter Constant
(⊙ = 2-4 m)
(□ = 6-10 m)
V_{max} (Km hr^{-1})
Background Wind (Km hr^{-1})
1
2
3
4
5
10
20
30

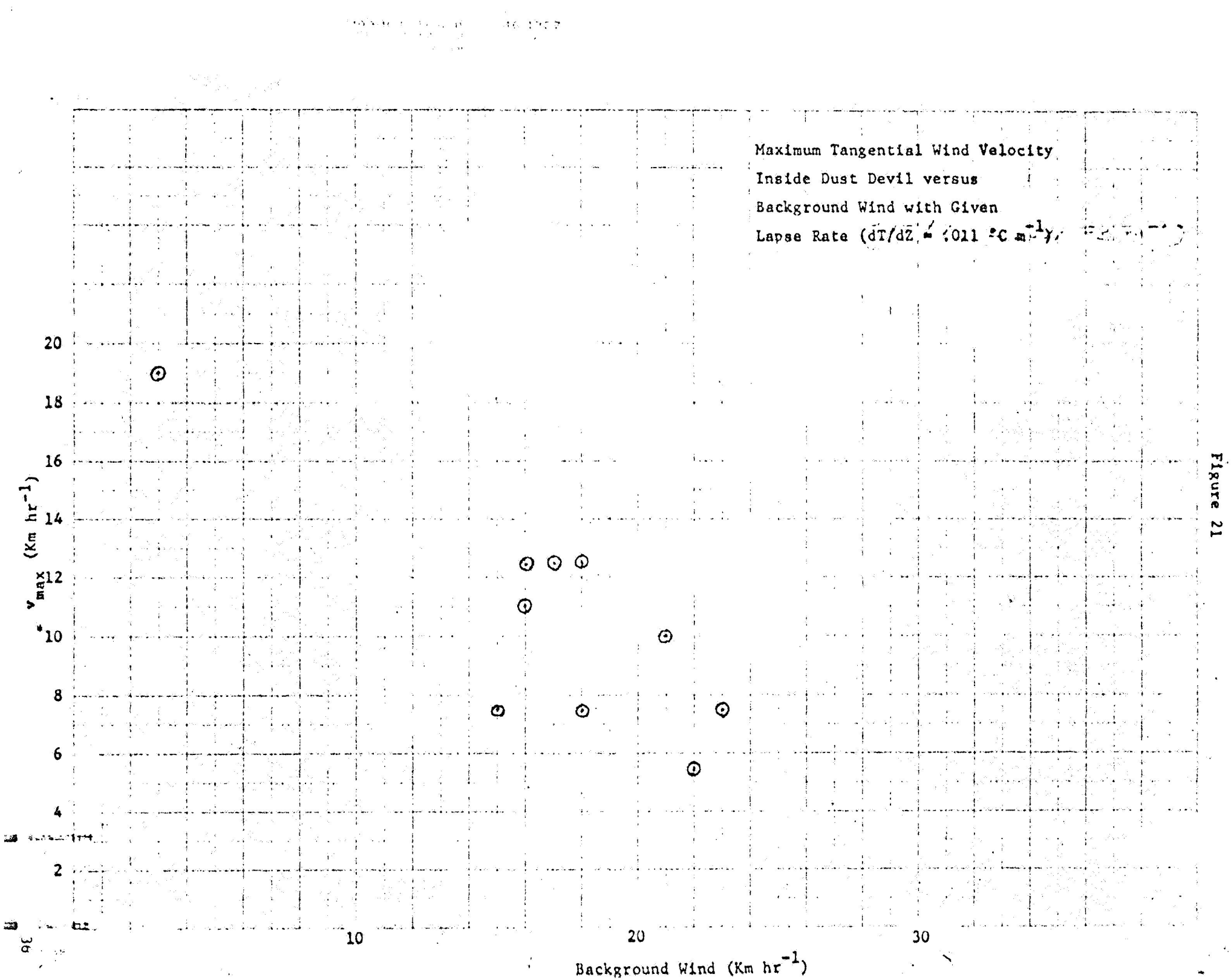
Maximum Tangential Wind Velocity
Inside Dust Devil versus
Background Wind with Given
Lapse Rate (dT/dZ = .011 °C m⁻¹)
v_{max} (Km hr^{-1})
20
18
16
14
12
10
8
6
4
2
10
20
30
Background Wind (Km hr^{-1})

Figure 21

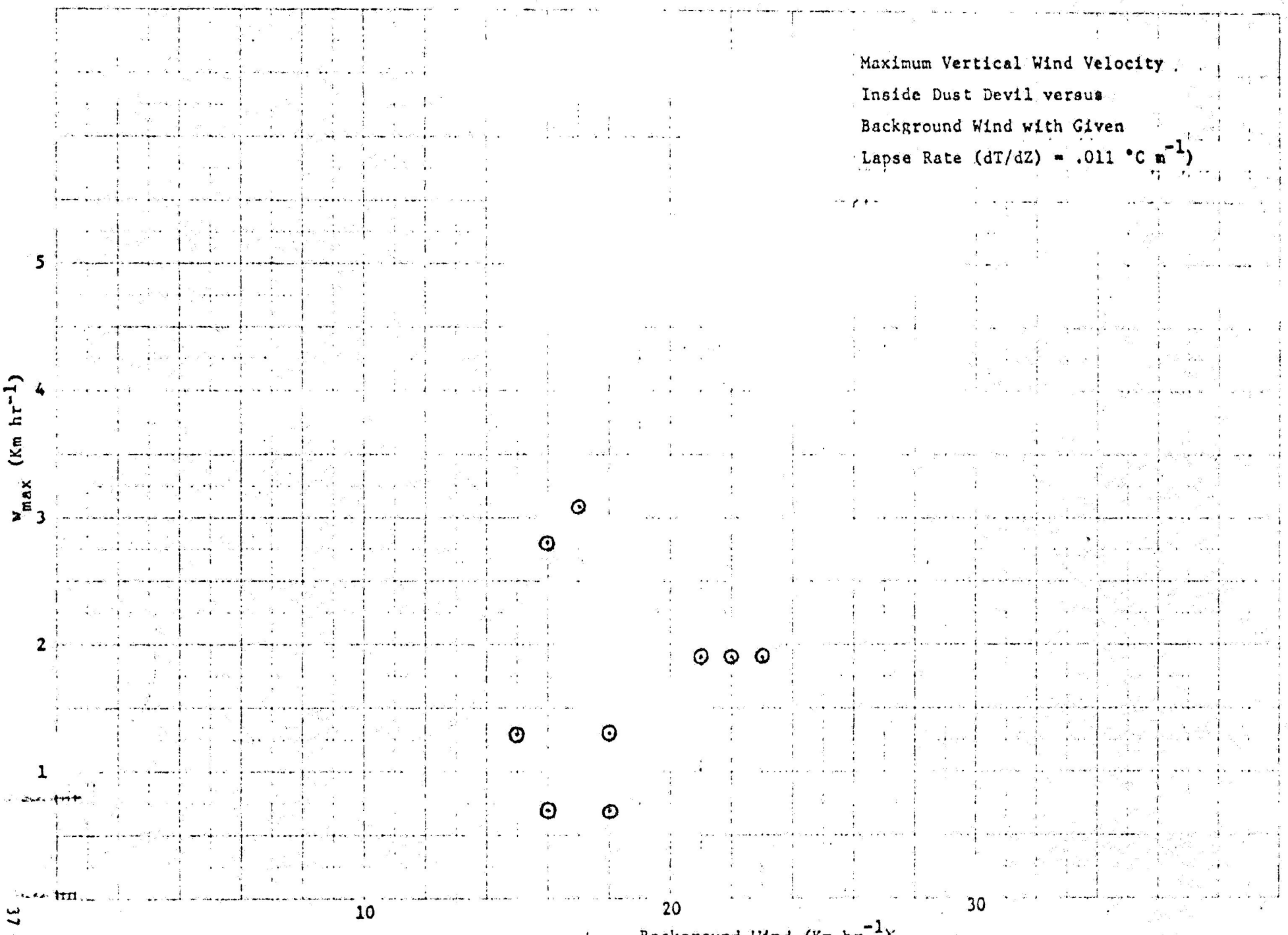
Maximum Vertical Wind Velocity
Inside Dust Devil versus
Background Wind with Given
Lapse Rate (dT/dZ) = .011 °C m^{-1})
w_{max} (Km hr^{-1})
5
4
3
2
1
10
20
30
Background Wind (Km hr^{-1})

Figure 22

TABLE 2

Dependence of Dust Devil Wind Velocities

on Lapse Rate in Superadiabatic Layer

for Given Diameter

$\frac{dT/dZ}{\text{Lapse Rate } (^\circ C\ m^{-1})}$ $\frac{(T_{.3} - T_h) - \Delta Ts}{h - h_s}$	v_{max} (Ave) (km hr^{-1})	w_{max} (Ave) (km hr^{-1})
1. Diameter <1 m		
.014	3.7 (2)*	1.5 (2)
.016	4.6	1.1
.017	4.3 (2)	1.1 (2)
2. Diameter = 1 m		
.013	4.6	3.3
.014	7.5 (3)	3.6 (3)
.016	6.5 (2)	6.0 (2)
3. Diameter = 2-3 m		
.011	7.5	< 0.7
.012	9 (3)	1.3 (3)
.013	4.6	2.6
.014	9.7 (2)	2.6 (2)
.016	9.2	6.9
4. Diameter = 3-5 m		
.011	9.2 (5)	1.5 (5)
.012	10 (2)	2.0 (2)
.013	4.6	2.6
.014	9.7 (2)	2.6 (2)
5. Diameter = 5-10 m		
.011	8.9 (4)	1.6 (4)
.018	11	No measurement
.020	32	No measurement
6. Diameter >10 m		
.011	19	No measurement
.012	20	1.9
.013	25	No measurement
.019	20	2.2

* Values in brackets indicate number of samples

diameters less than one meter, w_{max} increases as dT/dZ increases, for a given diameter. Conversely, there is no trend evident for v_{max}, except possibly for the larger diameters. There are two likely reasons why the w_{max} correlation fails at the smallest diameters. First, it is difficult to penetrate these small devils properly and the instrument and operator have a significant disruptive effect upon them. Second, these smallest of devils are most sensitive to local eddies and other perturbative influences.

The finding that w_{max} increases as dT/dZ increases provides strong evidence for the role of bouyancy forces in dust devil generation and provides data for determining the functional dependence. That v_{max} is not so correlated provides indirect evidence that v_{max} is determined primarily by the atmospheric angular momentum available (vorticity could not be solely responsible since the surface area from which angular momentum can be concentrated will depend upon the rate at which mass is transferred upward.

Dust Devil Diameter

Inspection of Table 2 shows that v_{max} has a decided tendency to increase as dust devil diameter increases. This is in accord with the conclusion reached in the previous report. Conversely, w_{max} shows no such tendency. This provides further evidence that w_{max} is dependent upon bouyancy forces which themselves are independent of the areal extent of the updraft.

3.2.4 Atmospheric Vorticity Correlation with Dust Devil Rotation

The rotation census and vorticity meter data are shown in Figure 16-18. The vertical scale on each is the vorticity meter two minute trends and the horizontal axis is time. Up represents a counterclockwise trend (filled in sections); down represents a clockwise trend (lined sections). The scale shown for vorticity (0-3) has the following meaning: '1' corresponds to revolutions per minute of between 0.1 and 0.5; '2', between 0.5 and 1.0; and '3', greater than 1.0. Dust devil counts are plotted above and below each vorticity plot, those above representing dust devils with counterclockwise rotation, those below rotating clockwise. Those shown as dots were over 100 meters from the station, those shown as crosses were within 100 meters. Those dust devils circled rotated in a sense opposite to the vorticity meter. In almost all cases analyzed thus far these "anamolous" dust devils were quite small (< 1 meter) and short lived, and/or occurred during a period where very little vorticity was present. This would indicate that small, local gusts were responsible.

The rotation census data indicate rather strongly that the direction of dust devil rotation is correlated to background vorticity. Correlation checks were made by taking those dust devils occurring during times of significant trends of the vorticity meter. The results of this are as follows:

Date	Correlation Coefficient	
	All	Near
6-13	+ 0.45	+ 0.80
6-26	+ 0.39	+ 0.22
6-27	+ 0.41	+ 0.52

Note that these were obtained using all dust devils. As noted above, many of the "anamolous" devils were very small and short lived. Removal of these from the counts would significantly increase the correlation coefficients. This is particularly so for 6-26 where several occurred at the station and could have been formed through vorticity produced in the air stream by station equipment. More detailed studies are underway, but are not far enough along to be included in this report. These preliminary studies, however, indicate the role played by background vorticity in dust devil generation.

3.2.5 Atmospheric Vorticity Correlation with Dust Devil Frequency

It was noted in Section 3.2.2 that dust devil frequency was correlated with ΔT_s. The vorticity data indicate a possible correlation with vorticity magnitude also. On 6-13 very few dust devils appeared. At the same time, vorticity magnitude rarely exceeded a few tenths of a revolution per minute. Many more dust devils appeared on 6-26 and the greatest number appeared on 6-27. Vorticity magnitude increased correspondingly. This correlation can be seen in a general manner in Figure 16-18.

4.1 Dust Devil Mechanisms

The results of particular interest to date are:

a) Dust devil frequency appears to be a function of ΔT_s and vorticity.

b) The maximum vertical velocity appears to be a function of $\partial T/\partial Z$ and independent of dust devil diameter.

c) The maximum tangential wind velocity appears to be independent of $\partial T/\partial Z$.

d) Dust devil rotation appears to correlate with background vorticity.

e) For a given diameter, the maximum tangential velocity appears to decrease as background wind velocity increases.

Finding (a) provides strong empirical support for the theoretical arguments presented in the previous report which concluded that the necessary conditions for dust devil formation are an unstable thermal stratification and sufficient environmental angular momentum available for the spin-up process. It is interesting to note that dust devil frequency is more dependent on the instability near the ground than on that of the whole unstable layer. This implies that the triggering mechanism must extend sufficiently close to the ground to tap this energy, and that dust devil formation and maintenance requires greater buoyant energy than the more prevalent plume or bubble convective modes (these other modes also do not require environmental angular momentum). This implication is enhanced by the fact that as the vortical motion increases, the radial inflow is increasingly confined to the lowest levels so that the updraft air supply is derived from the very buoyant air near the ground.

Finding (b) indicates that the maximum vertical velocity attainable in the core will depend on the vertically integrated buoyancy, which will be determined principally by the thick superadiabatic layer overlying the thin highly superadiabatic layer adjacent to the surface.

The apparent independence of v_{max} and dT/dZ [Finding (c)] would, in view of Finding (b), indicate an independence of v_{max} on w_{max}. If so, this would be contrary to the hypothesis that updraft produces vorticity convergence which produces the spin-up. However, since the updraft in a well developed dust devil is confined to a small area, the increased vertical mass flux associated with an increase in w requires only a relatively small increase in inflow rate and extent due to the much larger source area. Thus, v_{max} is expected to be much less a function of dT/dZ than is w_{max}. Unfortunately, the scatter in the data is at present too large to detect any functional dependence of v_{max} on dT/dZ.

The correlation between observed sense of rotation of dust devils and the background vorticity [Finding (d)] as well as adding more support to the previous comments, gives some indication of the scale of ζ_e and its source. The most obvious feature of the correlation is that on the 13th and 27th the correlations are higher than on the 26th and they improve if one considers only the near dust devils. On the 26th the correlation is worse for the near dust devils. Although the sample is small, this implies that on windy days the scale of ζ_e is larger than on calm days. The dust devil occurrences plotted in Figs. 1, 4, 7, 10, and 13 indicate the tendency for dust devils to occur in groups. Also, there is a tendency for these dust devil groups to occur with increases in the wind speed i.e. on the leading edges of "gusts". (This tendency is shown most clearly on the original wind velocity recordings.) These findings taken together strongly suggest that ζ_e is due to the shear of the horizontal wind in the boundary of "gust" elements. The sources of these gust elements probably range from those produced by local convection cells, to terrain effects, to large mesoscale phenomena such as the sea breeze front, with the importance of each dependent on the mean background wind.

Finding (e) is interpreted as a reflection of the role of friction. When the background wind is low, the amount of turbulent momentum exchange is small and confined to the very lowest layers. In such an environment the dissipation of angular momentum during the convergence process is minimal so one would expect a higher tangential velocity (for a given dust devil diameter). As the background wind increases, the depth and magnitude of turbulent dissipation of momentum increases in general and this is reflected in the loss of angular momentum for the dust devil.

4.2 Computer Calculations of Temperature Lapse Rates on Mars

Determination of the temperature lapse rates that could occur in the lower Martian atmosphere is important to this program since these lapse rates play an important role in determining whether or not dust devils could occur on Mars. This section describes a model for computing the diurnal variation of temperature and presents some of the results obtained to date.

Atmospheric temperature changes are assumed to be due primarily to turbulent heat transfer processes in the vertical direction (radiative transfer and advection have been ignored for the present calculations). At the surface a balance of net solar radiation, turbulent heat transfer, and conductive heat exchange with the subsurface layer is assumed. Temperature changes in the subsurface layer are due to molecular conduction of heat, the thermal diffusivity of the Martian soil being assumed constant with depth and time.

The rate of temperature change at any subsurface level is

$$\frac{\partial T}{\partial t} = K \frac{\partial^2 T}{\partial Z^2} \qquad (1)$$

where Z is the depth in the soil, t is time, T is the temperature of the soil, and K is the thermal conductivity of the soil (assumed constant).

The rate of temperature change in the atmosphere due to turbulent heat transfer is

$$\frac{\partial T'}{\partial t} = \frac{\partial}{\partial Z'}\left[K'(Z')\left(\frac{\partial T'}{\partial Z'} + \Gamma\right)\right] \qquad (2)$$

where T' is the temperature of the atmosphere, Z' is height, $K'(Z')$ is the eddy diffusivity (varied with height), and Γ is the adiabatic lapse rate.

The boundary condition equation is

$$\sigma\epsilon T_o^4 - K_s \frac{\partial T}{\partial Z}\bigg|_{Z=0} - \rho_a C_p K'_s \frac{\partial T'}{\partial Z'}\bigg|_{Z'=0} - (1-A)S_o = 0 \qquad (3)$$

where

σ = Stefan-Boltzman constant

ϵ = emissivity of the surface

K_s = thermal diffusivity (near surface)

K'_s = eddy diffusivity (near surface)

ρ_a = density of air

C_p = heat capacity of air

A = planetary albedo

S_o = solar radiation at surface.

Equations 1-3 are put in finite difference form for solution on the Univac 1108 digital computer. The Dufart-Frankel finite difference approximation is used for Eq. 1 , and an extrapolation of this difference approximation is used for Eq. 2.

The finite difference equations are

$$\frac{T_j - T_j^{m-1}}{2\Delta t} = \frac{K}{(\Delta Z)^2}\left(T_{j+1}^m + T_{j-1}^m - T_j^{m+1} - T_j^{m-1}\right) \qquad (1')$$

and

$$\frac{T'_j - T'^{m-1}_j}{2\Delta t} = \frac{1}{4(\Delta Z')^2}\left(K'_{j+1} - K'_{j-1}\right)\left(T'^m_{j+1} - T'^m_{j-1} + 2\Gamma\Delta Z'\right) \qquad (2')$$

where the subscript refers to distance and the superscript to time. Equations (1') and (2') can be solved for T_j^{m+1} and T'^{m+1}_j respectively to give

$$T_j^{m+1} = \frac{T_j^{m-1} + \frac{2K\Delta t}{(\Delta Z)^2}\left(T_{j+1}^m + T_{j-1}^m - T_m^{m-1}\right)}{1 + \frac{2K\Delta t}{(\Delta Z)^2}} \qquad (1'')$$

$$T_j'^{m+1} = \left\{ T_j^{m-1} + \frac{2\,t}{(\Delta Z')^2} \frac{\left(K'_{j+1} - K'_{j-1}\right)\left(T'^{m}_{j+1} - T'^{m}_{j-1} + 2\Gamma\Delta Z'\right)}{4} \right. \qquad (2'')$$

$$\left. + K_j\left(T'^{m}_{j+1} + T'^{m}_{j-1} - T_j'^{m-1}\right) \right| \frac{1}{1 + \frac{2\Delta t K'_j}{(\Delta Z')^2}}$$

The finite difference analog of Eq. 3 is

$$\sigma\varepsilon T_o^4 + \frac{K_s}{\Delta Z}\left(T_o - T_1\right) + \frac{\rho_a C_p K'_s}{\Delta Z'}\left(T_o - T'_1 - \Gamma\Delta Z'\right) - \left(1-A\right)S_o = 0 \qquad (3')$$

The root, T_o, satisfying (3') is found. This T_o is the surface temperature for the time iteration under consideration. Subsurface and air temperatures are obtained by solving (1'') and (2'') going up and down from the surface.

The numerical values used in the computations are:

$K_s = 2.50\text{x}10^3$ cm^2/sec

$K'_s = \begin{cases} T_o > T_{20\text{ meters}} & 5.2\text{x}10^4 \text{ cm}^2/\text{sec} \\ T_o < T_{20\text{ meters}} & 1\text{x}10^3 \text{ cm}^2/\text{sec} \end{cases}$

$\rho_a = 2.975\text{x}10^{-3}/T$ gm cm^{-3}

$\varepsilon = .85$

$A = .15$

$\Delta Z = 0.2$ cm

$\Delta Z' = 2{,}000$ cm

$\Delta t = 61.5574$ sec = 1 Martian minute

$C_p = (514 + 1.1T)\times10^4$

$\sigma = 5.67\times10^{-5}$ cgs

Solar Constant at Mars = $.626\times10^6$ erg/cm^2 sec

$K = .474\times10^{-4}$ cm^2/sec

$$K'(Z') = \begin{cases} Z' \leq 120 \text{ met.} \begin{cases} \text{unstable air} = 2.2\times10^3\, Z'^{4/3} & \text{cm}^2/\text{sec} \\ \text{stable} = 1.\times10^3 & \text{cm}^2/\text{sec} \end{cases} \\ Z' > 120 \text{ met.} \begin{cases} \text{unstable} = 1.303\times10^6 & \text{cm}^2/\text{sec} \\ \text{stable} = 1.\times10^3 & \text{cm}^2/\text{sec} \end{cases} \end{cases}$$

The space grid utilized is as follows: for the ground, 20 layers of equal thickness (Z), underlain by 8 layers of thickness 100x Z; for the air, starting from the surface, 6 layers of equal thickness (Z') overlain by 5 layers of thickness 10x Z', in turn overlain by 9 layers of thickness 100x Z'. The top 20 layers in the ground were iterated every Martian minute, and the bottom 17 every 120 Martian minutes.

The bottom 6 layers of the atmosphere were 20 meters thick, but because K' is large, they were iterated every 5 Martian seconds. The next 4 layers were iterated every 1 minute (K' is somewhat larger for them) and the top 8 layers every 120 minutes.

Preliminary results of the computer computations of the model are illustrated in Figures 23 through 26. In these initial computations the temperature at time t = 0 is 237°K at 6 A.M. on Mars at all levels. The computer program is then allowed to run for ten days and the data for the tenth day is used. Figures 23a and b depict the change in the 6 a.m. temperature through the ten-day cycle. From the graphs it can be seen that by the ninth day the temperatures are approaching steady state values at all the selected levels.

Figures 24a and b illustrate the diurnal change in temperature at selected levels for the Martian equator at equinox. Inspection of the curves indicates that the temperature changes throughout the day are similar in manner to the changes observed in the earth's atmosphere and ground. In particular, it should be noted that the daytime surface temperature curve agrees fairly well with the Martian temperatures determined by remote sensing techniques (Sinton, W. M. and J. Strong; "Radiometric Observations of Mars," Astrophys. J., 131, 459-464, 1960, and Gifford, F., Jr.; "Surface Temperatures of the Planet Mars: 1962 to 1943," The Study of Planetary Atmospheres, a Final Report, Lowell Obs., Flagstaff, Ariz., 208-249, 1952). In addition, the maximum surface temperature agrees with the maximum temperature obtained by Ohring, et al. (Ohring, George, W. Tang, J. Mariano, and G. Desanto, "Planetary Meteorology," Final report, Contract No. NASw-1574, GCA-TR-68-4-N, 54 pp., May 1968) with their constant K model. However, their minimum temperature is approximately thirty-five degrees colder. On the other hand, the preliminary results of their variable K model give a similar minimum temperature as shown in Figure 24, but a much colder maximum temperature (i.e., 240°K). As can be seen from Figure 24 the dirunal range computed for the Martian surface is 96°K. The observed range on desert surfaces on Earth is approximately 40-50°K. At 20 meters the computed range is 53°K while the observed range on Earth at 20 meters is approximately 5-10°K.

The vertical temperature profiles computed for different times of the day at the equator at equinox are presented in Figures 25a & b. Although the temperature change with height between the surface and 20 meters at the time of the surface maximum (1 p.m.) temperature is -29.8°C, the greatest change with height is -30.2°C at noon. A similar temperature change over deserts on the earth would be approximately 15°K. Actually in the earth's atmosphere most of this temperature

change takes place in the first ten meters with over 70% of the change generally in the first meter above the surface. Ohring, et al. computed an approximate 80°K maximum change in the first km compared to 46°K from Figure 25a. Part of this difference is undoubtedly due to the fact that the Ohring, et al. model has a constant eddy diffusivity while our model has a variable eddy diffusivity with the largest values near the ground, and a function of the stability. These curves illustrate quite well the response of the atmosphere to the eddy flux of heat from the surface.

The variation of the ground and 20 meter temperature with latitude is shown in Figures 26a & b. Figure 26a is for the equinox ($\delta = 0$) while b is for the summer and winter solstice ($\delta \pm 25$). These curves are based on calculations made for latitudes 0°, 30°, 45° and 90°. Although the temperature at the equator and low latitudes agree fairly well with previous estimates the polar regions do not (Michaux, C. M., 1967, NASA SP3030, Handbook of Mars). The summer temperatures are higher and the winter temperatures are lower.

In summary, the results of the calculations made from this analytical model and the finite difference analog give quite reasonable results. Future work will include 1) determining the vertical temperature profiles at different latitudes and seasons; 2) comparing profiles observed over desert conditions with those predicted by the model under similar conditions; and 3) comparing these data with those of others. All three of these objectives will involve varying the eddy diffusivity in accord with emperically derived values and theoretical considerations.

Figure 23a

Atmospheric temperature at Martian equator at 6 AM over a ten-day period.

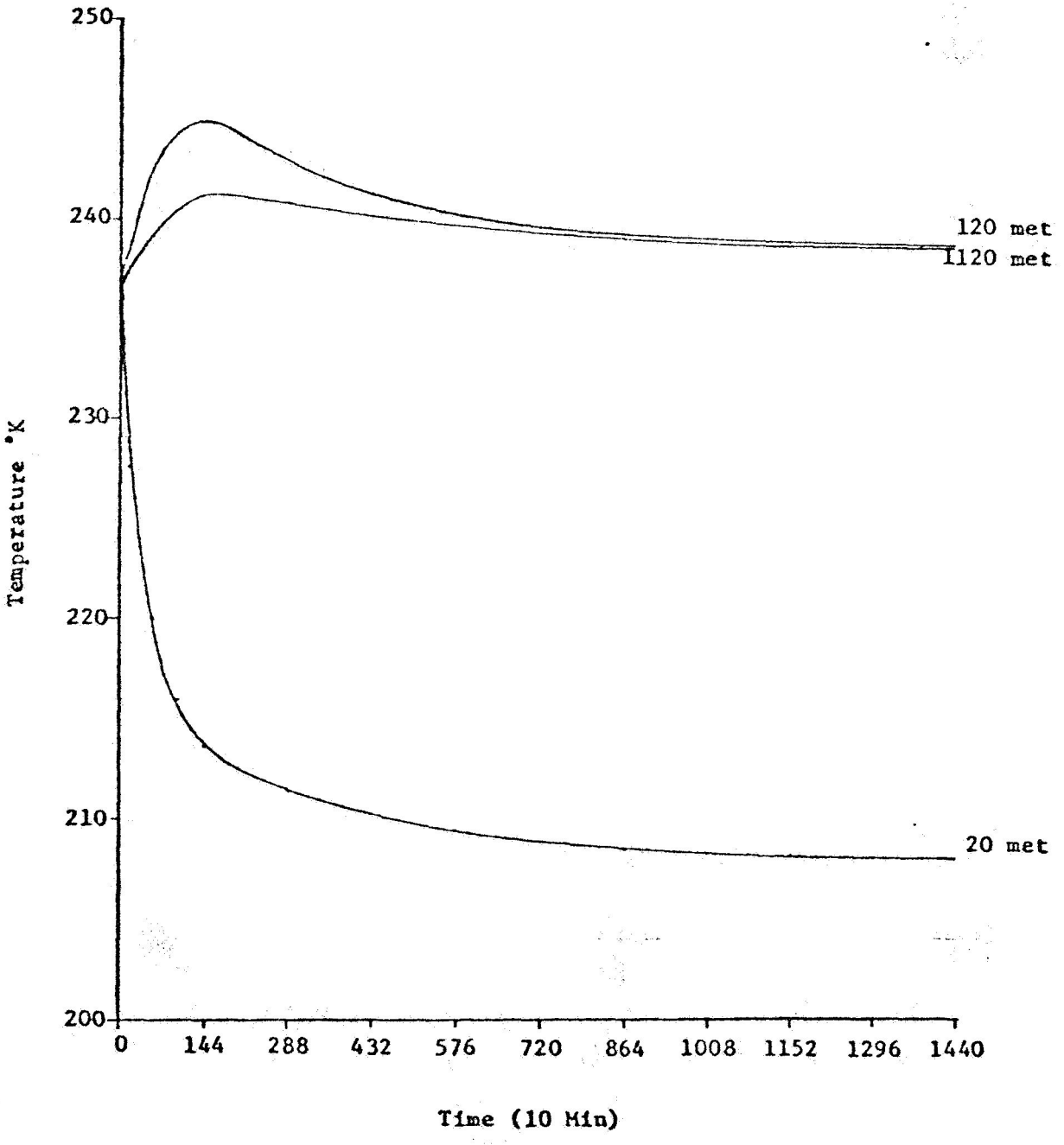

Figure 23b

Surface and interior temperatures at Martian equator at 6 AM over a ten-day period.

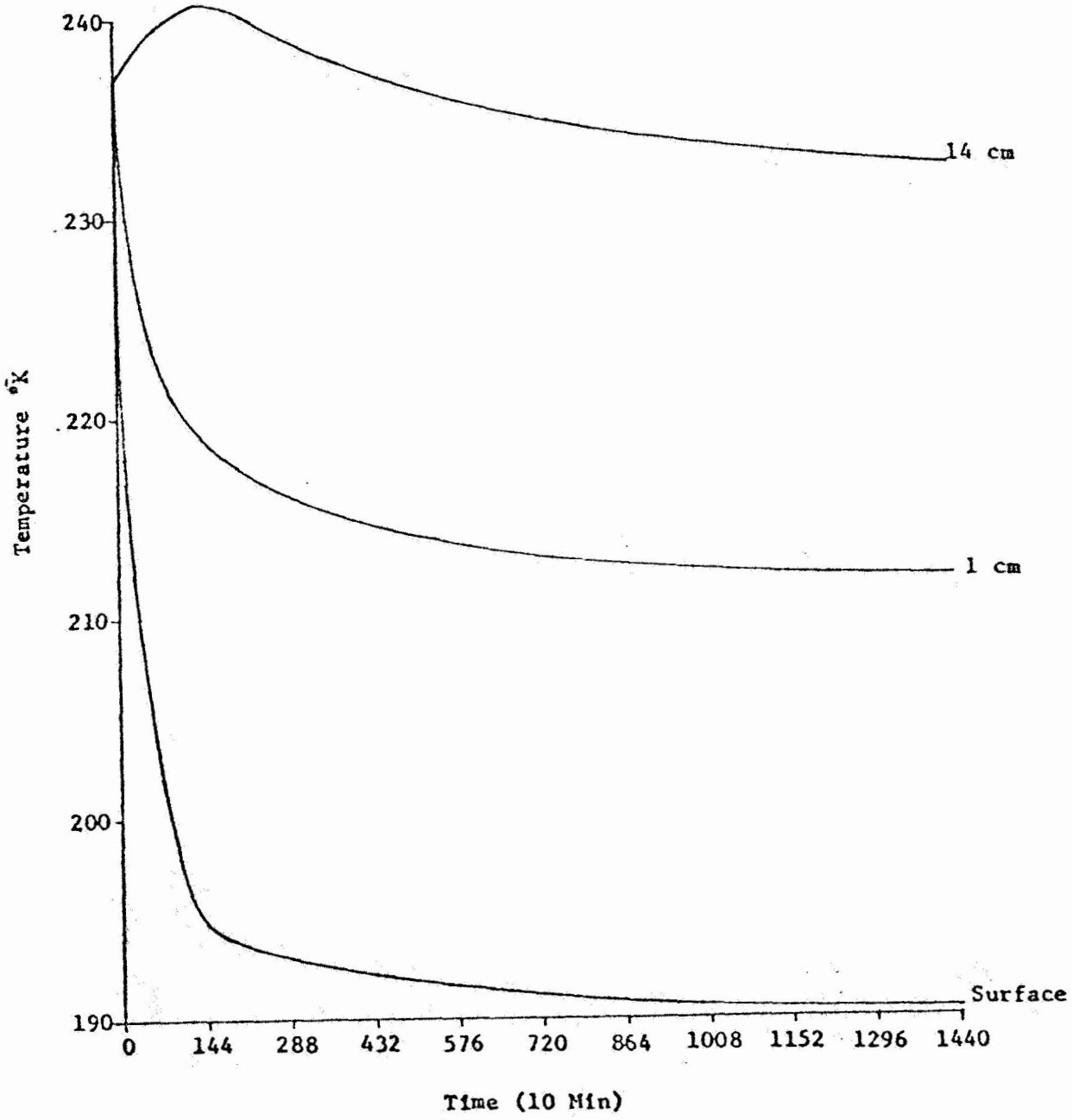

Figure 24a

Computed diurnal variation of the Martian atmospheric temperature at the equator at equinox.

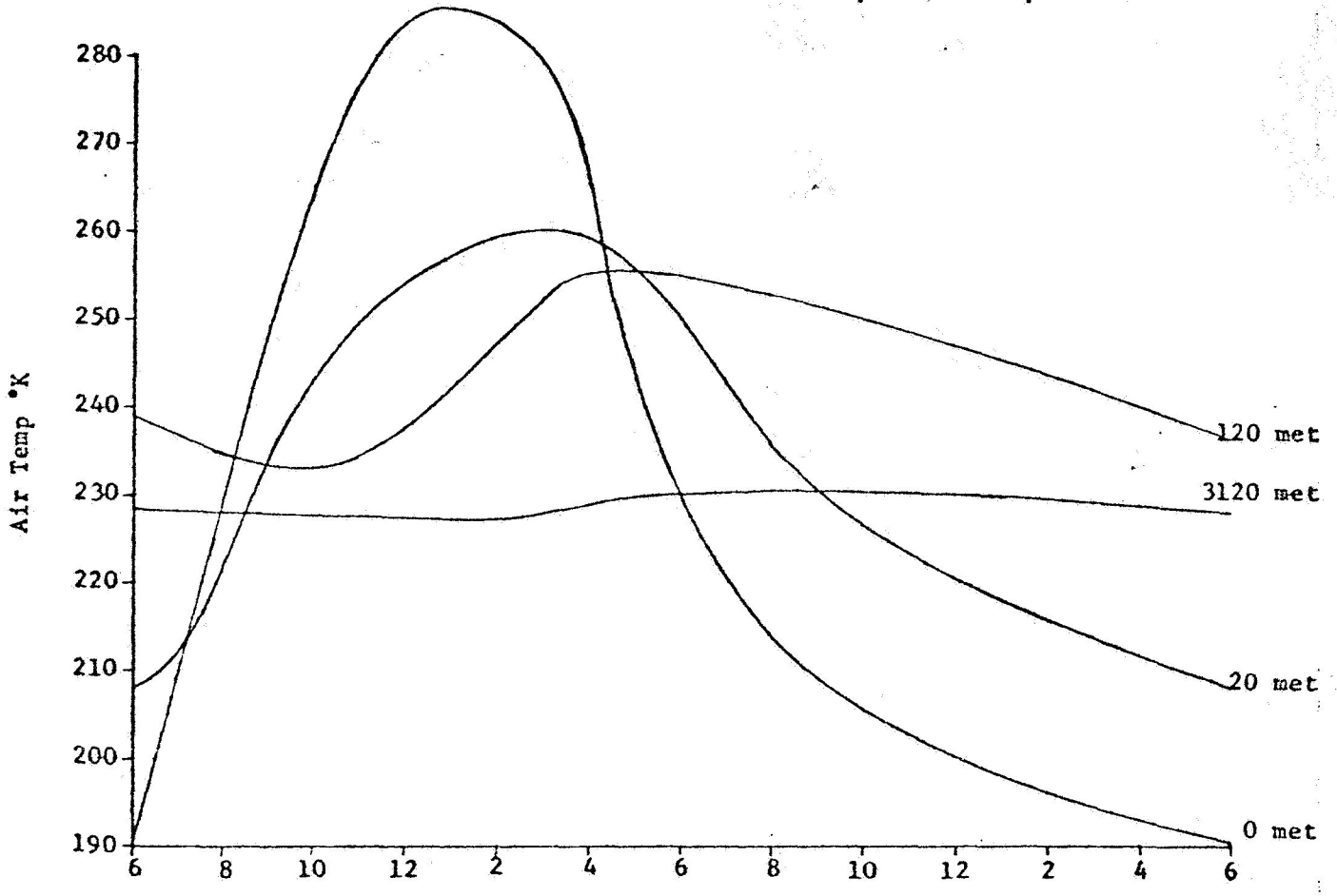

Figure 24b

Computed diurnal variation of interior temperature of Mars at the equator at equinox.

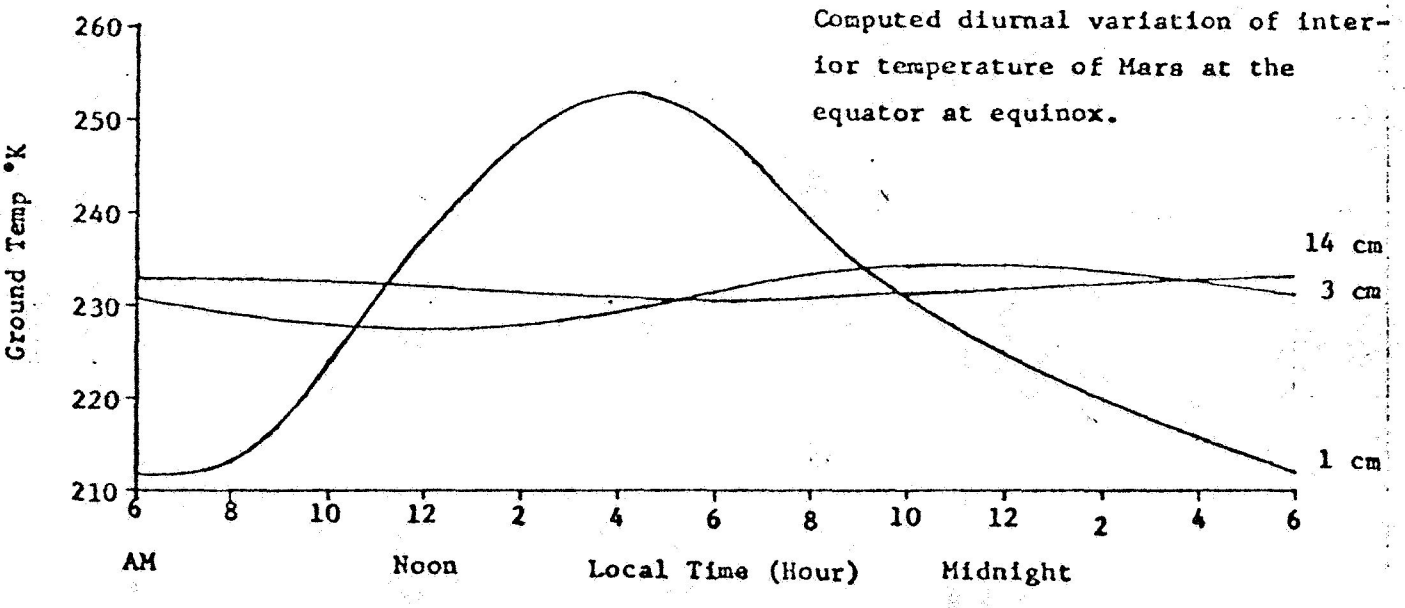

Figure 25a

Computed atmospheric temperature profiles for various times of day at Martian equator at equinox.

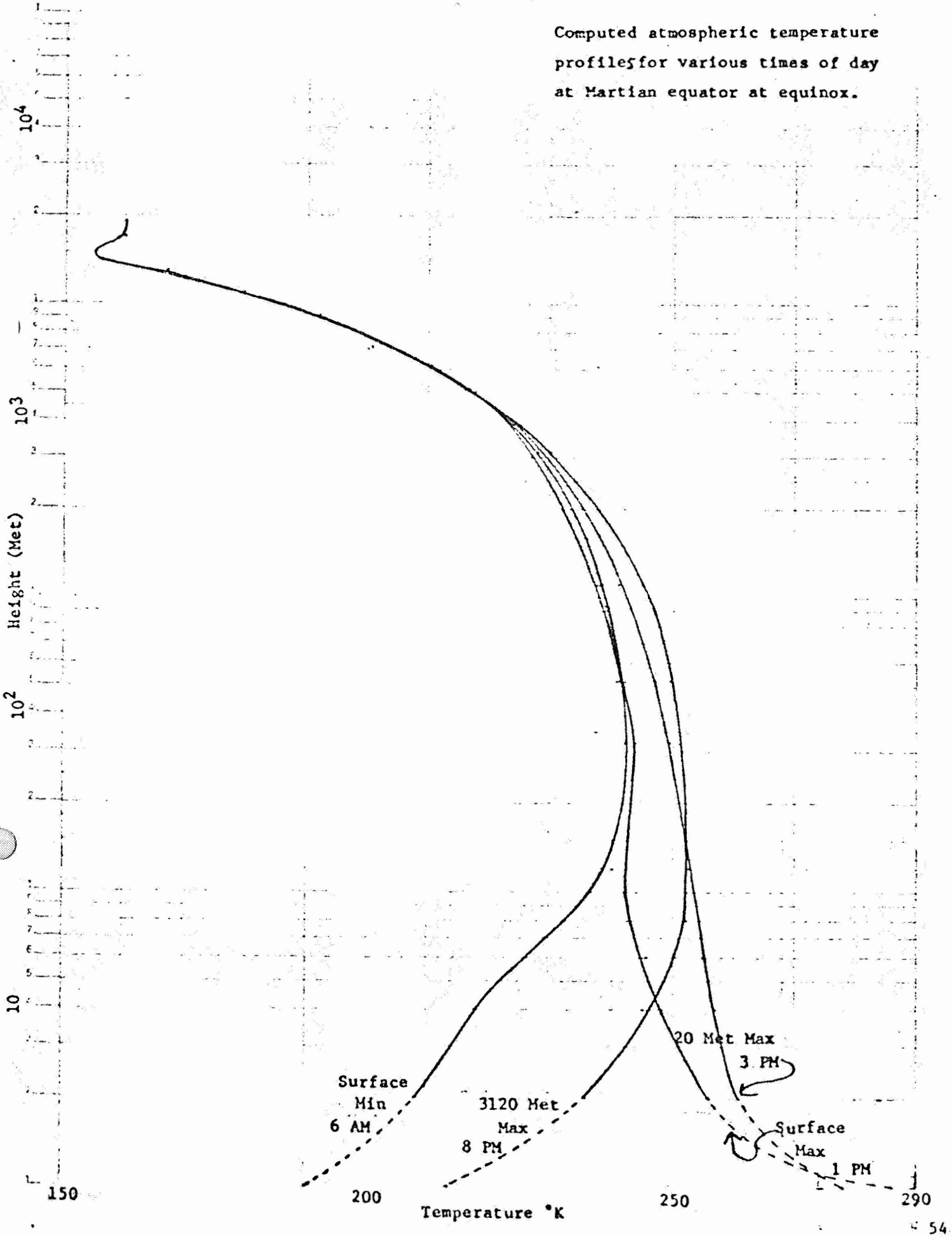

Figure 25b

Computed ground temperature profile for various times of day at Martian equator at equinox.

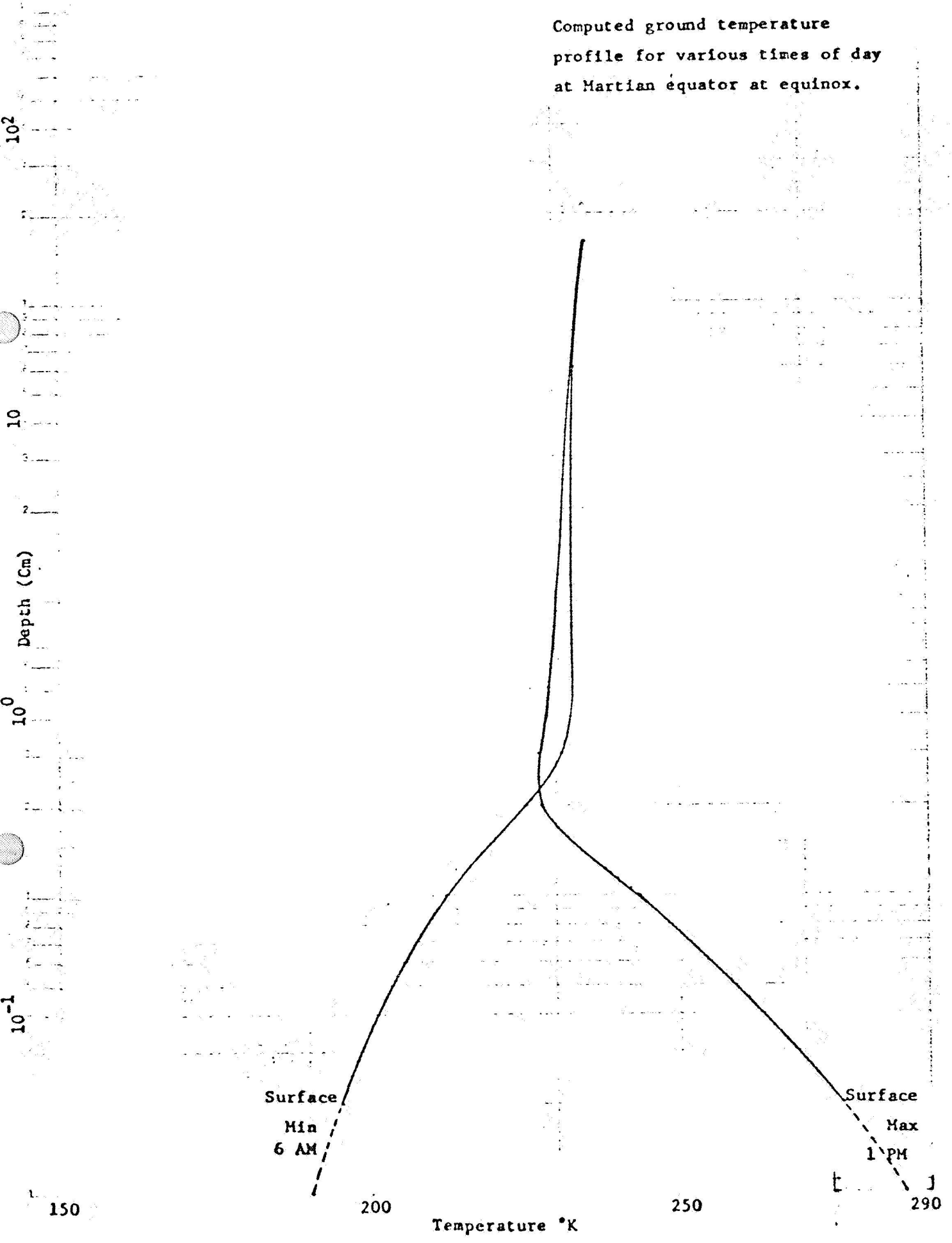

Figure 26a

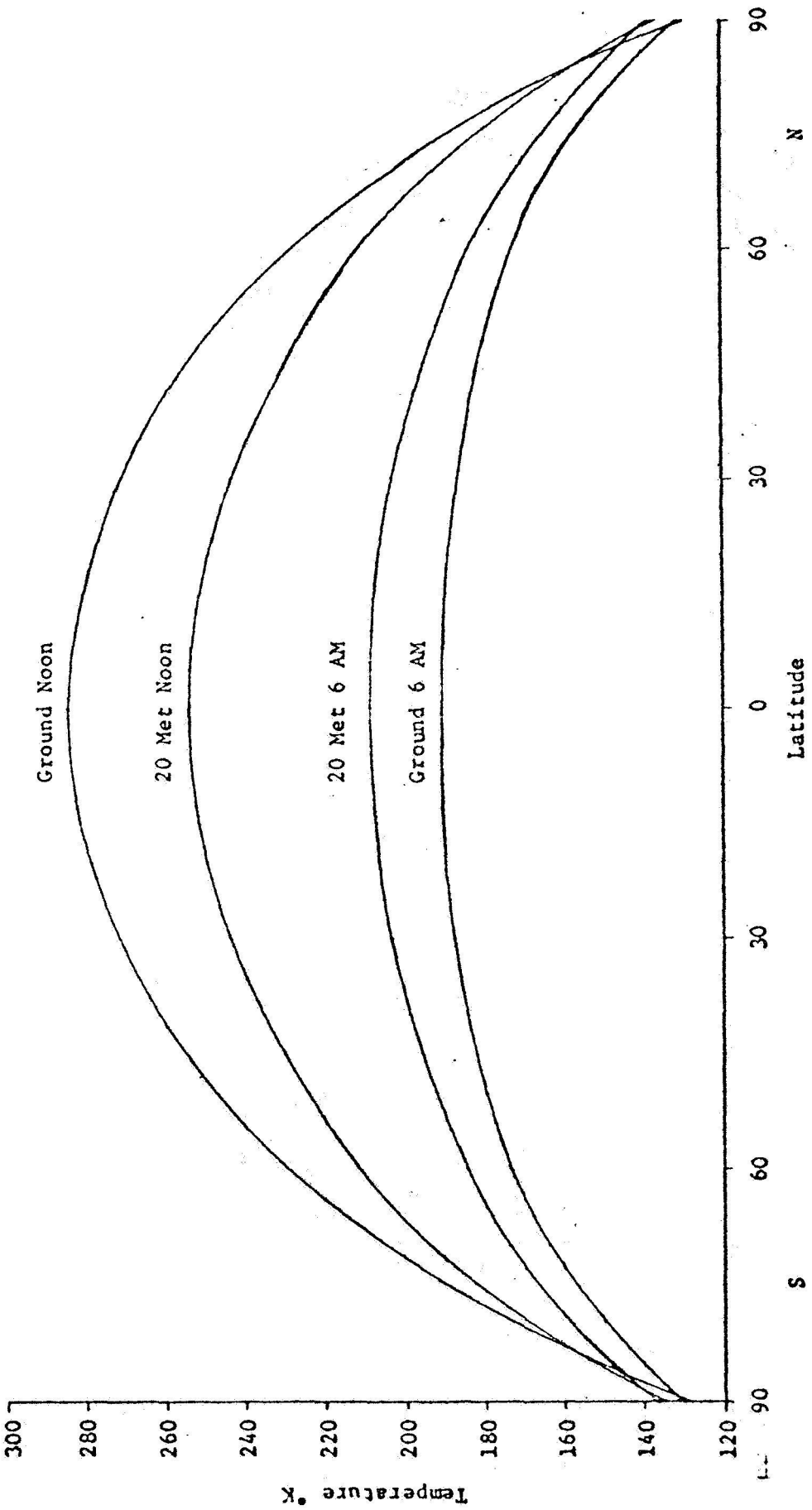

Computed latitudinal variations of the 20 meter and surface temperatures of Mars (solar declination is 0°).

Figure 26b

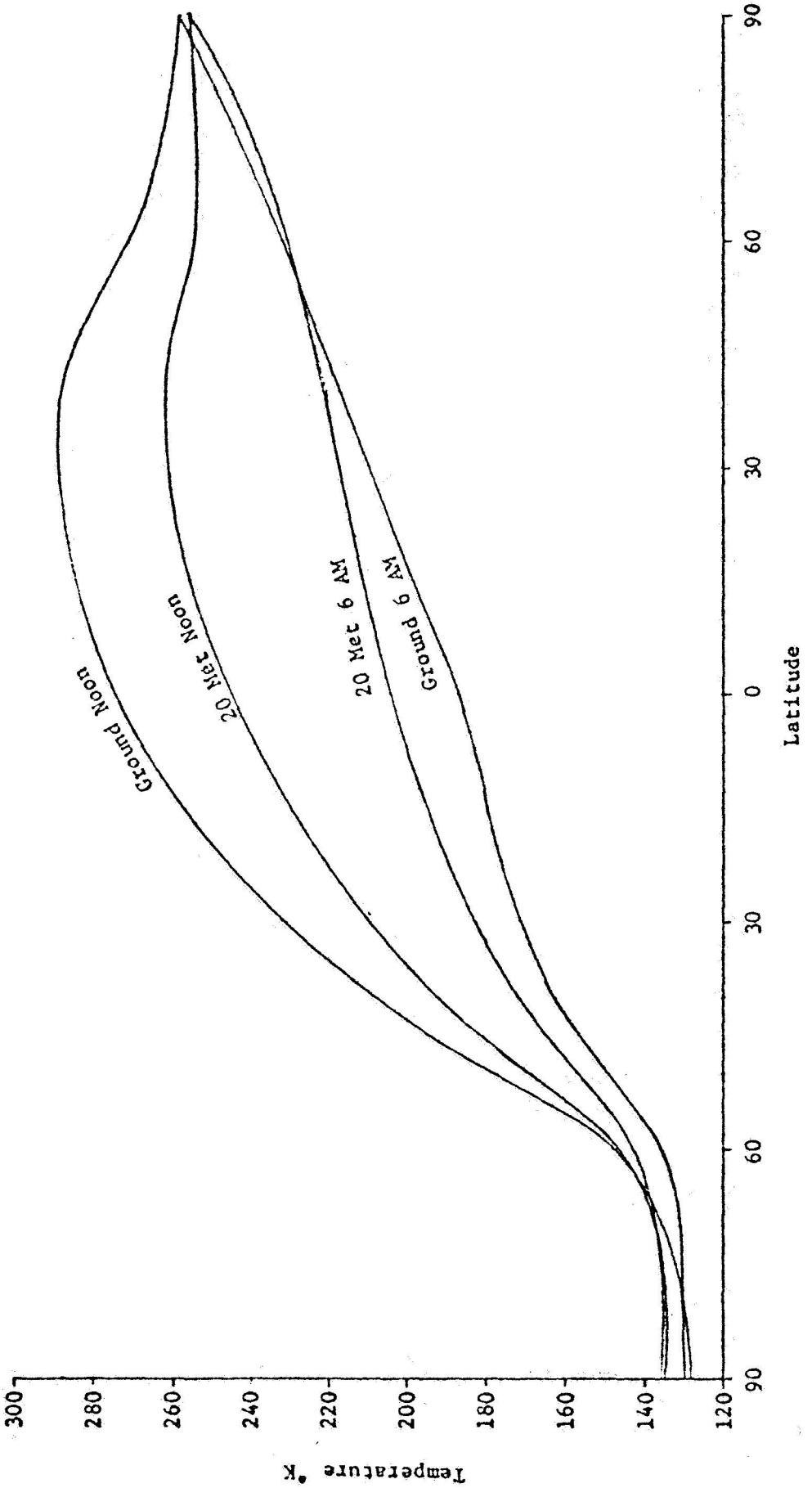

Computed latitudinal variations of the 20 meter and surface temperatures of Mars (solar declination is ± 25°).

APPENDIX A

TEMPERATURE DATA

TEMPERATURE DATA FOR MARCH 28, 1968

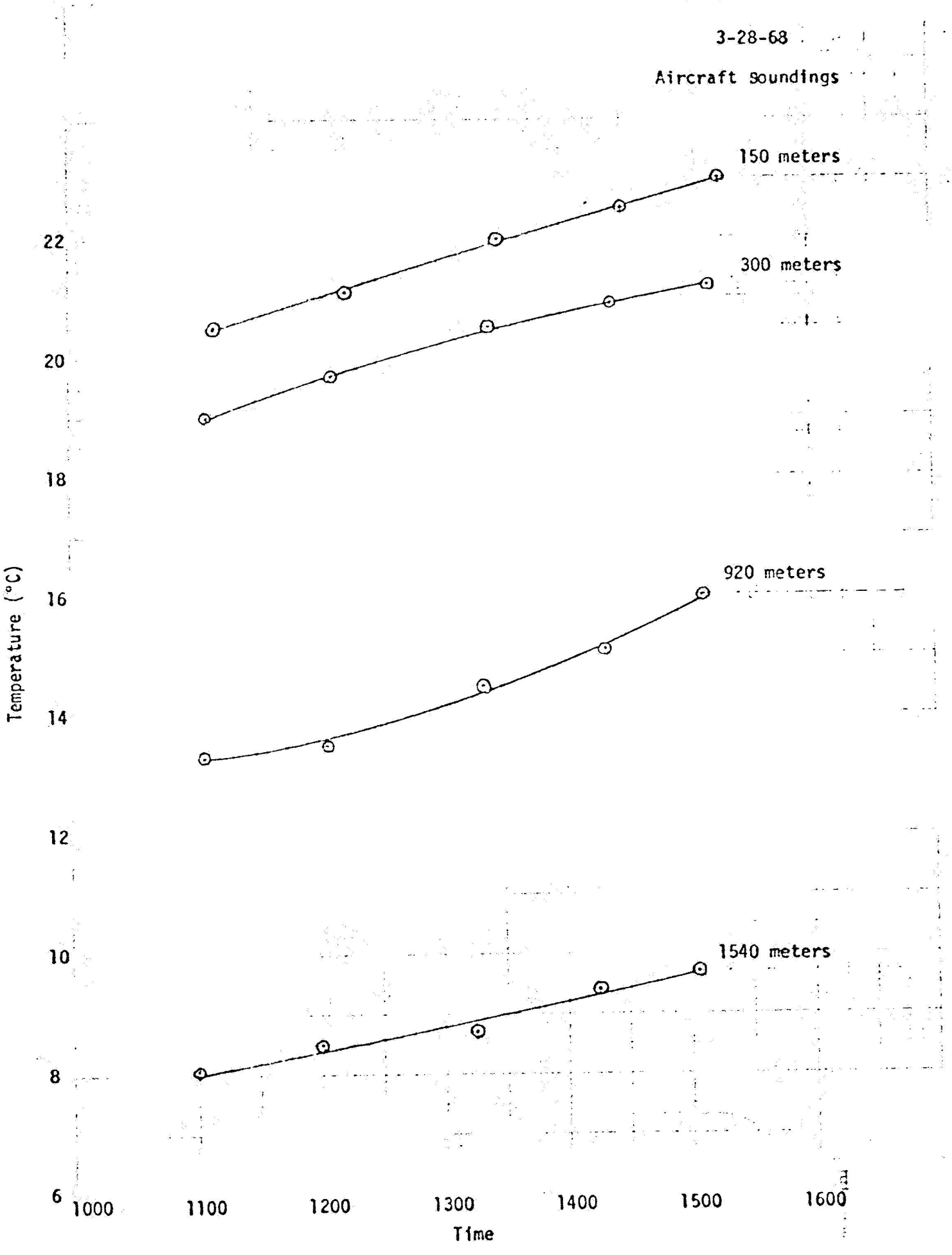
3-28-68
Aircraft Soundings
150 meters
300 meters
920 meters
1540 meters
Temperature (°C)
22
20
18
16
14
12
10
8
6
1000
1100
1200
1300
1400
1500
1600
Time

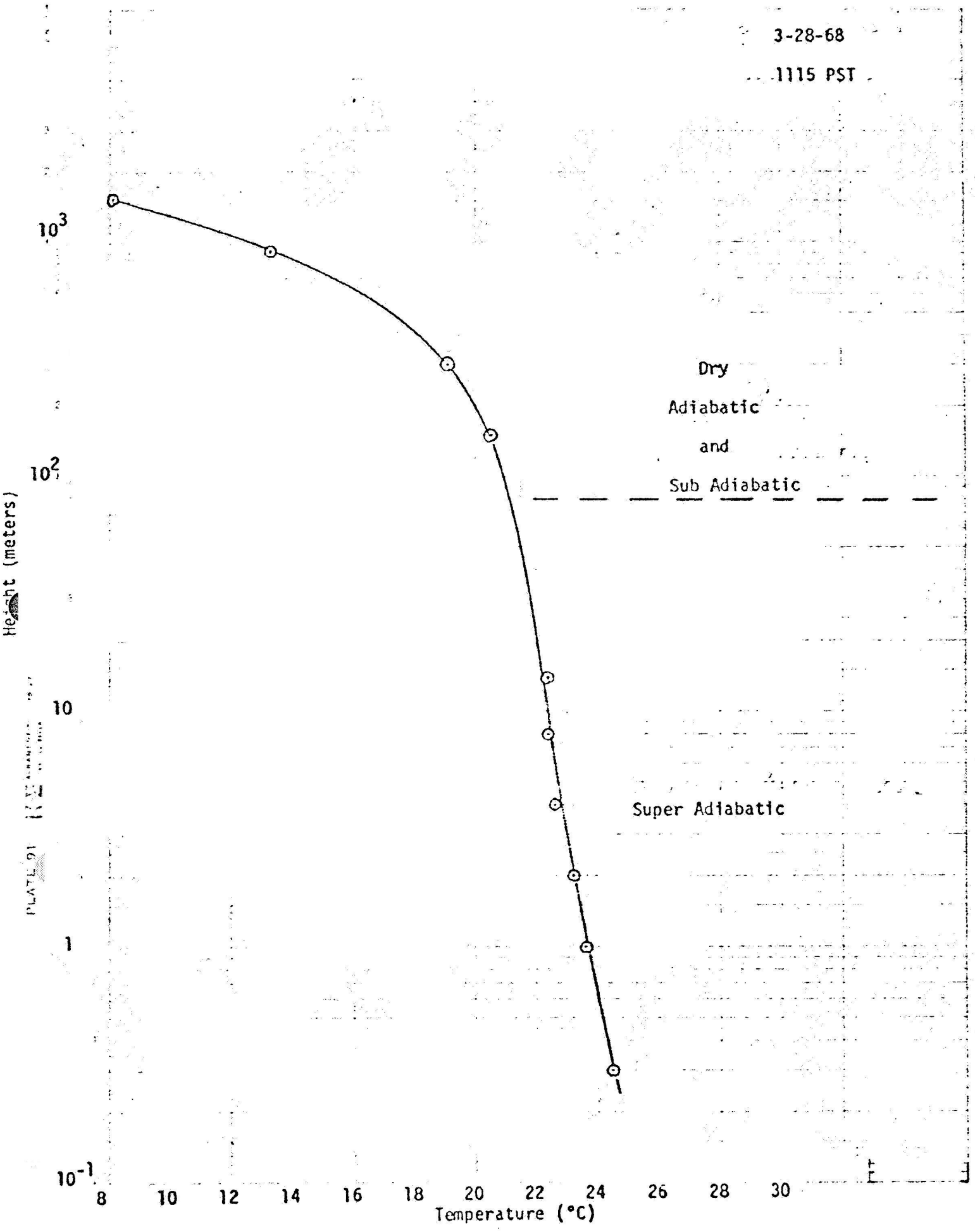
3-28-68
1115 PST
Dry
Adiabatic
and
Sub Adiabatic
Super Adiabatic
Height (meters)
10^3
10^2
10
1
10^{-1}
8
10
12
14
16
18
20
22
24
26
28
30
Temperature (°C)

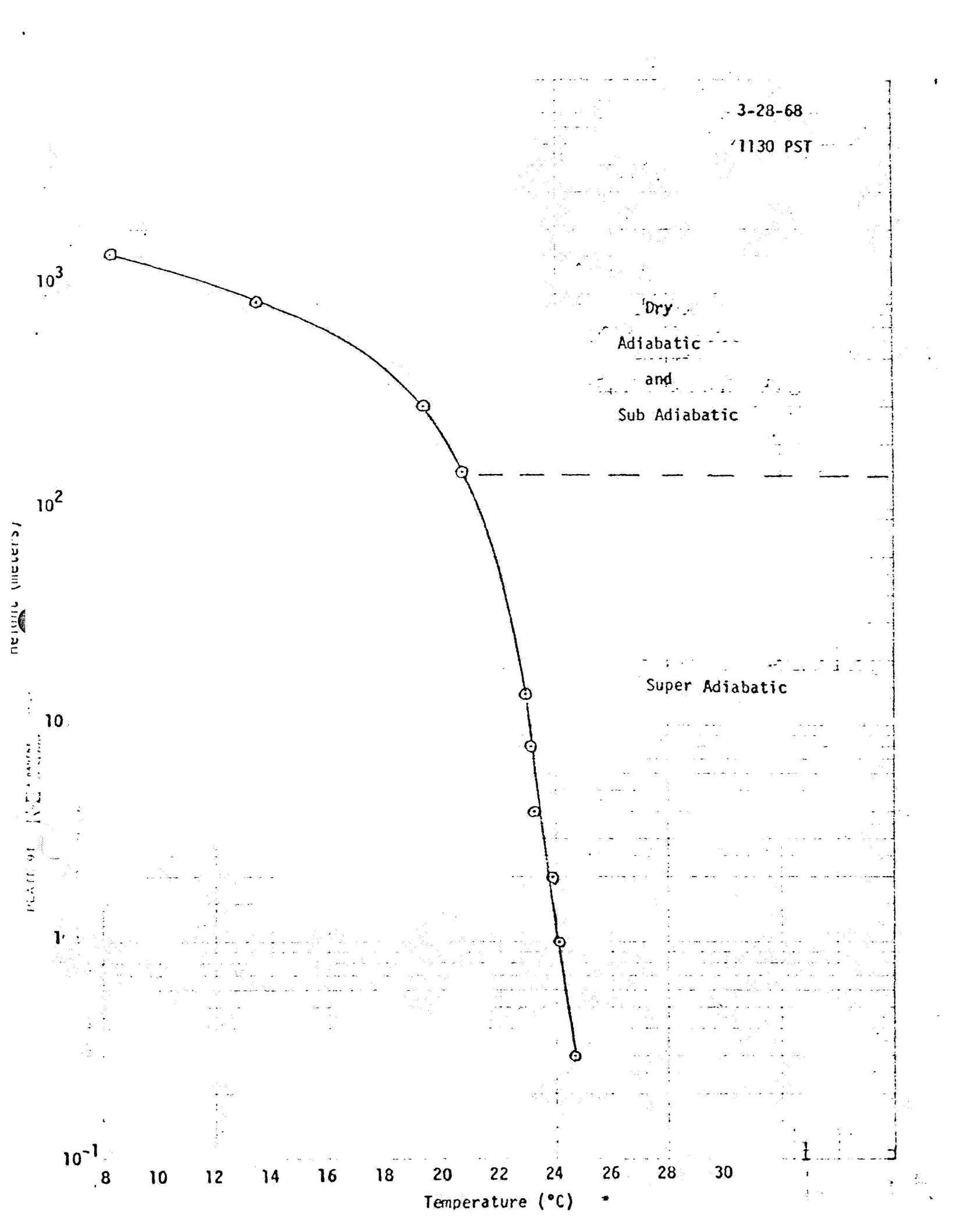
3-28-68
1130 PST
Dry
Adiabatic
and
Sub Adiabatic
Super Adiabatic
10^3
10^2
10
1
10^{-1}
8
10
12
14
16
18
20
22
24
26
28
30
Temperature (°C)

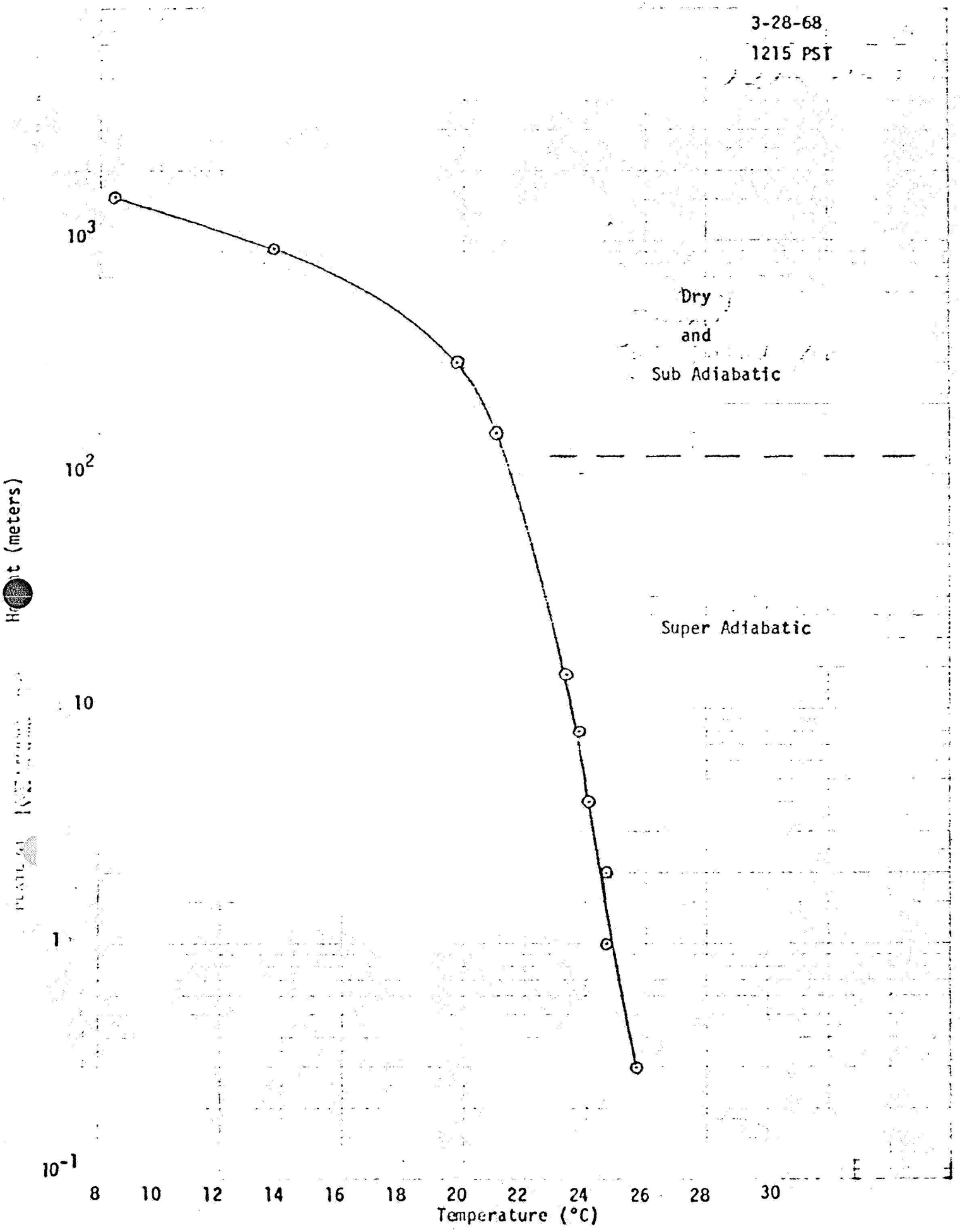
3-28-68
1215 PST
Dry
and
Sub Adiabatic
Super Adiabatic
10^3
10^2
10
1
10^{-1}
Height (meters)
8
10
12
14
16
18
20
22
24
26
28
30
Temperature (°C)

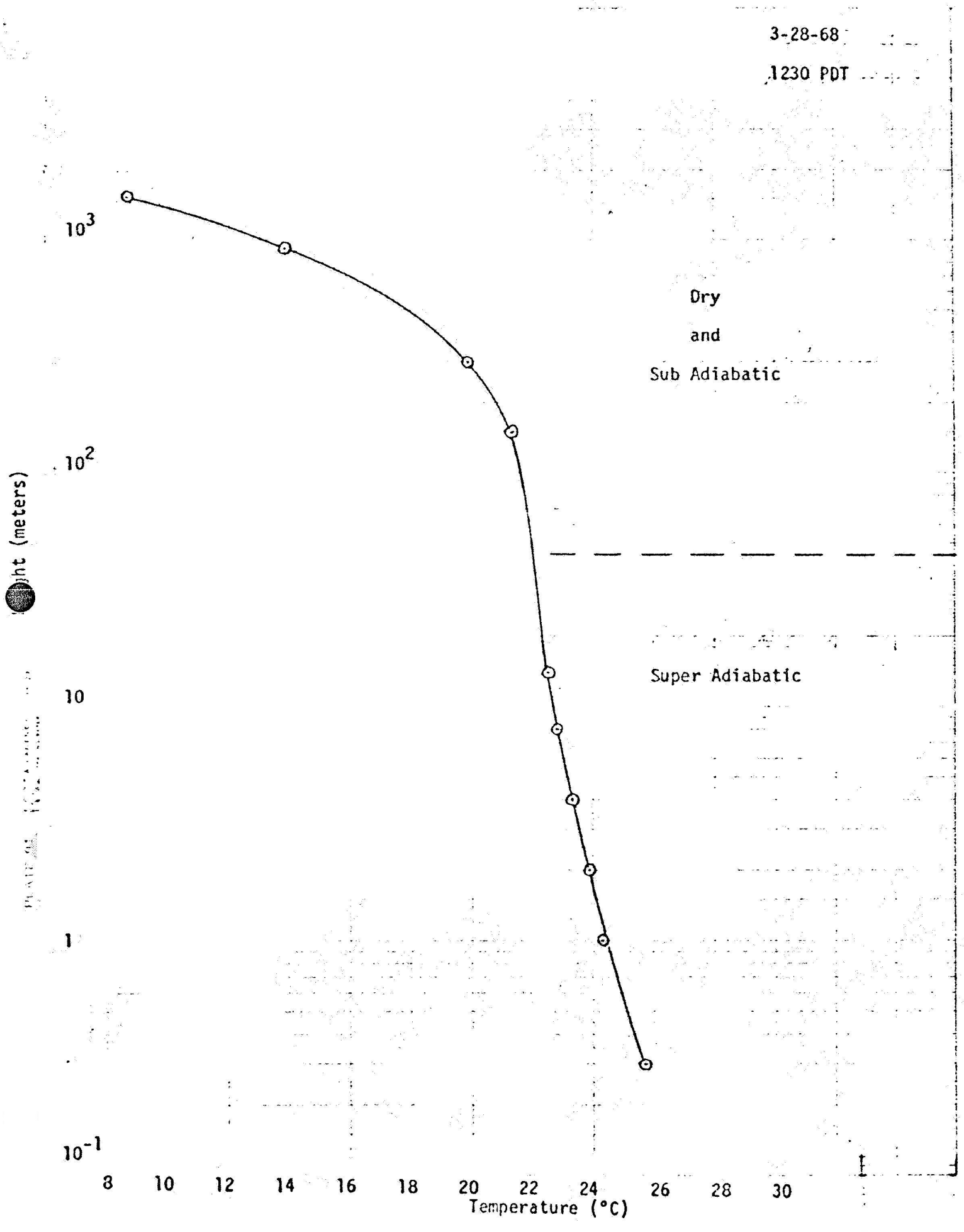
3-28-68
1230 PDT
Dry
and
Sub Adiabatic
Super Adiabatic
10^3
10^2
10
1
10^{-1}
ht (meters)
8
10
12
14
16
18
20
22
24
26
28
30
Temperature (°C)

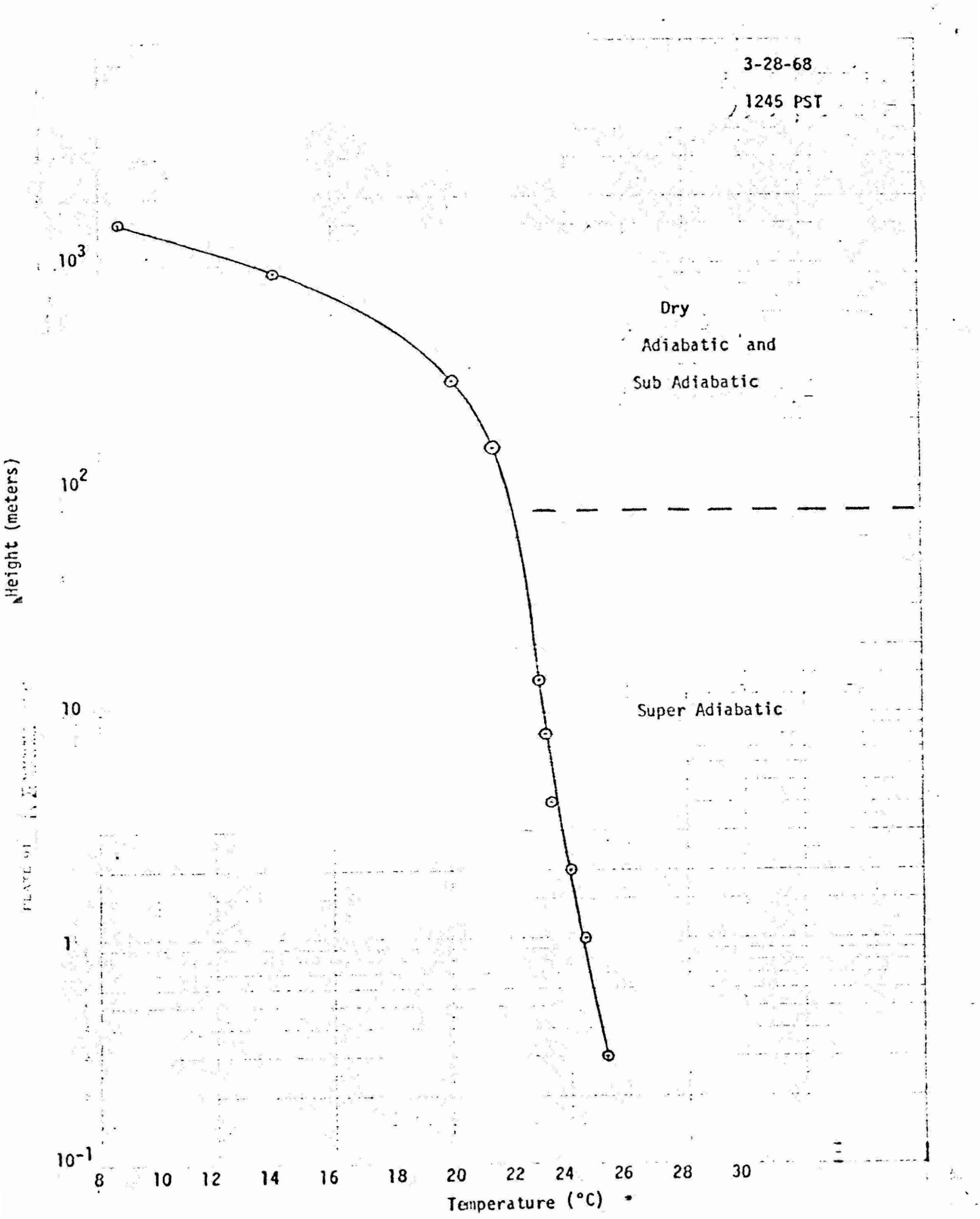
3-28-68
1245 PST
Dry
Adiabatic and
Sub Adiabatic
Super Adiabatic
Height (meters)
10^3
10^2
10
1
10^{-1}
8
10
12
14
16
18
20
22
24
26
28
30
Temperature (°C)

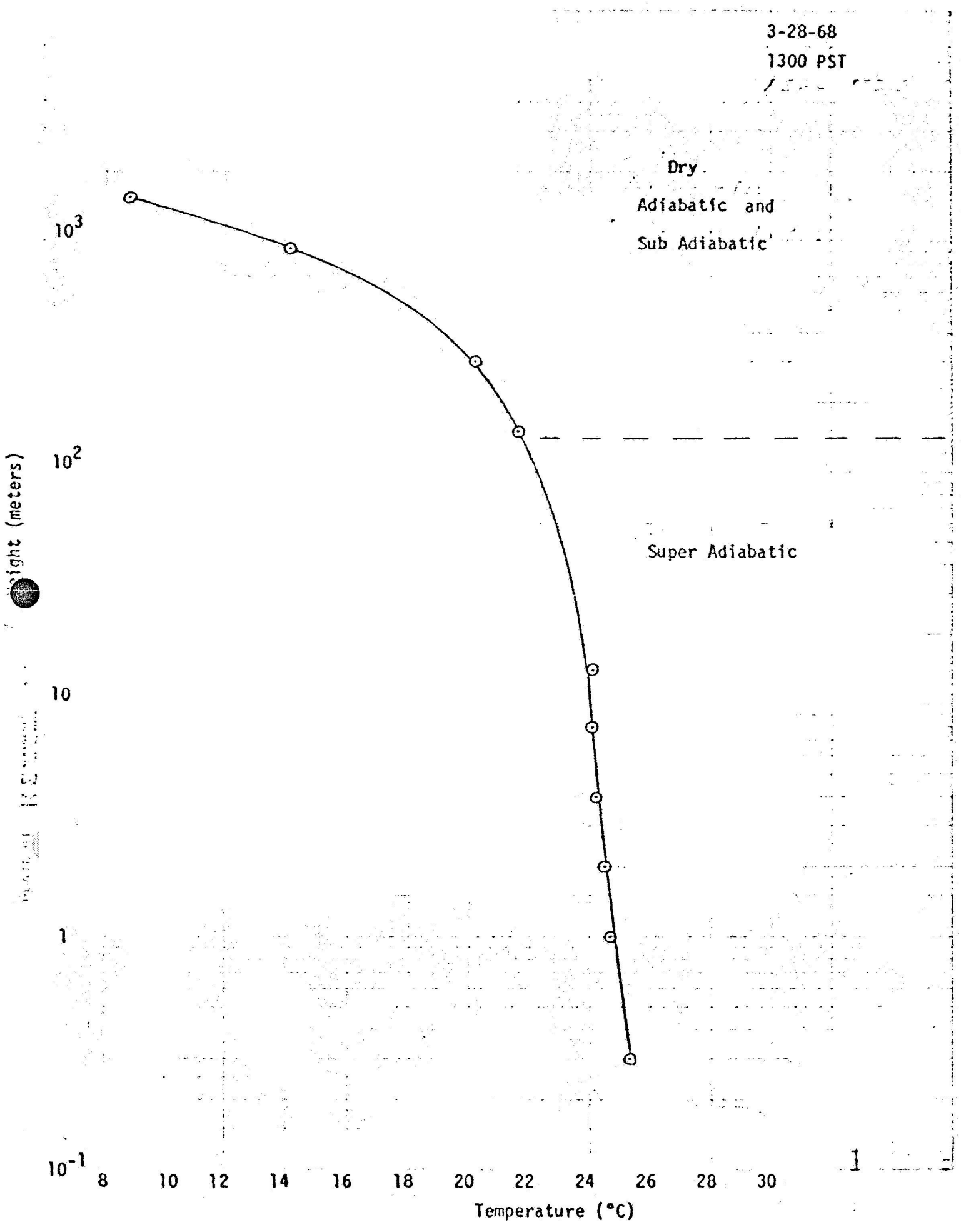
3-28-68
1300 PST
Dry
Adiabatic and
Sub Adiabatic
Super Adiabatic
10^3
10^2
10
1
10^{-1}
Height (meters)
8
10
12
14
16
18
20
22
24
26
28
30
Temperature (°C)

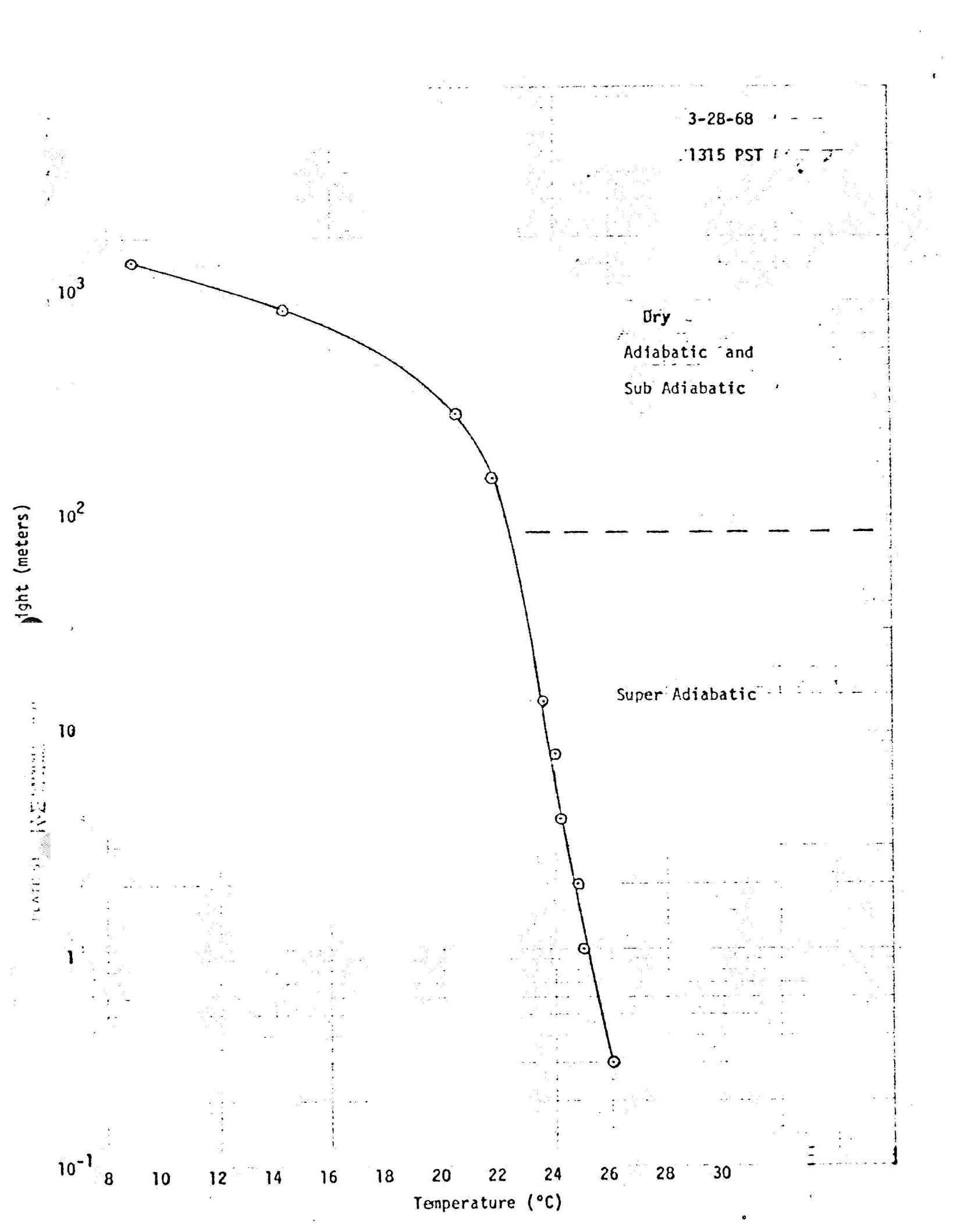
3-28-68
1315 PST
Dry
Adiabatic and
Sub Adiabatic
Super Adiabatic
10^3
10^2
10
1
10^{-1}
ight (meters)
8
10
12
14
16
18
20
22
24
26
28
30
Temperature (°C)

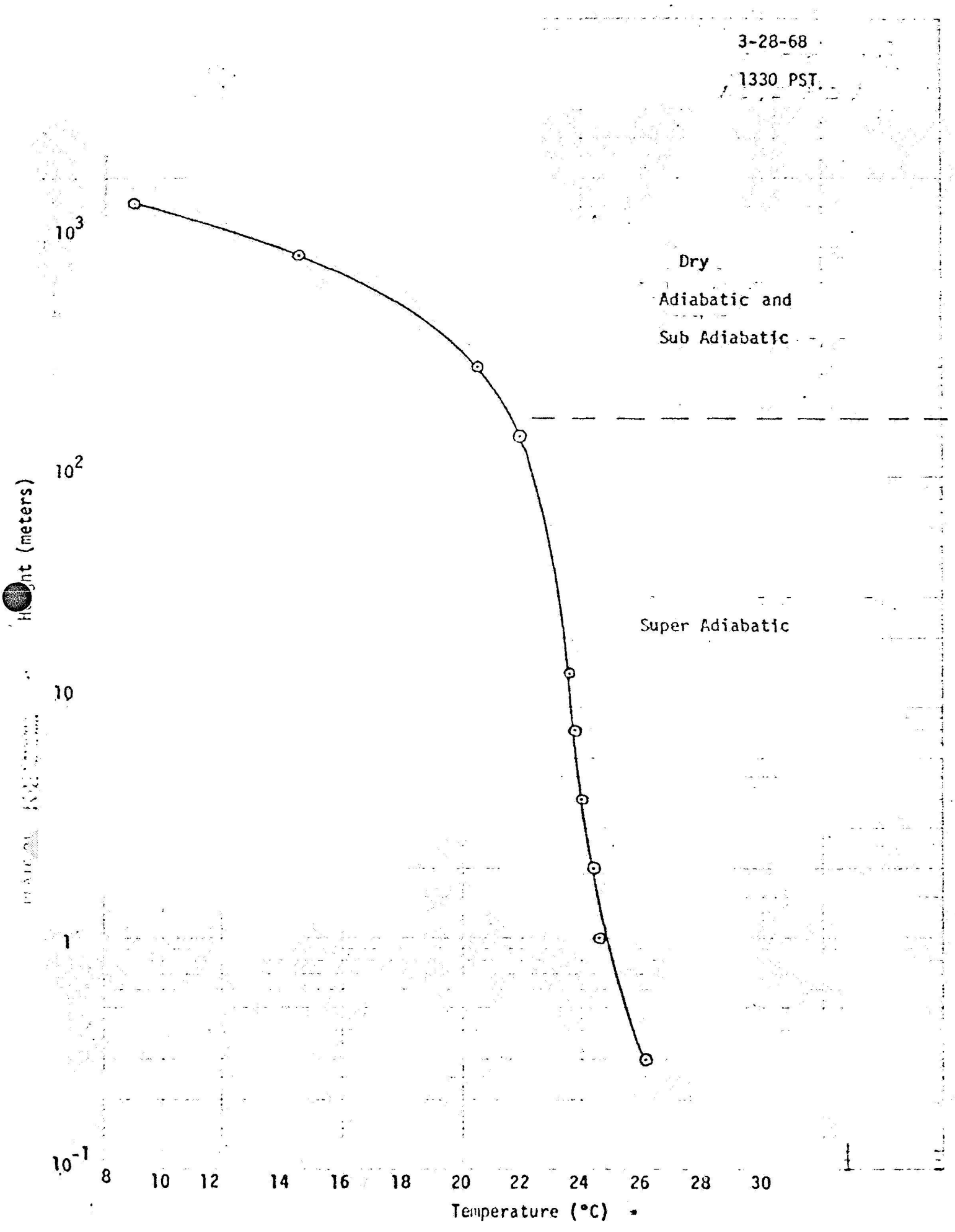
3-28-68
1330 PST
Dry
Adiabatic and
Sub Adiabatic
Super Adiabatic
10^3
10^2
10
1
10^{-1}
Height (meters)
8
10
12
14
16
18
20
22
24
26
28
30
Temperature (°C)

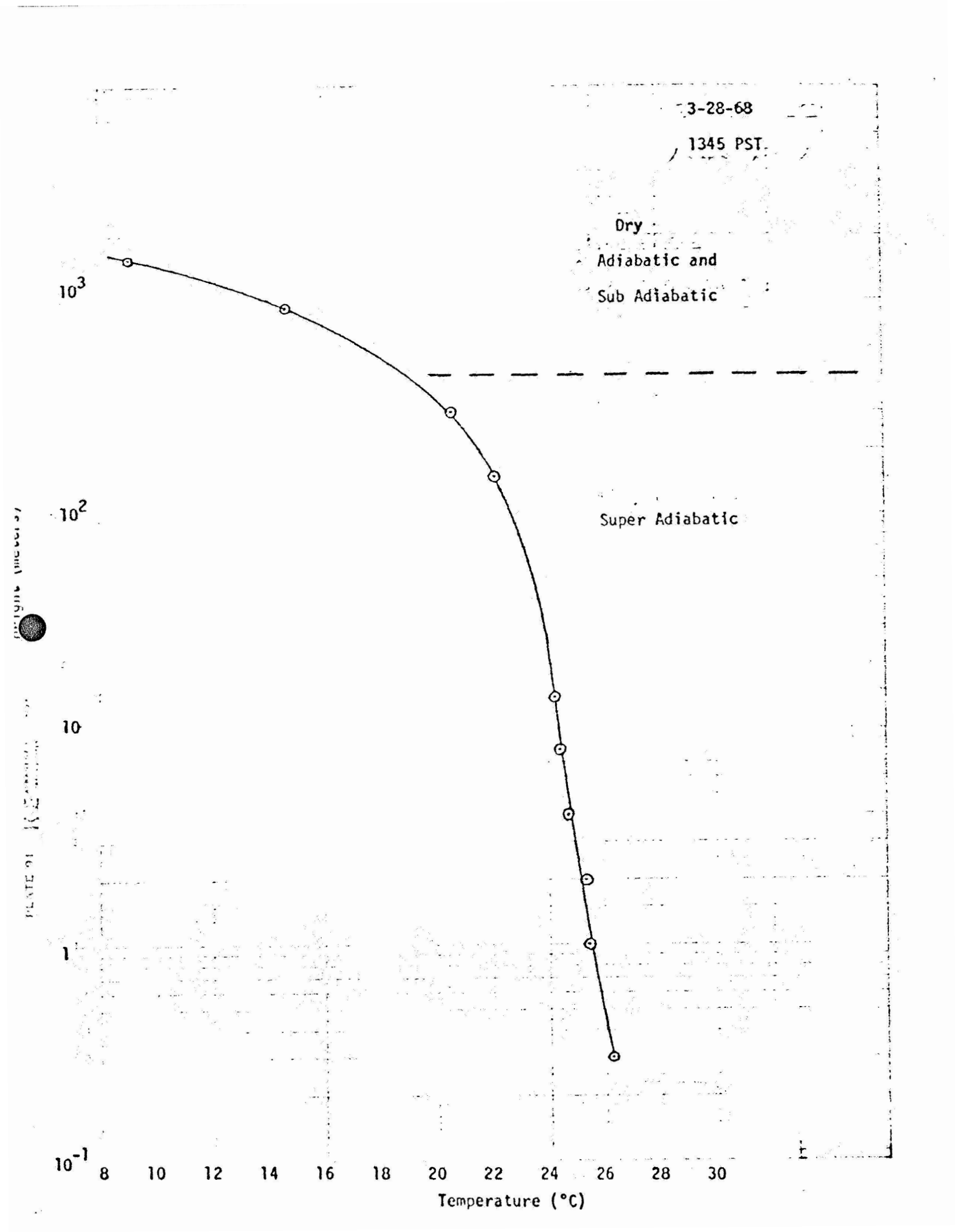
3-28-68
1345 PST
Dry
Adiabatic and
Sub Adiabatic
Super Adiabatic
10^3
10^2
10
1
10^{-1}
8
10
12
14
16
18
20
22
24
26
28
30
Temperature (°C)

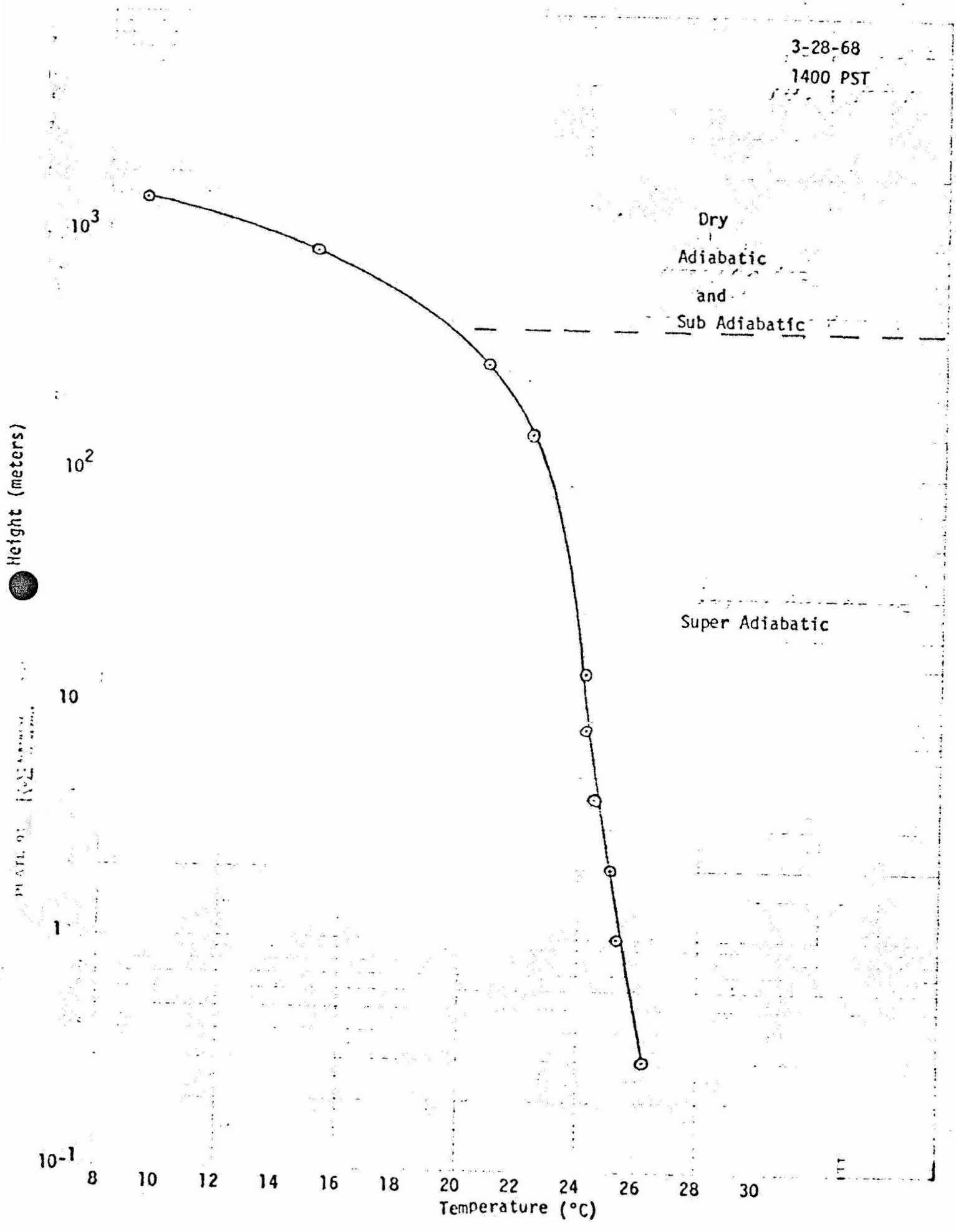
3-28-68
1400 PST
Dry
Adiabatic
and
Sub Adiabatic
Super Adiabatic
Height (meters)
10^3
10^2
10
1
10^{-1}
8
10
12
14
16
18
20
22
24
26
28
30
Temperature (°C)

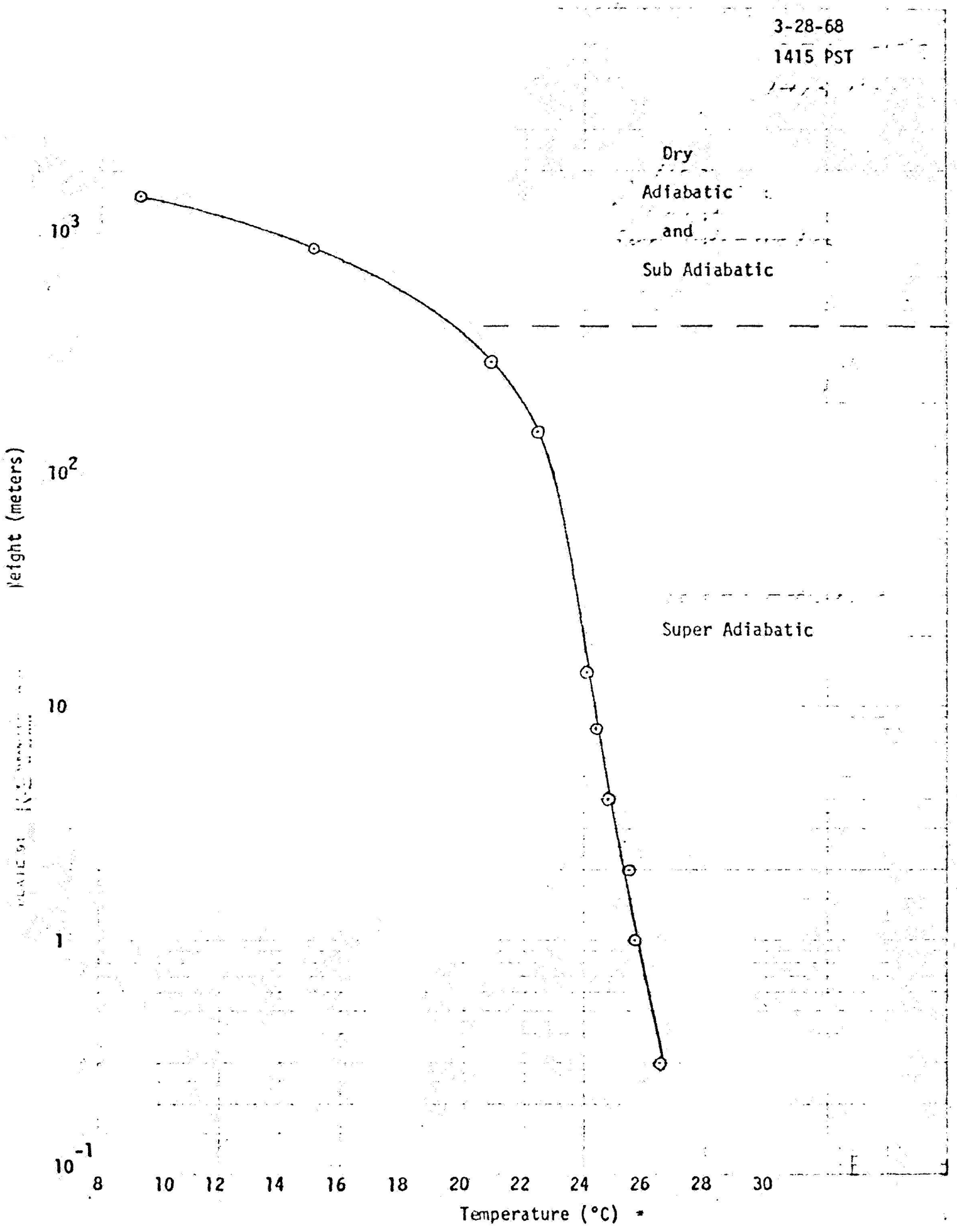
3-28-68
1415 PST
Dry
Adiabatic
and
Sub Adiabatic
Super Adiabatic
Height (meters)
10^3
10^2
10
1
10^{-1}
8
10
12
14
16
18
20
22
24
26
28
30
Temperature (°C)

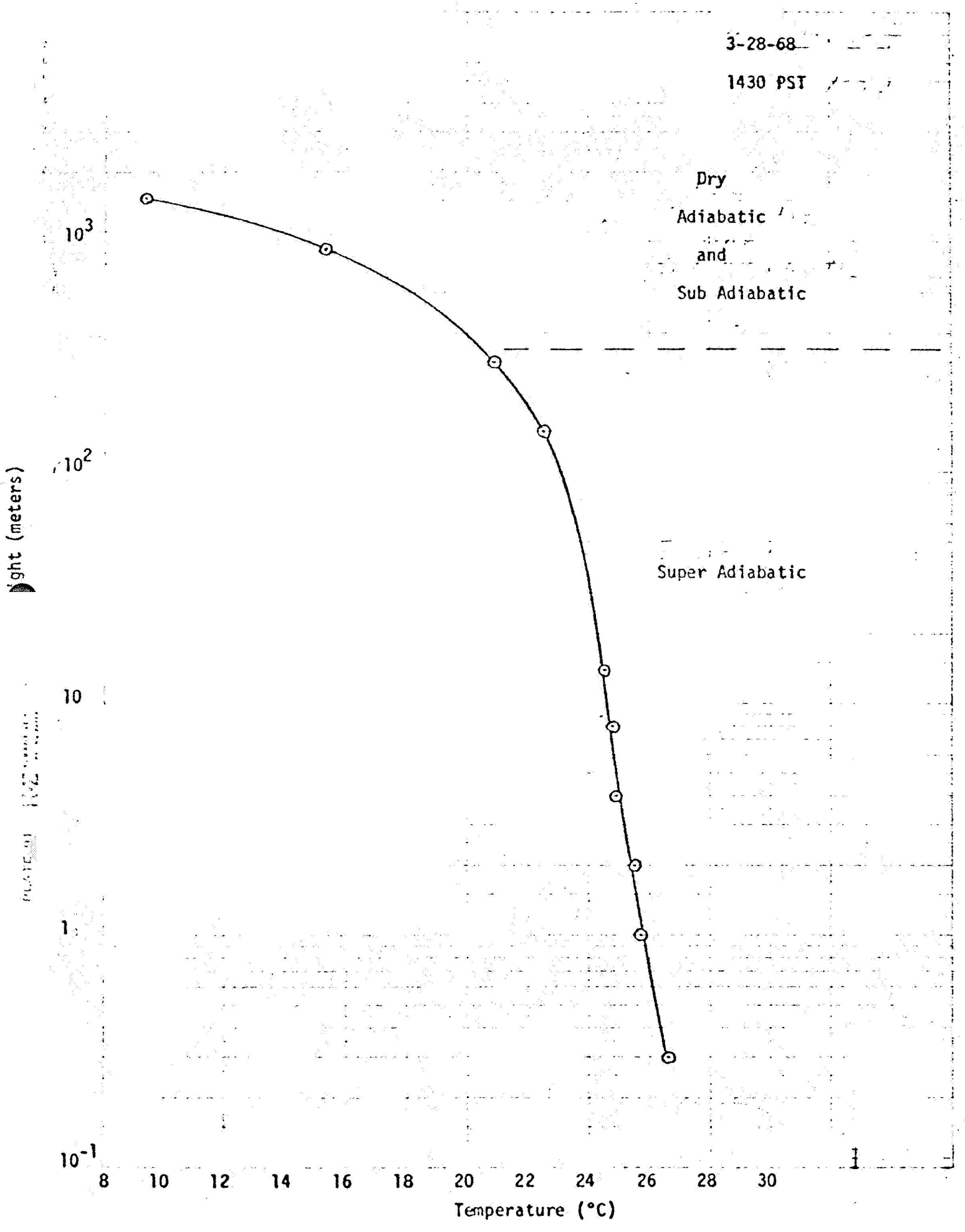
3-28-68
1430 PST
Dry
Adiabatic
and
Sub Adiabatic
Super Adiabatic
10^3
10^2
10
1
10^{-1}
ght (meters)
8
10
12
14
16
18
20
22
24
26
28
30
Temperature (°C)

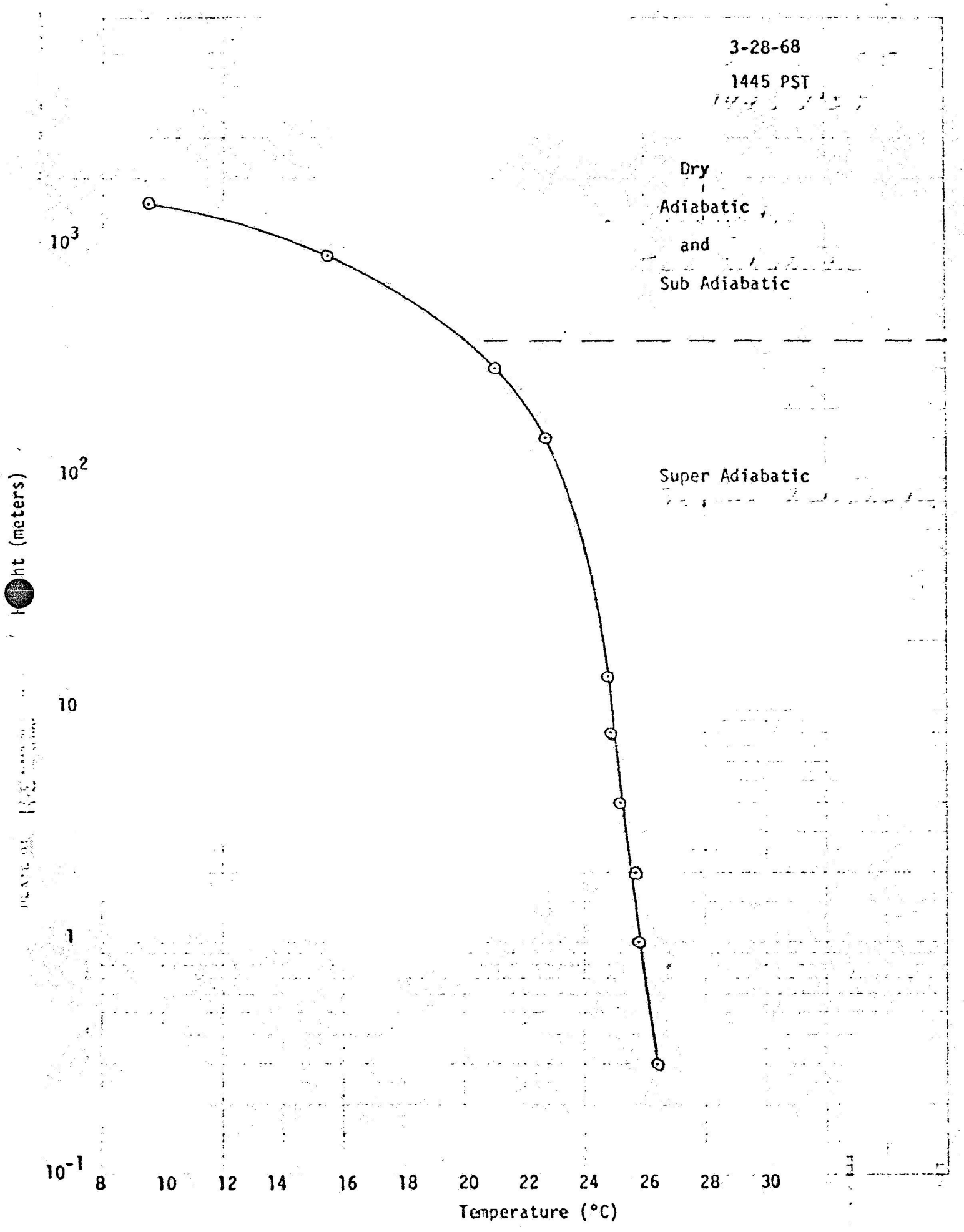
3-28-68
1445 PST
Dry
Adiabatic
and
Sub Adiabatic
Super Adiabatic
10^3
10^2
10
1
10^{-1}
ht (meters)
8
10
12
14
16
18
20
22
24
26
28
30
Temperature (°C)

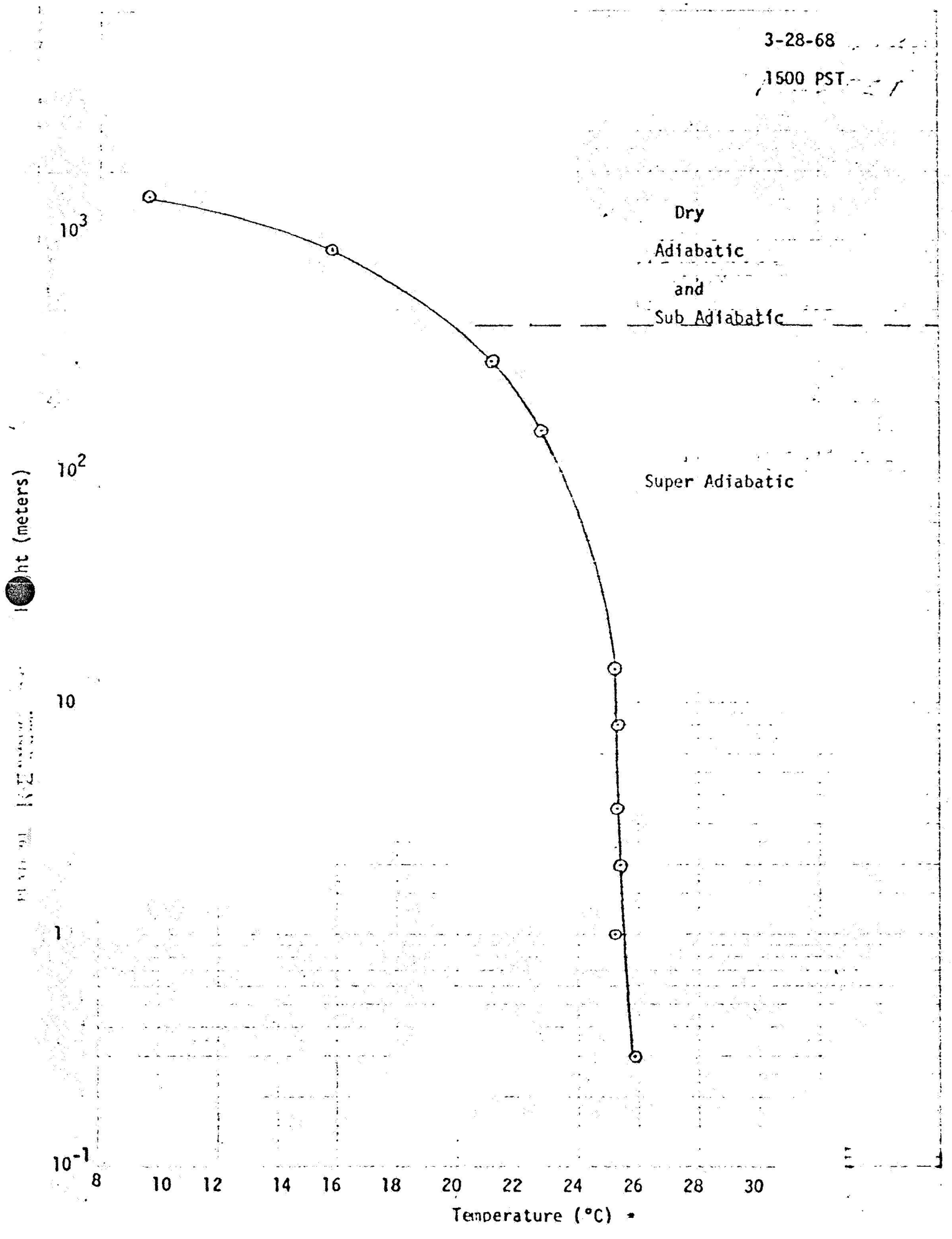
3-28-68
1500 PST
Dry
Adiabatic
and
Sub Adiabatic
Super Adiabatic
10^3
10^2
10
1
10^{-1}
ht (meters)
8
10
12
14
16
18
20
22
24
26
28
30
Temperature (°C)

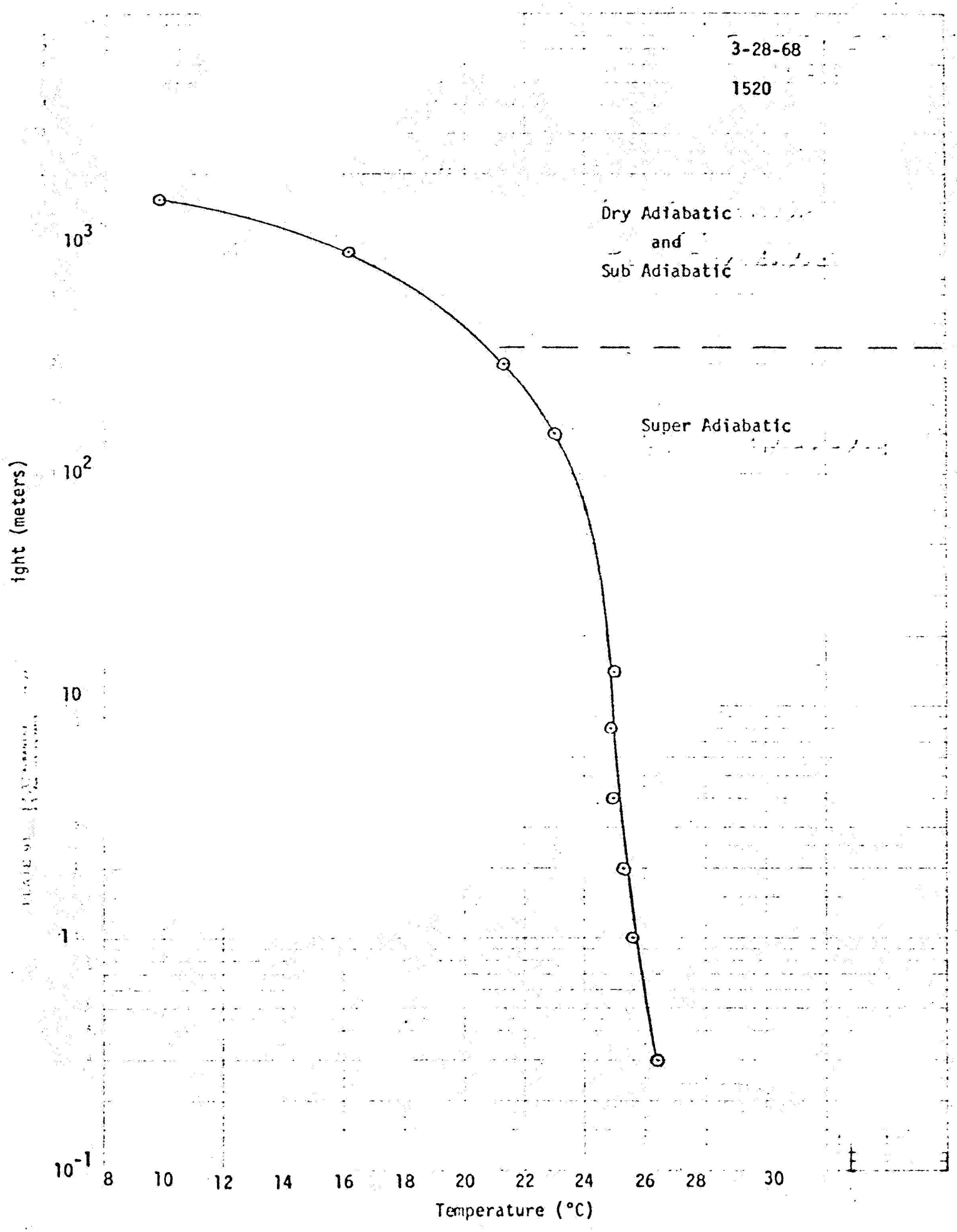
3-28-68
1520
Dry Adiabatic
and
Sub Adiabatic
Super Adiabatic
10^3
10^2
10
1
10^{-1}
ight (meters)
8
10
12
14
16
18
20
22
24
26
28
30
Temperature (°C)

TEMPERATURE DATA FOR MAY 3, 1968

5-3-68

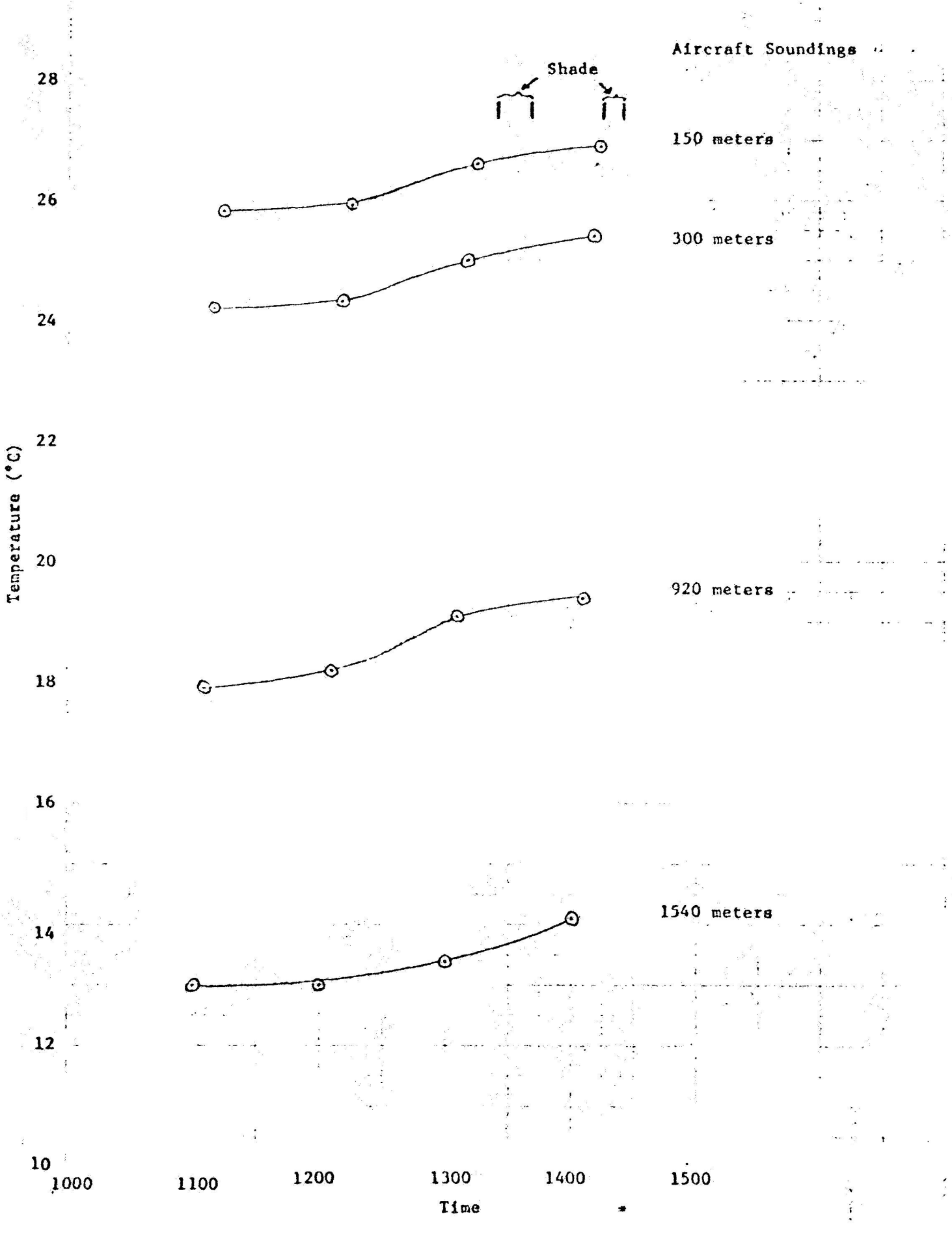
Aircraft Soundings
Shade
150 meters
300 meters
920 meters
1540 meters
Temperature (°C)
28
26
24
22
20
18
16
14
12
10
1000
1100
1200
1300
1400
1500
Time

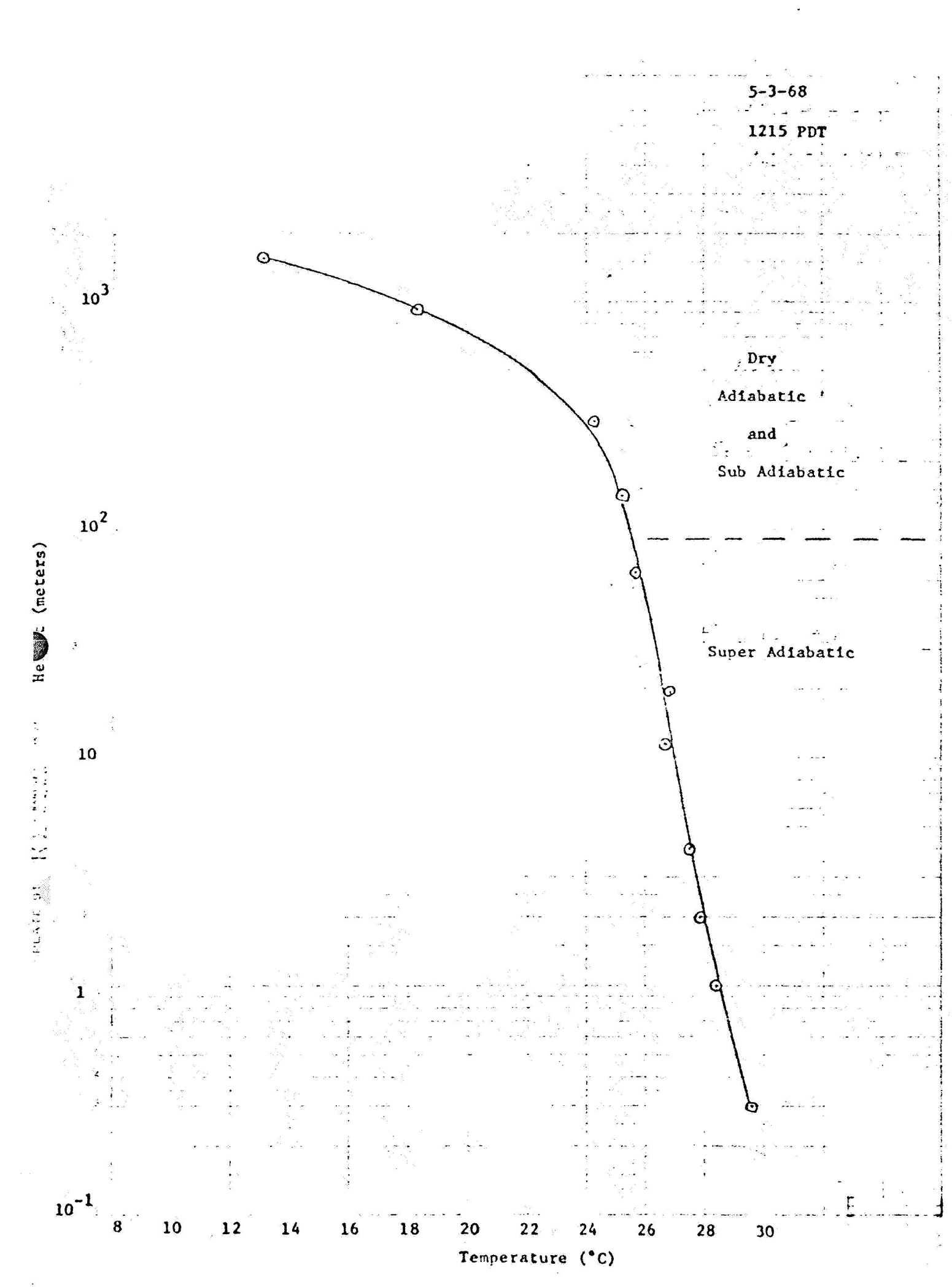
5-3-68
1215 PDT
Dry
Adiabatic
and
Sub Adiabatic
Super Adiabatic
10^3
10^2
10
1
10^{-1}
Height (meters)
8
10
12
14
16
18
20
22
24
26
28
30
Temperature (°C)

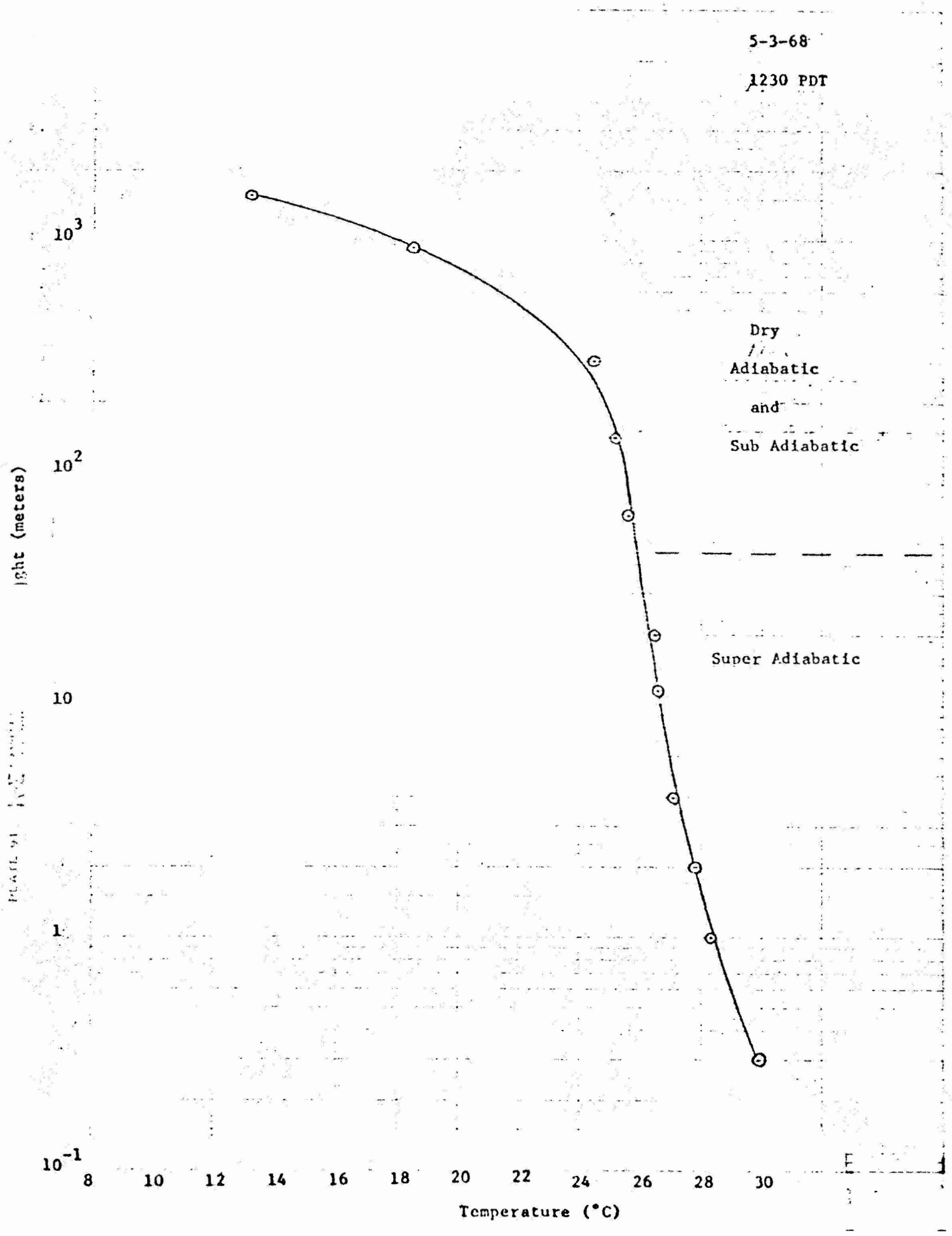
5-3-68
1230 PDT
Dry
Adiabatic
and
Sub Adiabatic
Super Adiabatic
10^3
10^2
10
1
10^{-1}
ght (meters)
8
10
12
14
16
18
20
22
24
26
28
30
Temperature (°C)

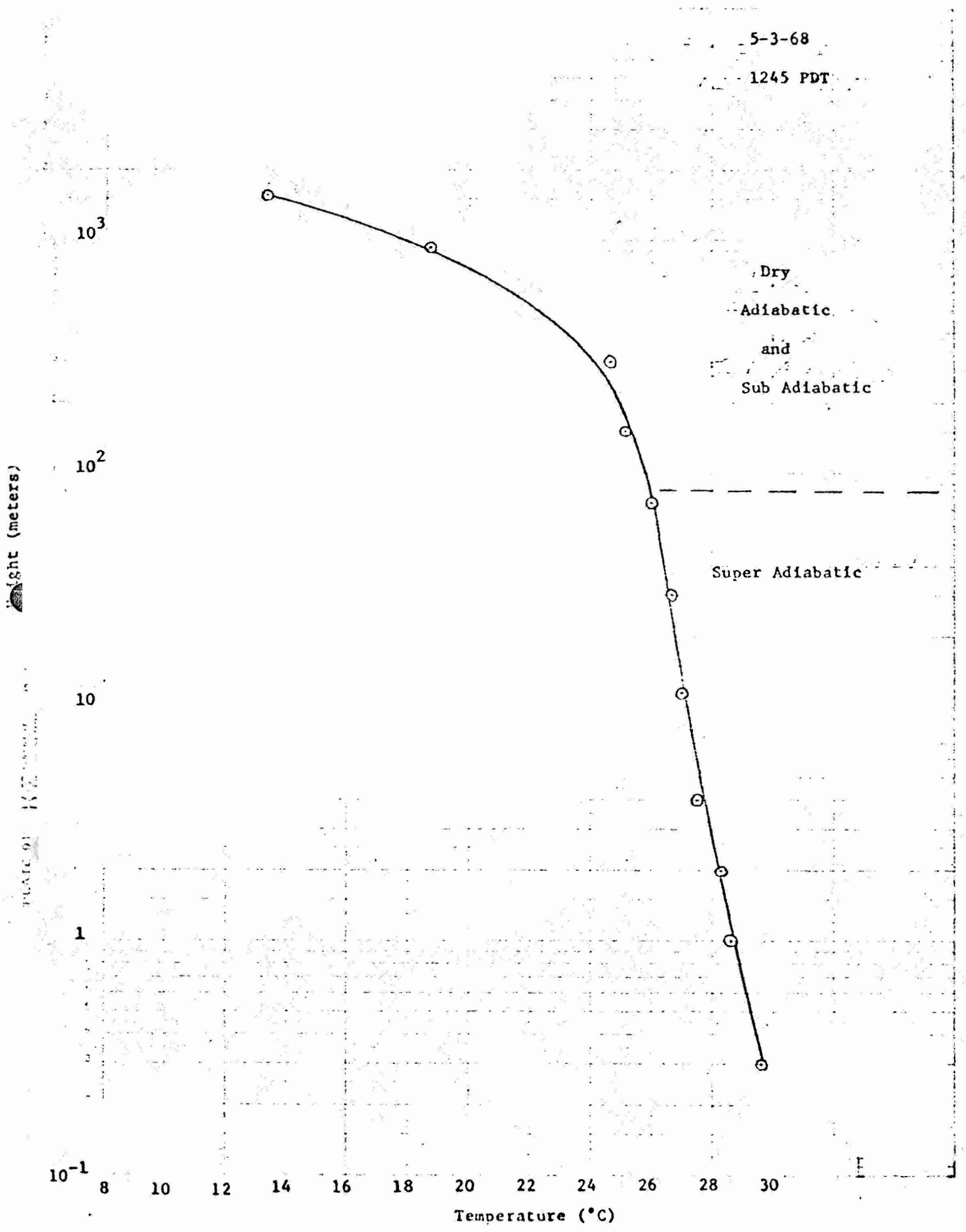
5-3-68
1245 PDT
Dry
Adiabatic
and
Sub Adiabatic
Super Adiabatic
10^3
10^2
10
1
10^{-1}
ight (meters)
8
10
12
14
16
18
20
22
24
26
28
30
Temperature (°C)

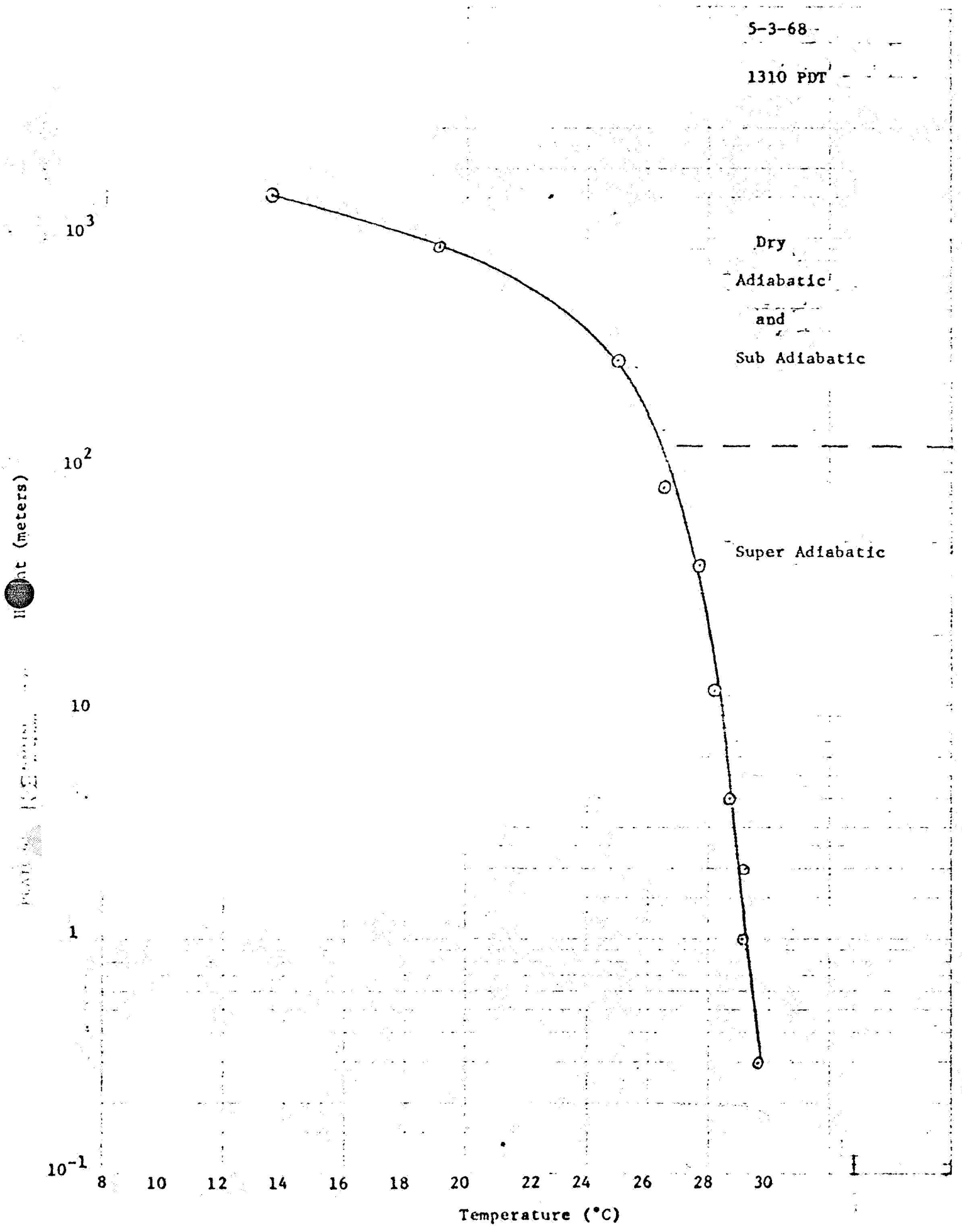
5-3-68
1310 PDT
Dry
Adiabatic
and
Sub Adiabatic
Super Adiabatic
10^3
10^2
10
1
10^{-1}
8
10
12
14
16
18
20
22
24
26
28
30
Temperature (°C)

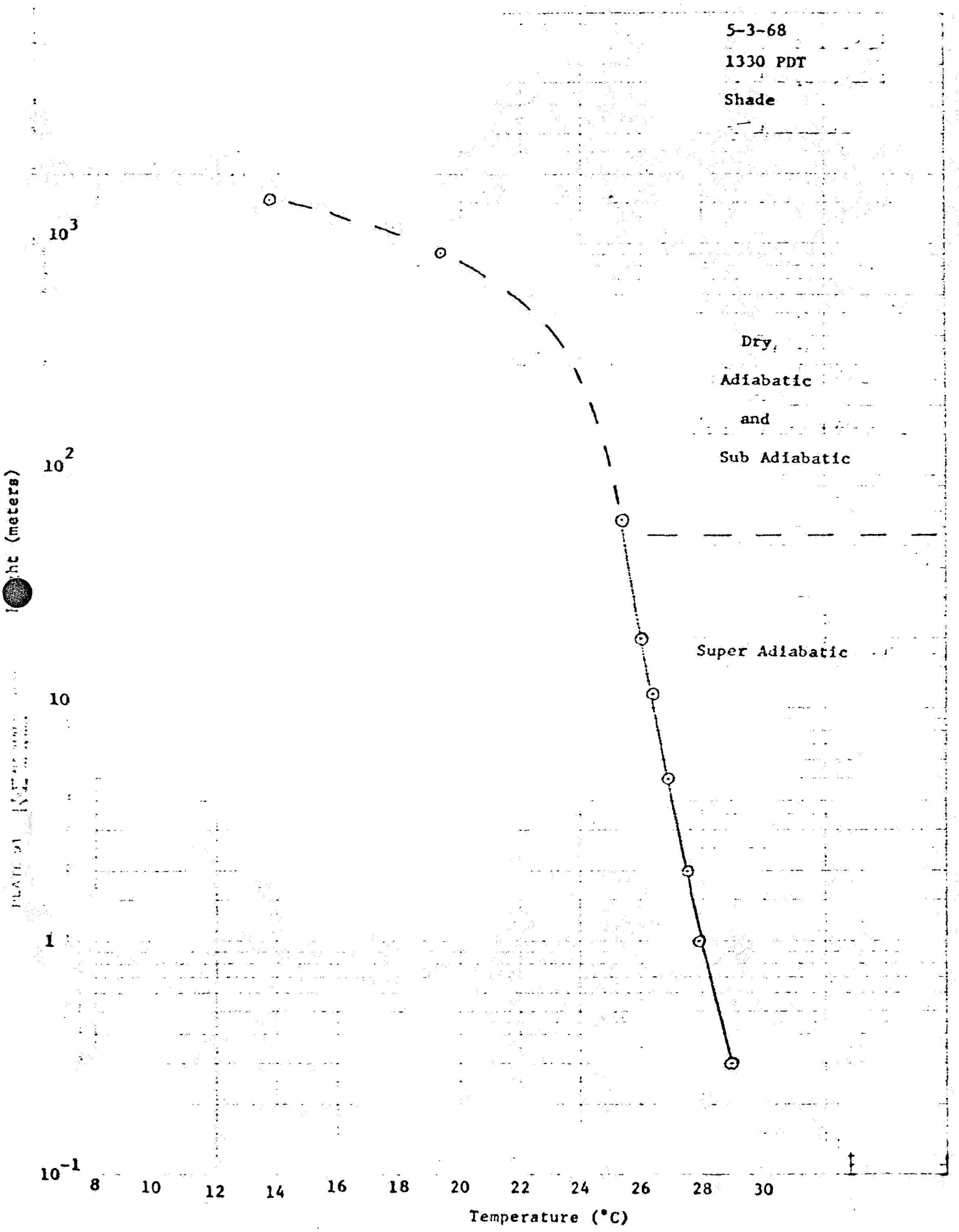
5-3-68
1330 PDT
Shade
Dry
Adiabatic
and
Sub Adiabatic
Super Adiabatic
10^3
10^2
10
1
10^{-1}
ht (meters)
8
10
12
14
16
18
20
22
24
26
28
30
Temperature (°C)

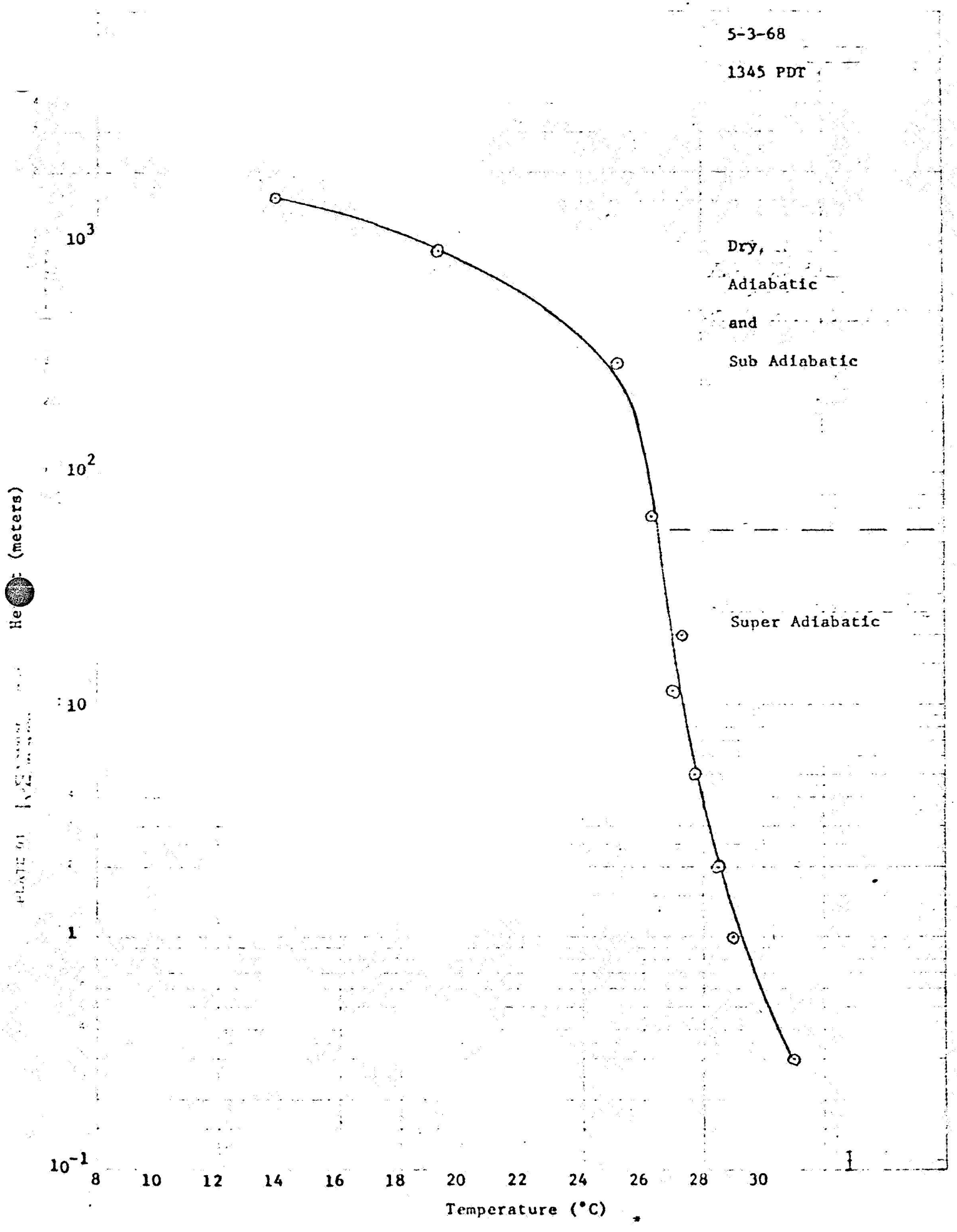
5-3-68
1345 PDT
Dry,
Adiabatic
and
Sub Adiabatic
Super Adiabatic
10^3
10^2
10
1
10^{-1}
Height (meters)
8
10
12
14
16
18
20
22
24
26
28
30
Temperature (°C)

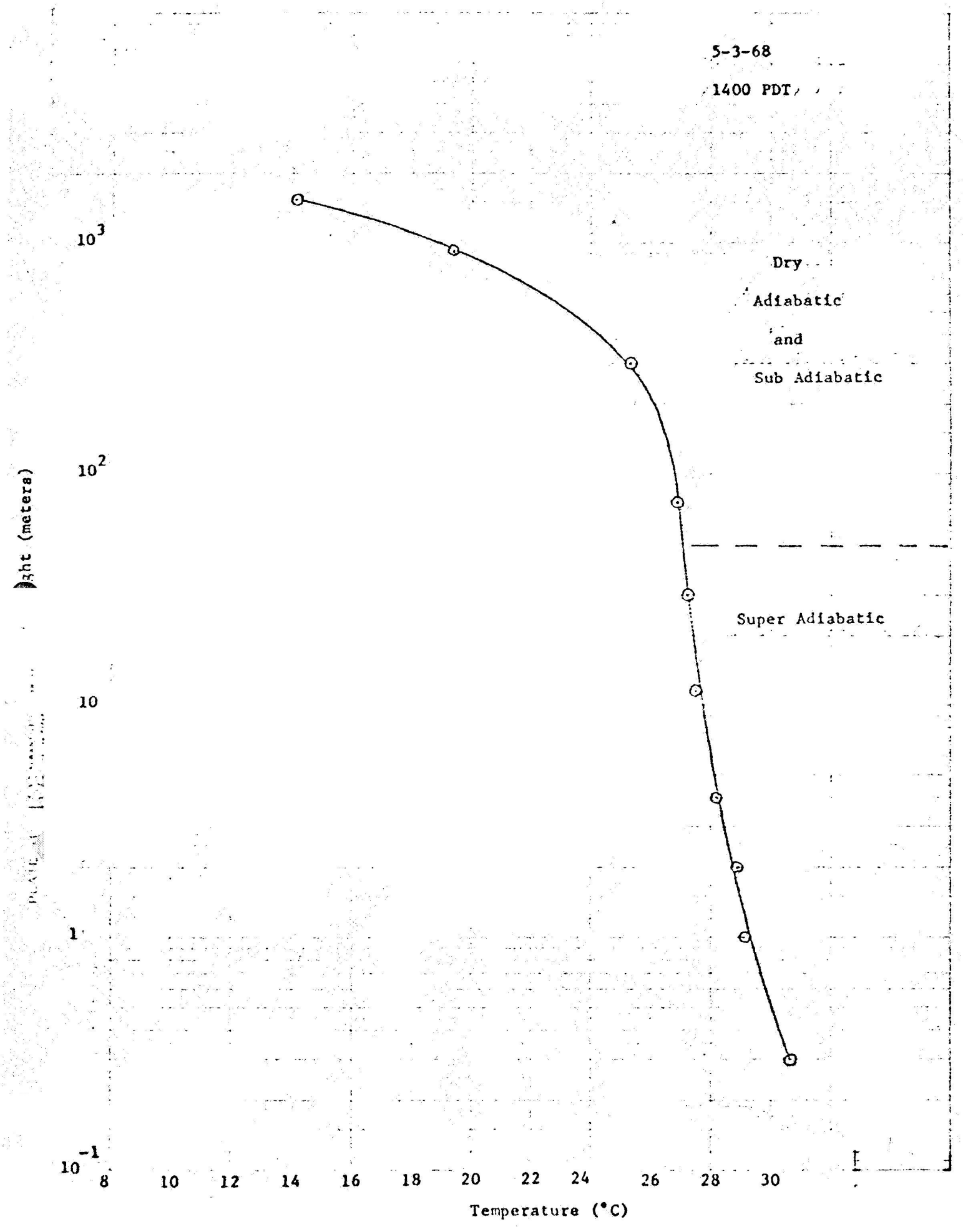
5-3-68
1400 PDT
Dry
Adiabatic
and
Sub Adiabatic
Super Adiabatic
10^3
10^2
10
1
10^{-1}
ght (meters)
8
10
12
14
16
18
20
22
24
26
28
30
Temperature (°C)

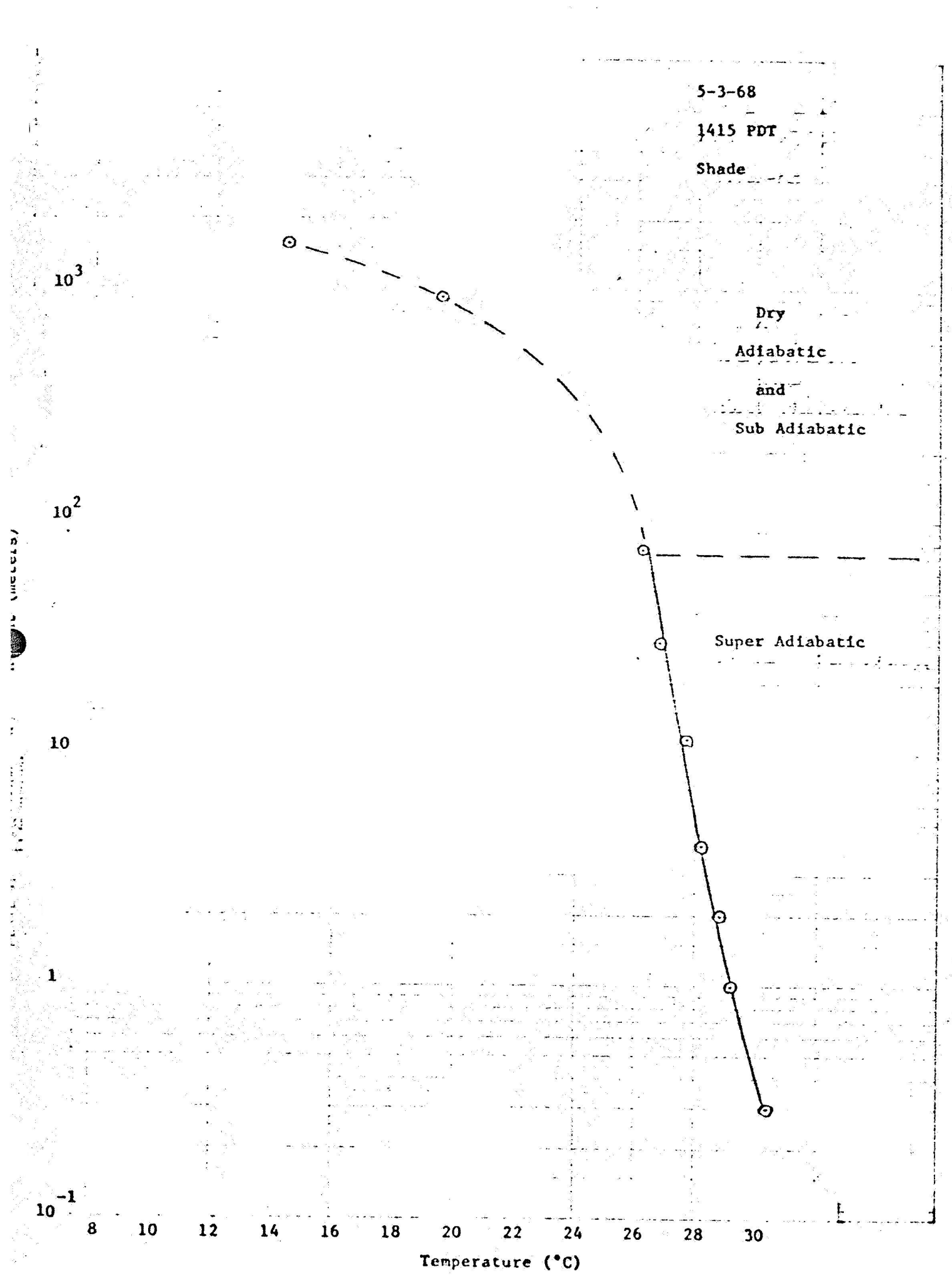
5-3-68
1415 PDT
Shade
Dry
Adiabatic
and
Sub Adiabatic
Super Adiabatic
10^3
10^2
10
1
10^{-1}
8
10
12
14
16
18
20
22
24
26
28
30
Temperature (°C)

TEMPERATURE DATA FOR JUNE 13, 1968

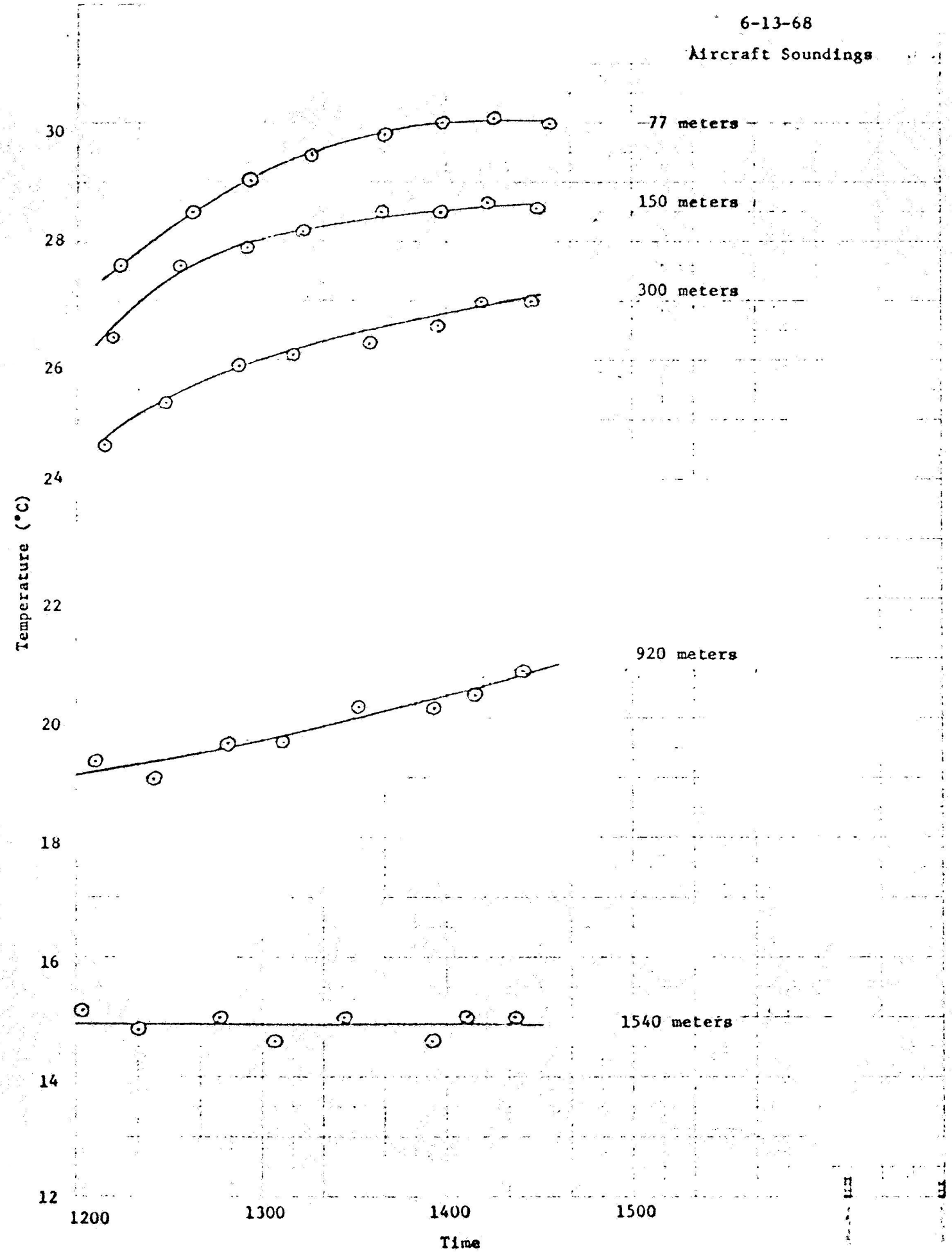
6-13-68
Aircraft Soundings
77 meters
150 meters
300 meters
920 meters
1540 meters
Temperature (°C)
30
28
26
24
22
20
18
16
14
12
1200
1300
1400
1500
Time

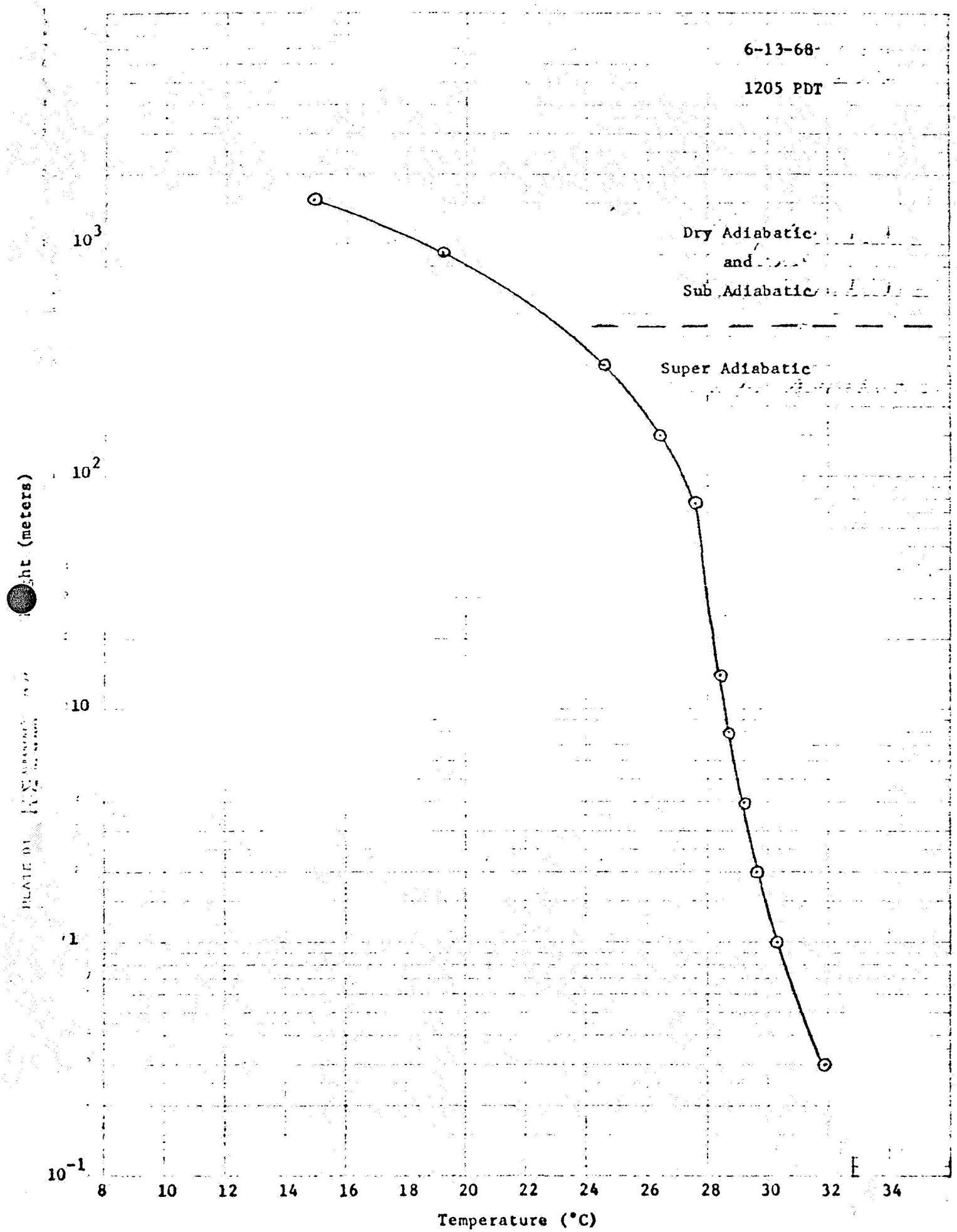
6-13-68
1205 PDT
Dry Adiabatic
and
Sub Adiabatic
Super Adiabatic
10^3
10^2
10
1
10^{-1}
ht (meters)
8
10
12
14
16
18
20
22
24
26
28
30
32
34
Temperature (°C)

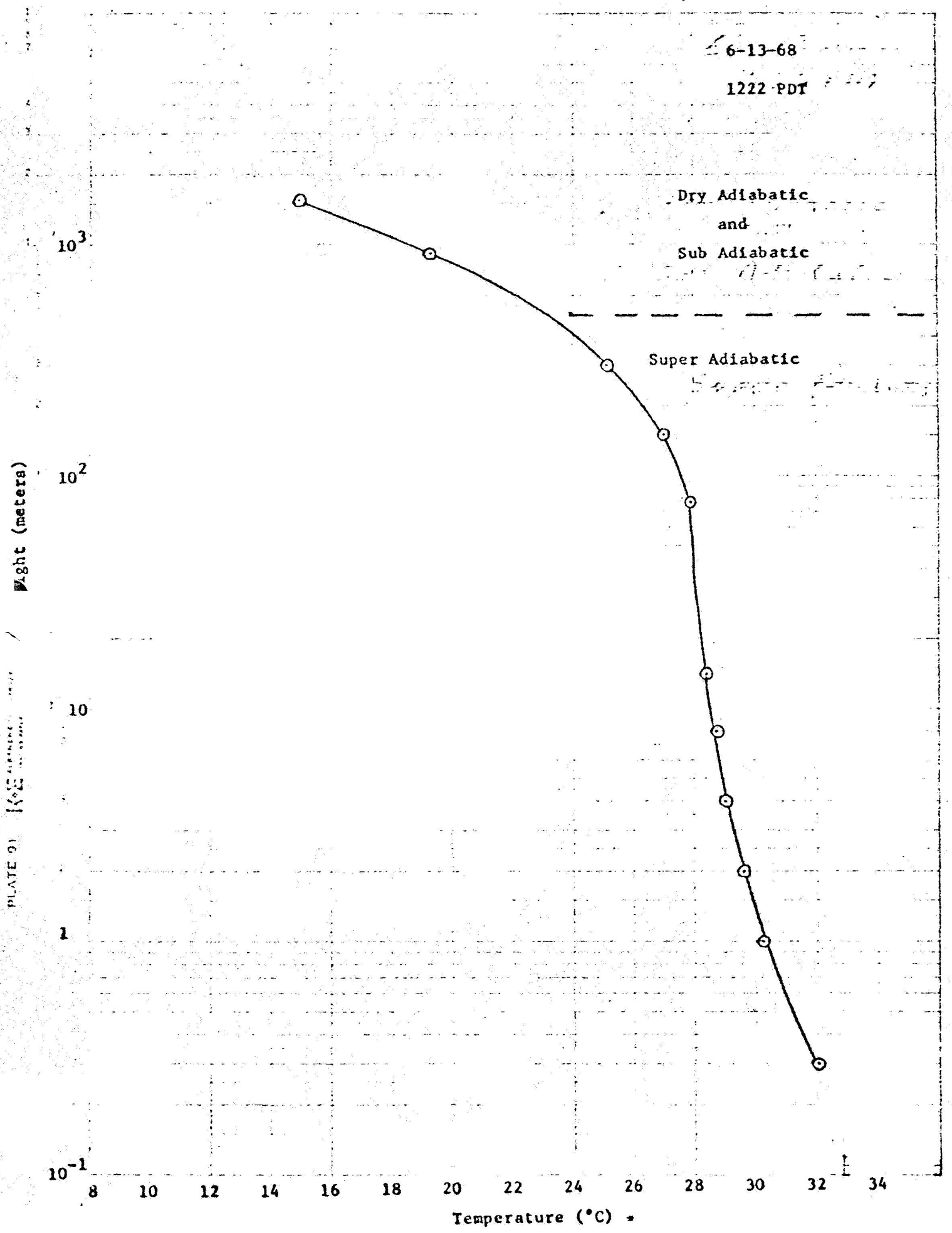
6-13-68
1222 PDT
Dry Adiabatic
and
Sub Adiabatic
Super Adiabatic
10^3
10^2
10
1
10^{-1}
ght (meters)
8
10
12
14
16
18
20
22
24
26
28
30
32
34
Temperature (°C)

PLATE 91

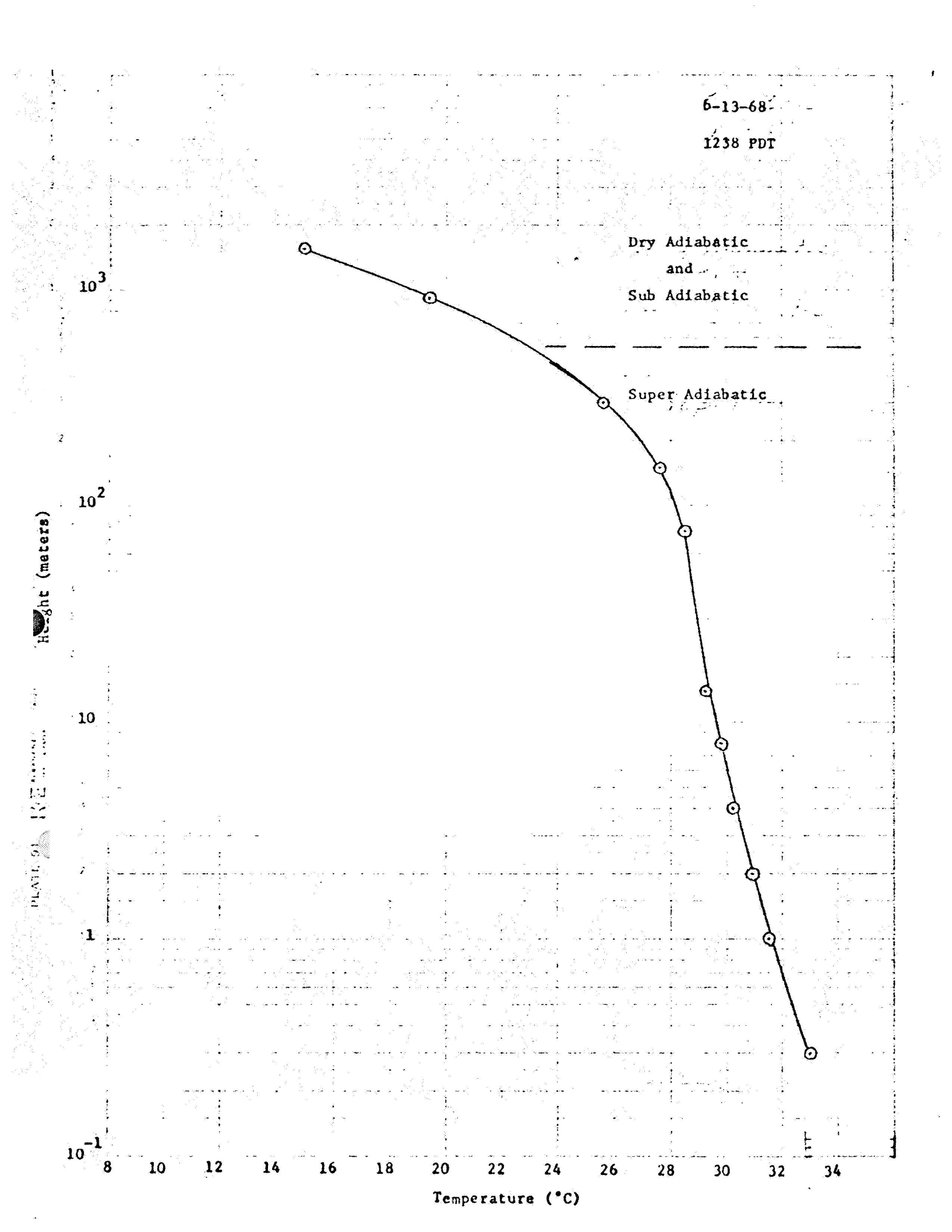
6-13-68
1238 PDT
Dry Adiabatic
and
Sub Adiabatic
Super Adiabatic
10^3
10^2
10
1
10^{-1}
Height (meters)
8
10
12
14
16
18
20
22
24
26
28
30
32
34
Temperature (°C)

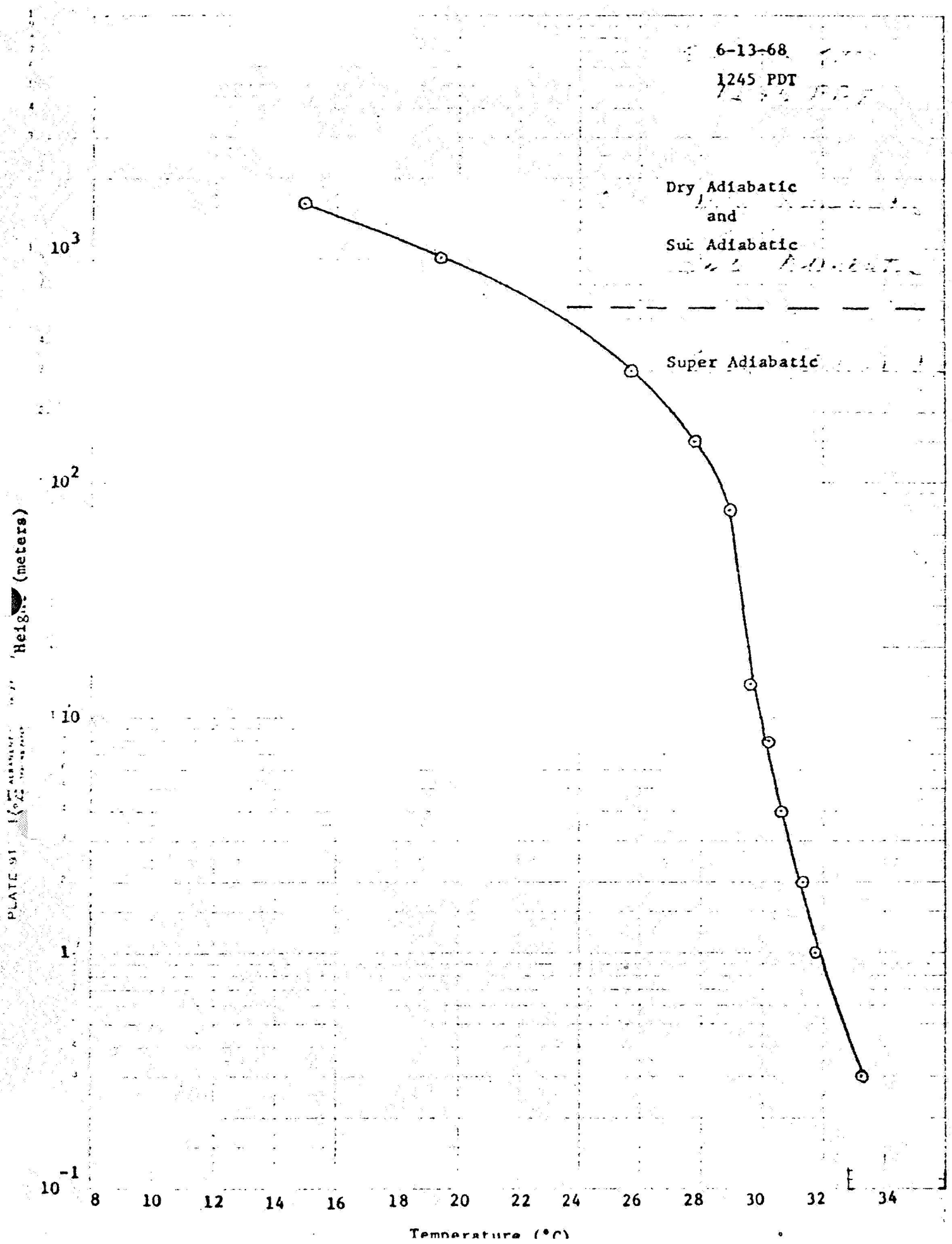
6-13-68
1245 PDT
Dry Adiabatic
and
Sub Adiabatic
Super Adiabatic
Height (meters)
10^3
10^2
10
1
10^{-1}
8
10
12
14
16
18
20
22
24
26
28
30
32
34
Temperature (°C)

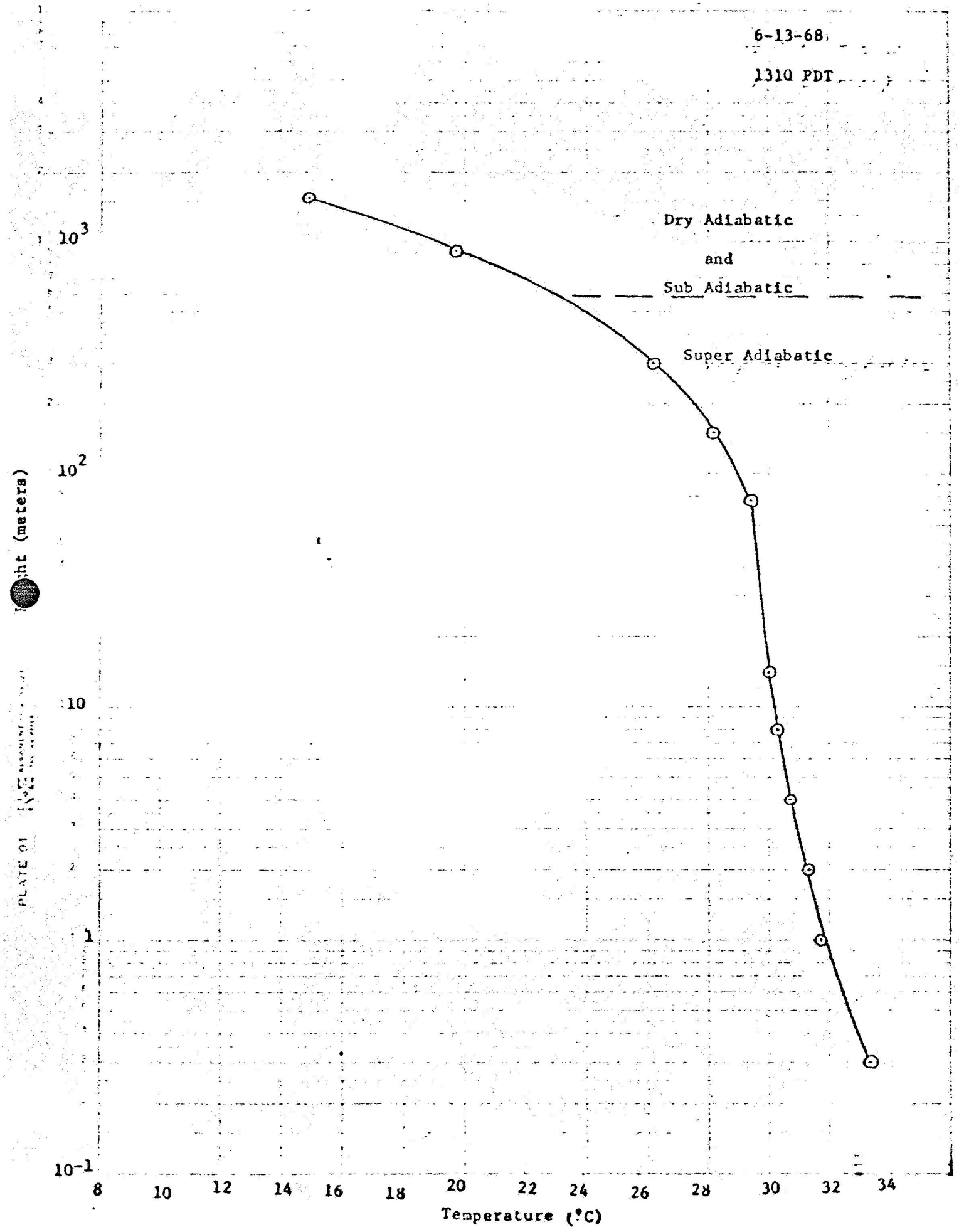
6-13-68
1310 PDT
Dry Adiabatic
and
Sub Adiabatic
Super Adiabatic
10^3
10^2
10
1
10^{-1}
ht (meters)
8
10
12
14
16
18
20
22
24
26
28
30
32
34
Temperature (°C)

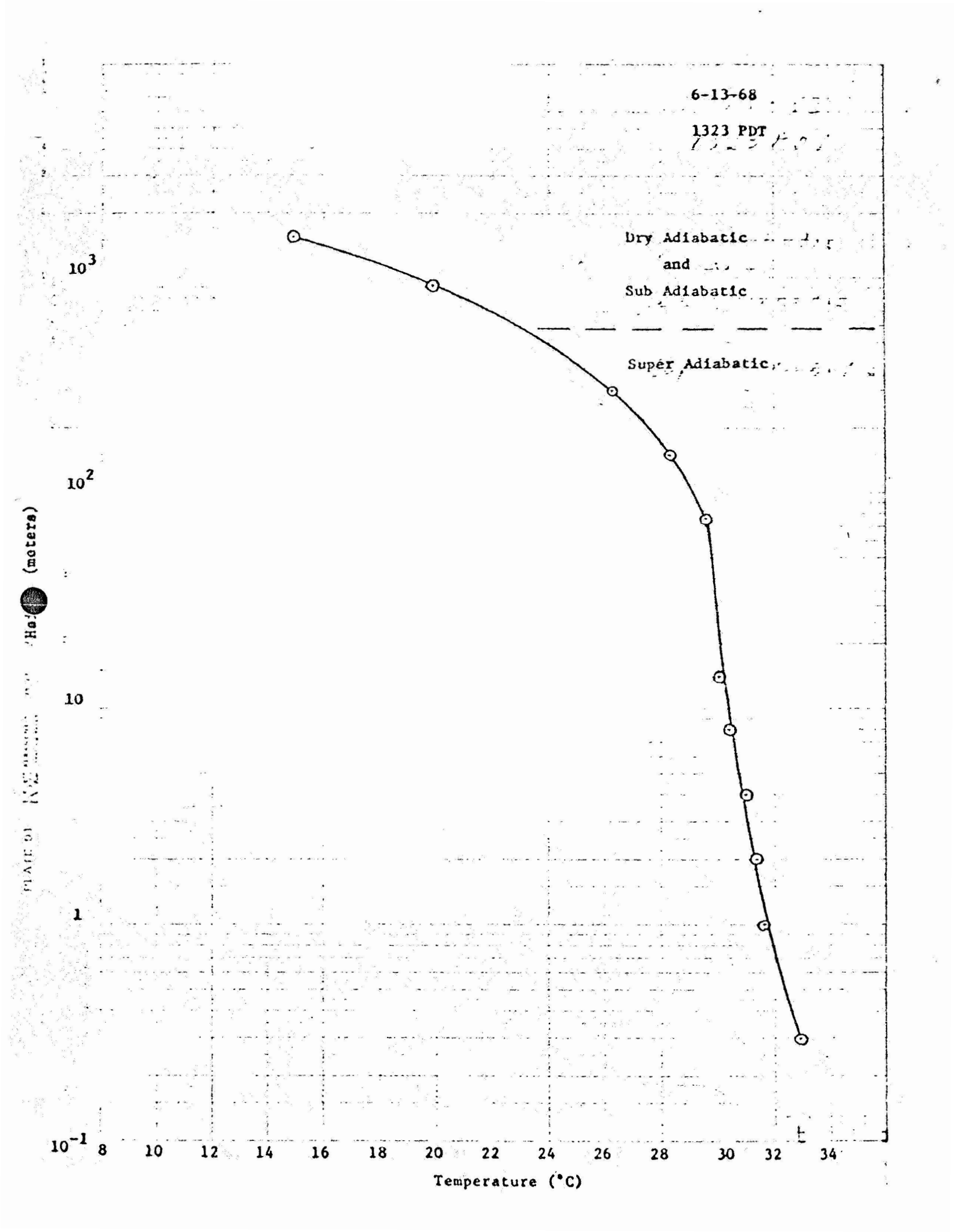
6-13-68
1323 PDT
Dry Adiabatic
and
Sub Adiabatic
Super Adiabatic
10^3
10^2
10
1
10^{-1}
Height (meters)
8
10
12
14
16
18
20
22
24
26
28
30
32
34
Temperature (°C)

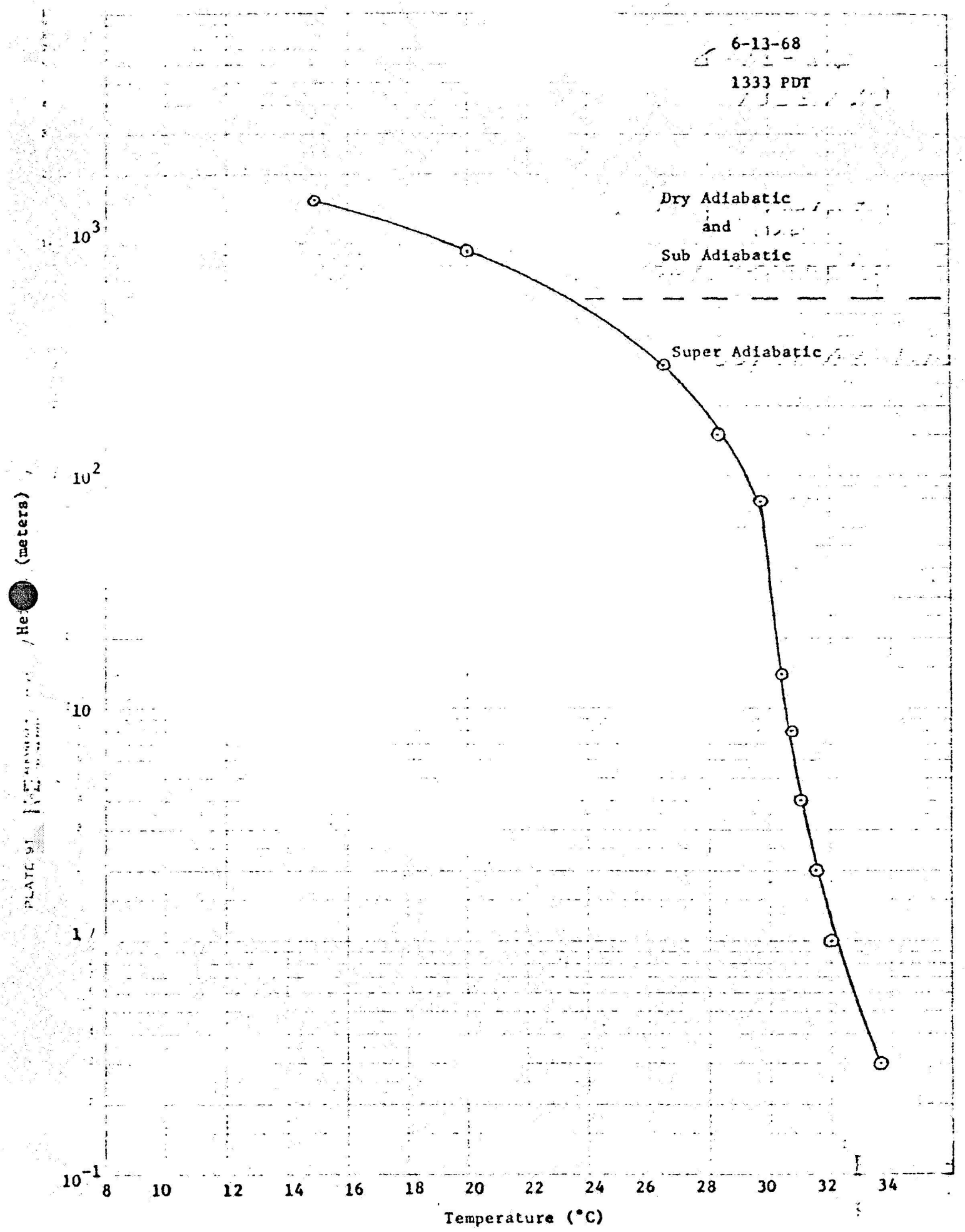
6-13-68
1333 PDT
Dry Adiabatic
and
Sub Adiabatic
Super Adiabatic
10^3
10^2
10
1
10^{-1}
(meters)
8
10
12
14
16
18
20
22
24
26
28
30
32
34
Temperature (°C)

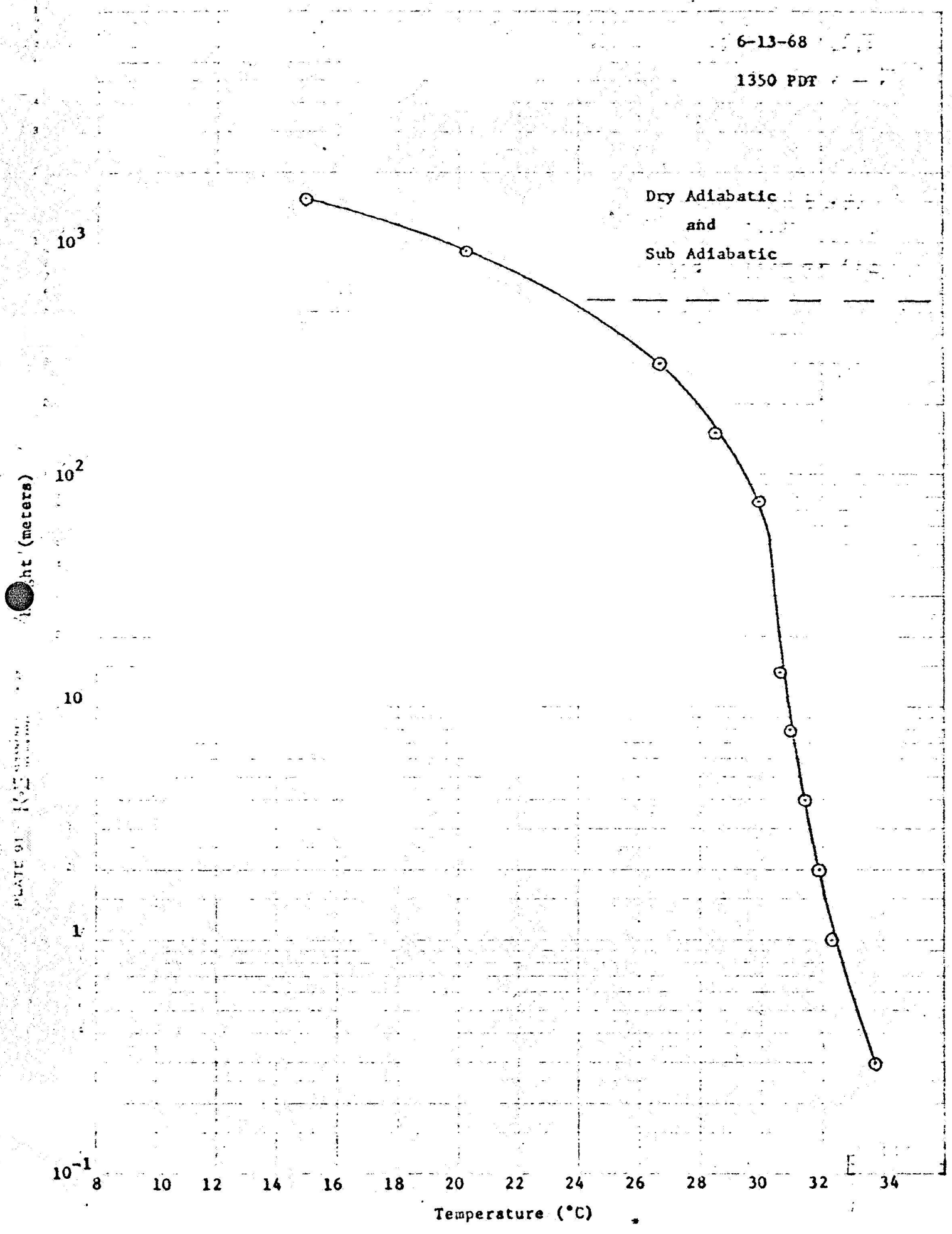
6-13-68
1350 PDT
Dry Adiabatic
and
Sub Adiabatic
10^3
10^2
10
1
10^{-1}
ht (meters)
8
10
12
14
16
18
20
22
24
26
28
30
32
34
Temperature (°C)

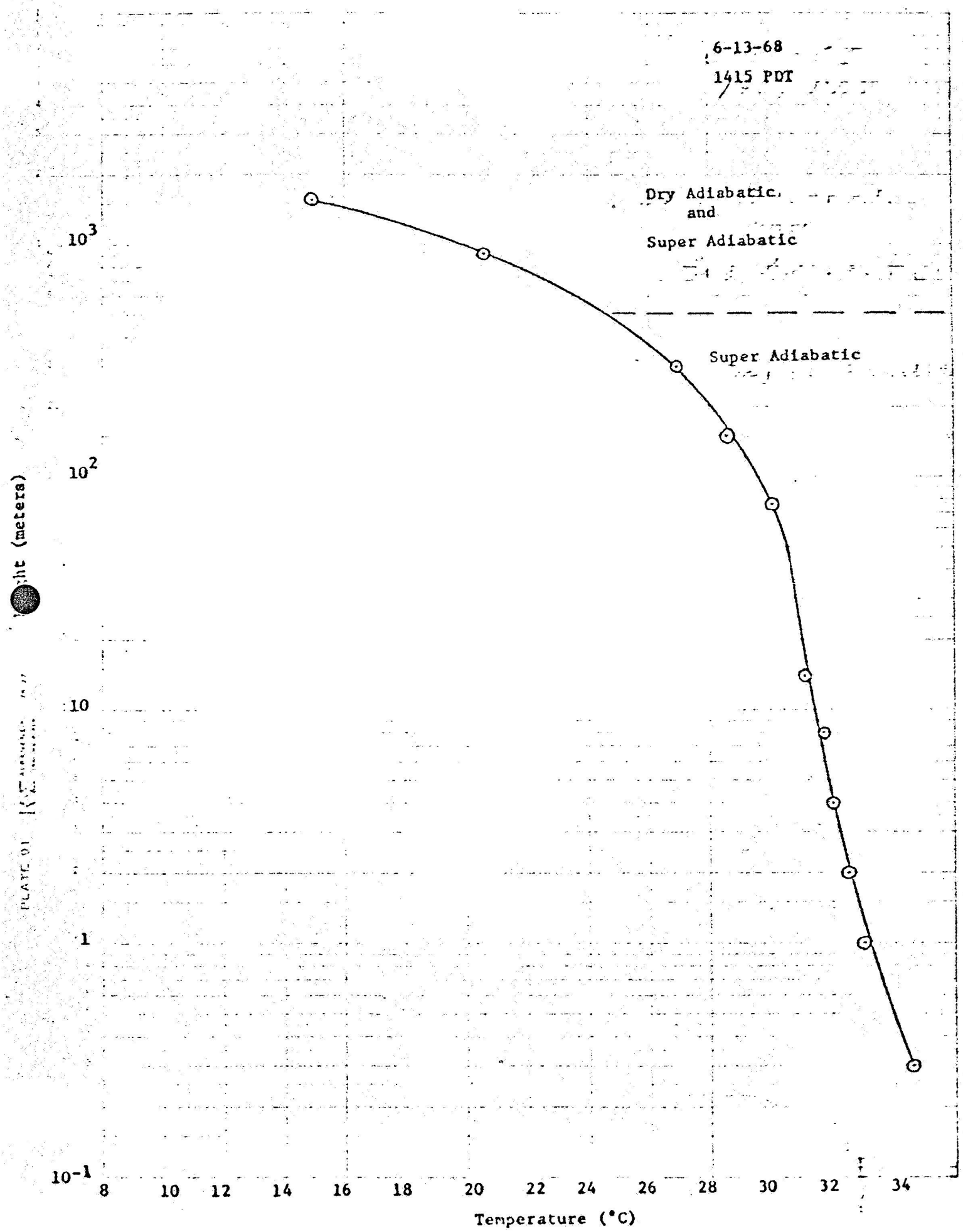
6-13-68
1415 PDT
Dry Adiabatic
and
Super Adiabatic
Super Adiabatic
10^3
10^2
10
1
10^{-1}
ht (meters)
8
10
12
14
16
18
20
22
24
26
28
30
32
34
Temperature (°C)

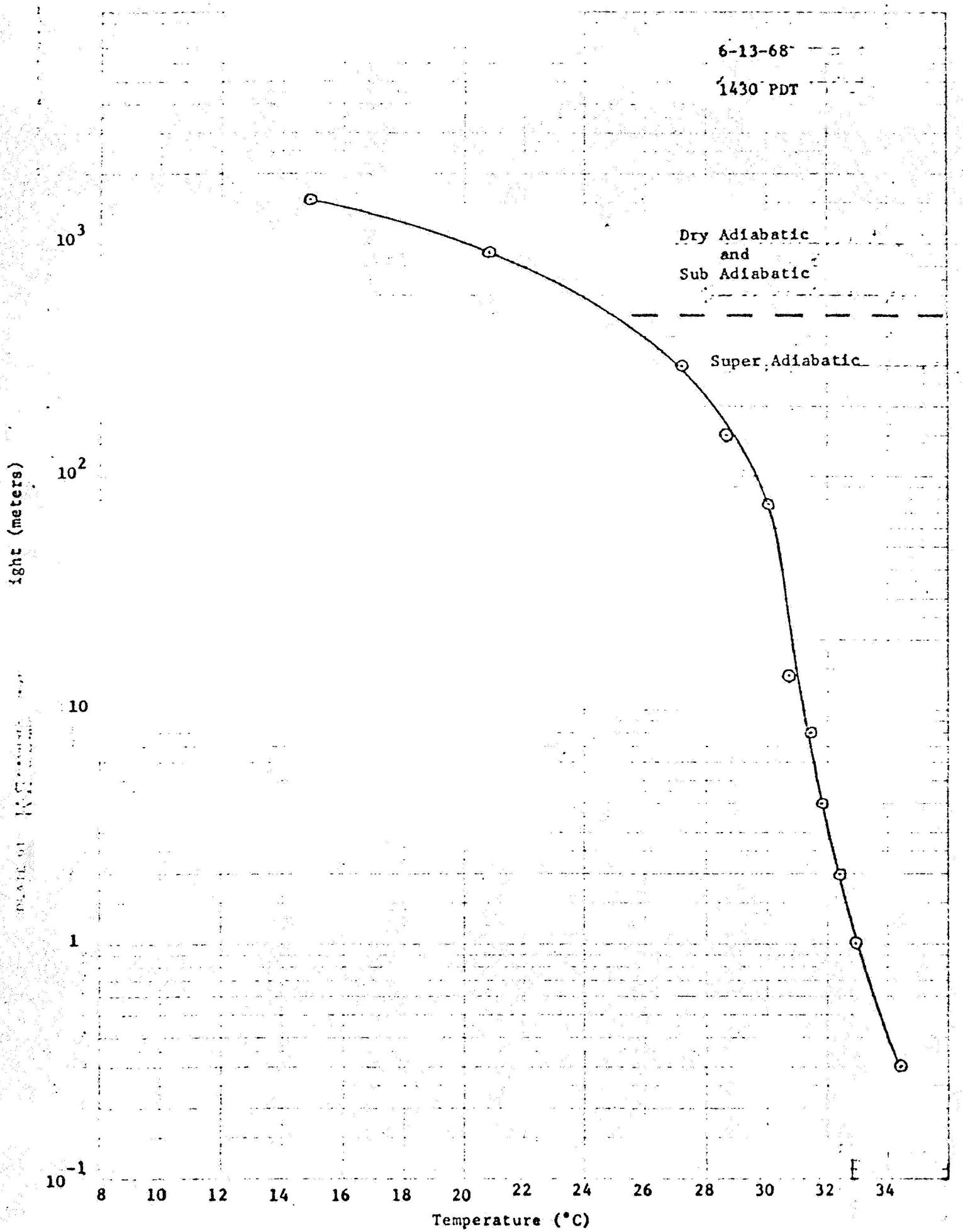
6-13-68
1430 PDT
Dry Adiabatic
and
Sub Adiabatic
Super Adiabatic
10^3
10^2
10
1
10^{-1}
ight (meters)
8
10
12
14
16
18
20
22
24
26
28
30
32
34
Temperature (°C)

TEMPERATURE DATA FOR JUNE 26, 1968

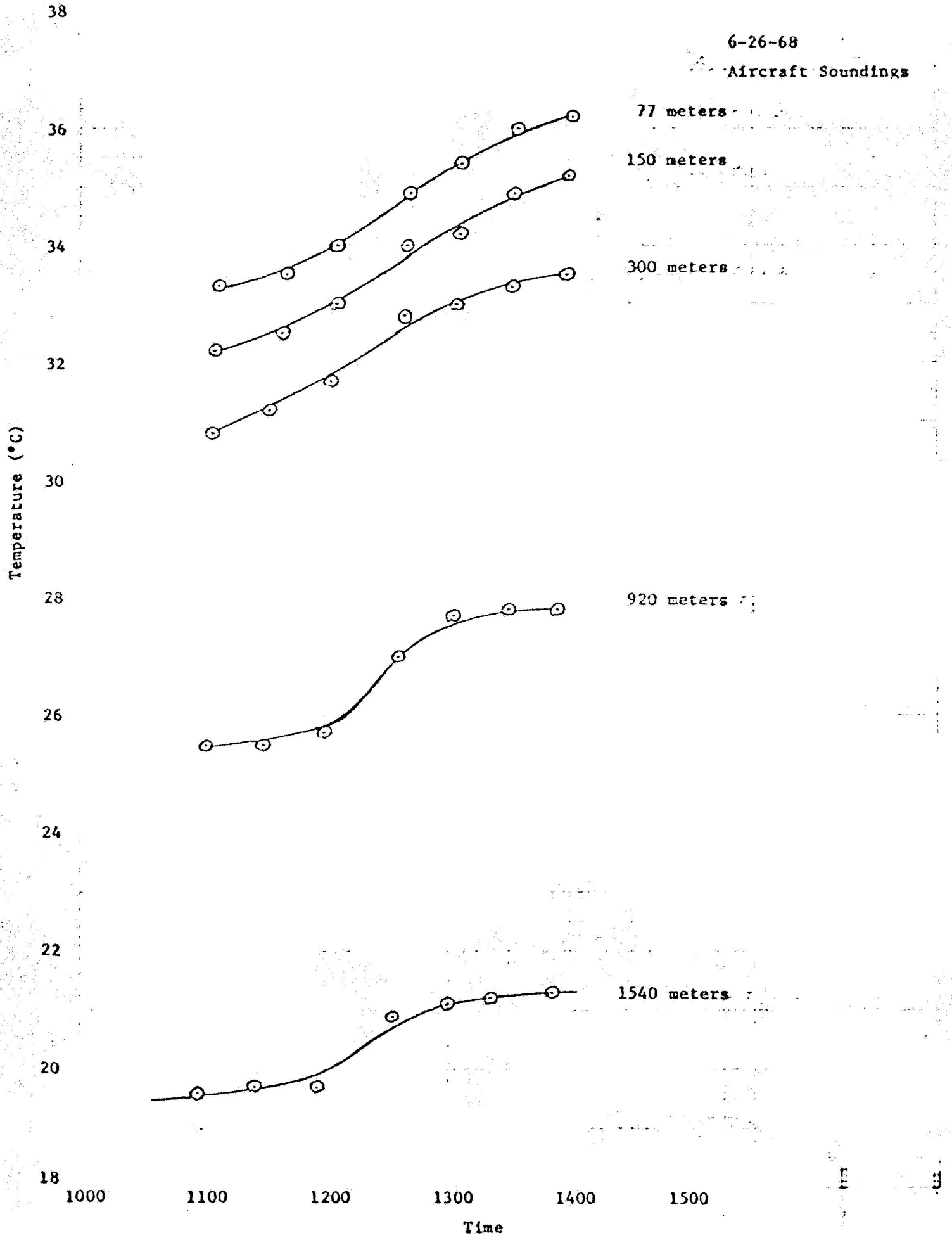
6-26-68
Aircraft Soundings
77 meters
150 meters
300 meters
920 meters
1540 meters
Temperature (°C)
38
36
34
32
30
28
26
24
22
20
18
1000
1100
1200
1300
1400
1500
Time

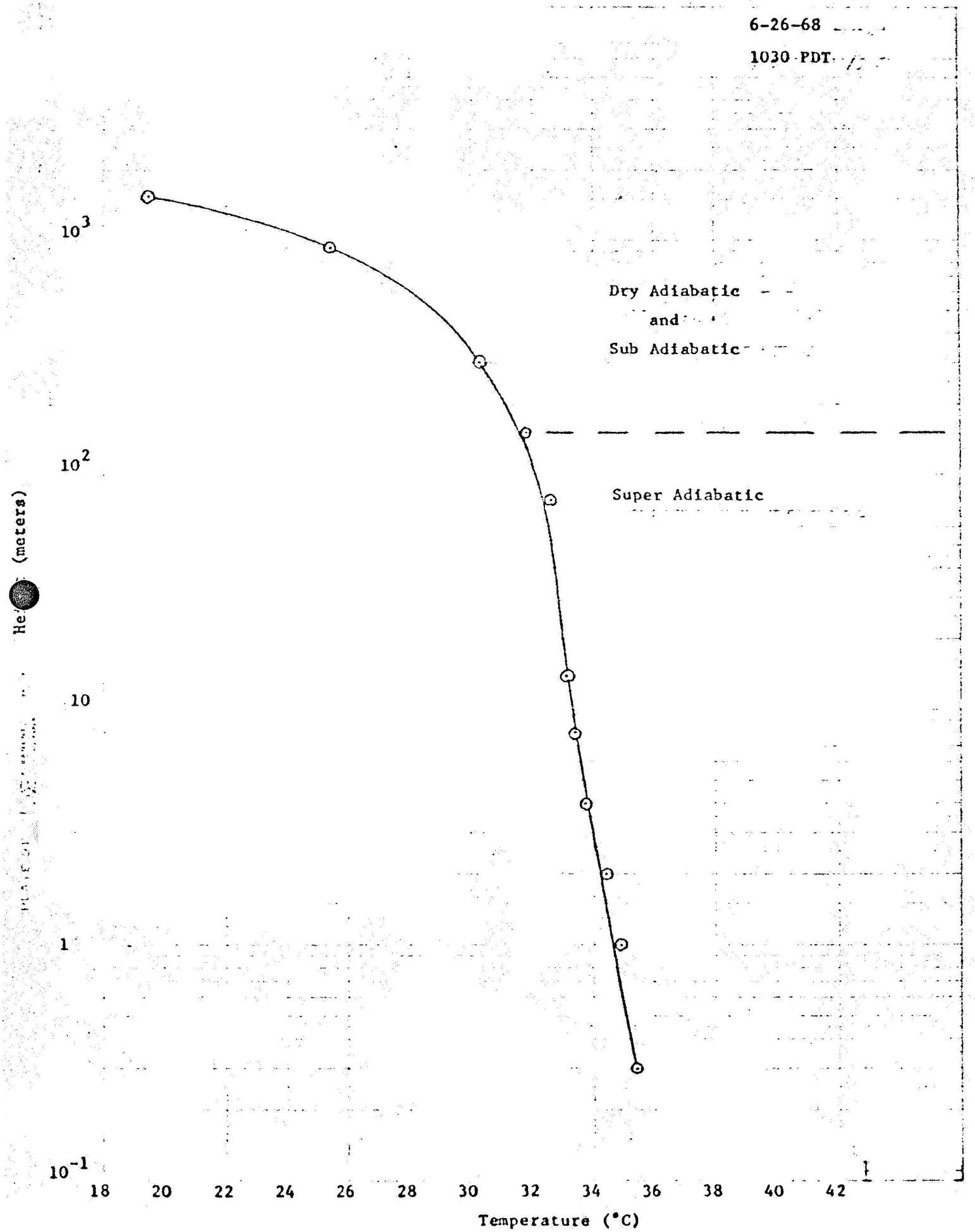
6-26-68
1030 PDT
Dry Adiabatic
and
Sub Adiabatic
Super Adiabatic
10^3
10^2
10
1
10^{-1}
Height (meters)
18
20
22
24
26
28
30
32
34
36
38
40
42
Temperature (°C)

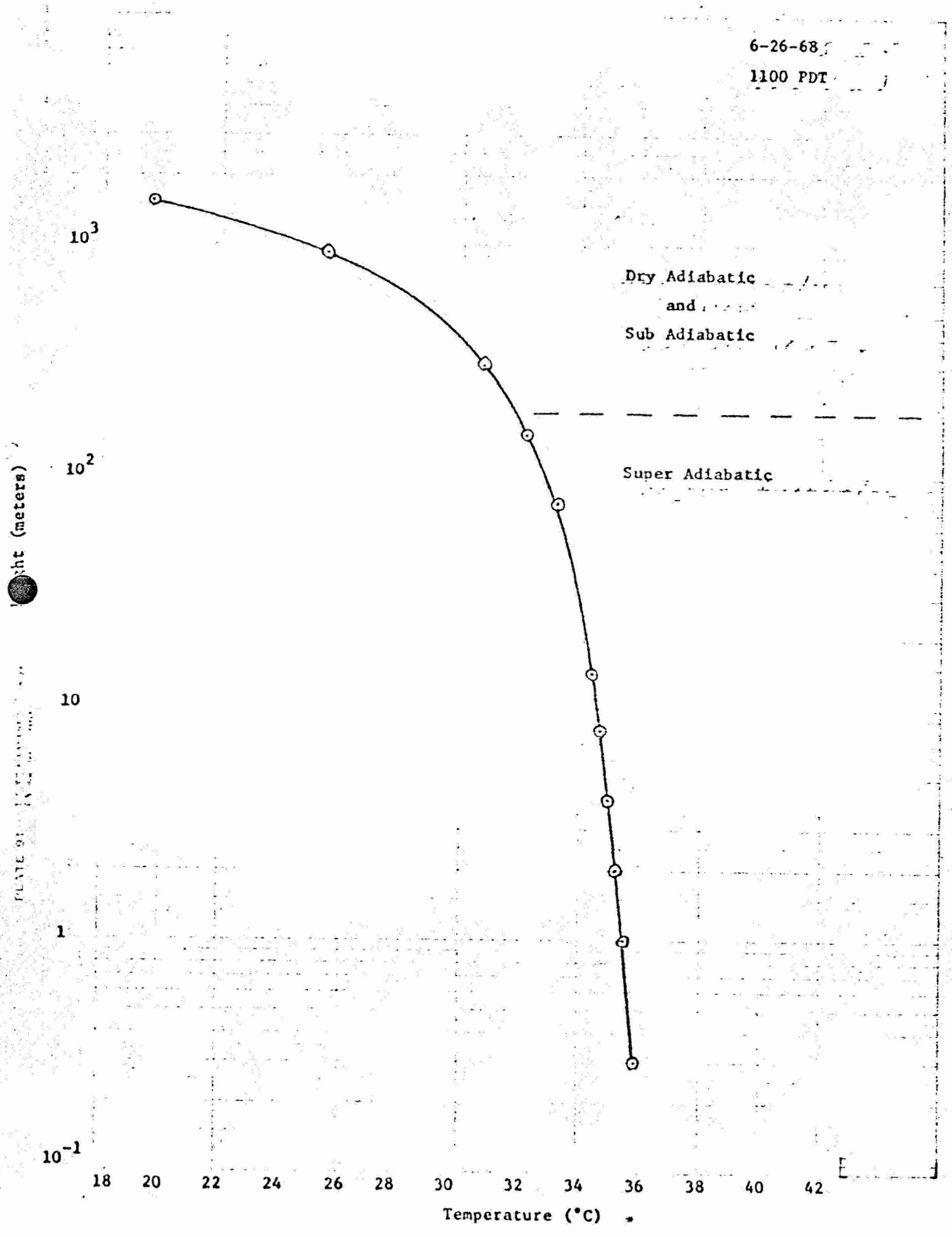
6-26-68
1100 PDT
Dry Adiabatic
and
Sub Adiabatic
Super Adiabatic
10^3
10^2
10
1
10^{-1}
ht (meters)
18
20
22
24
26
28
30
32
34
36
38
40
42
Temperature (°C)

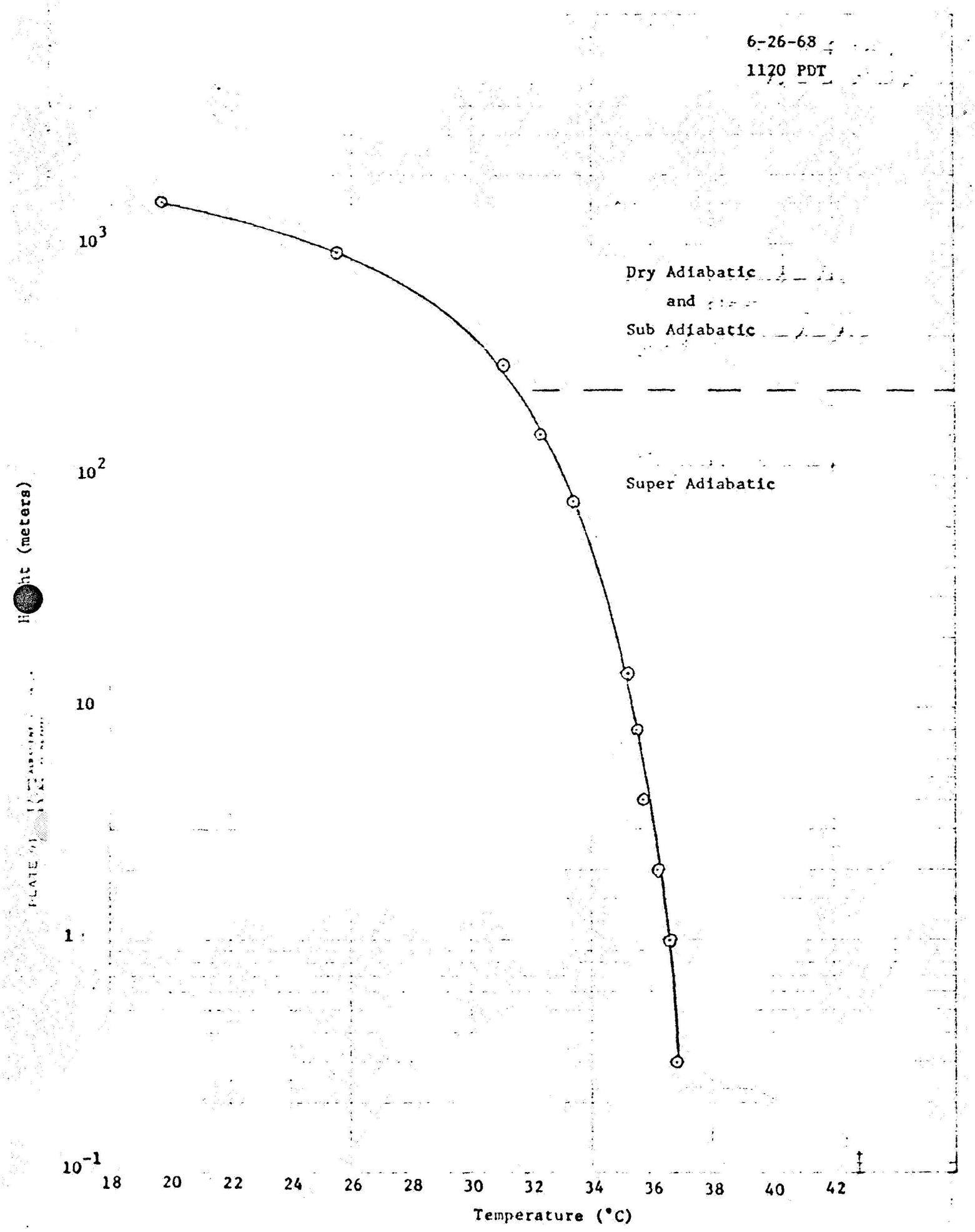
6-26-68
1120 PDT
Dry Adiabatic
and
Sub Adiabatic
Super Adiabatic
10^3
10^2
10
1
10^{-1}
ht (meters)
18
20
22
24
26
28
30
32
34
36
38
40
42
Temperature (°C)

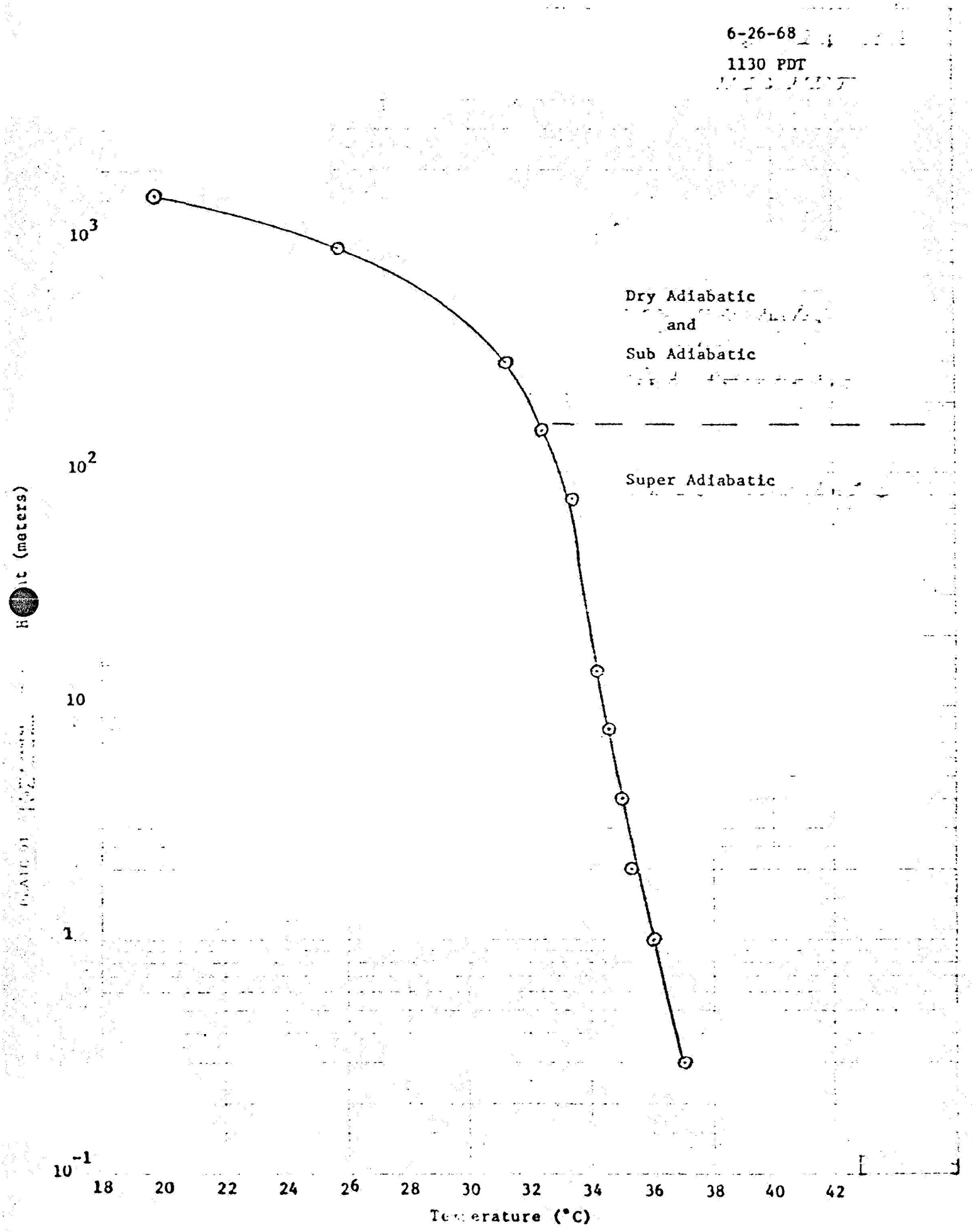
6-26-68
1130 PDT
Dry Adiabatic
and
Sub Adiabatic
Super Adiabatic
10^3
10^2
10
1
10^{-1}
18
20
22
24
26
28
30
32
34
36
38
40
42
Temperature (°C)

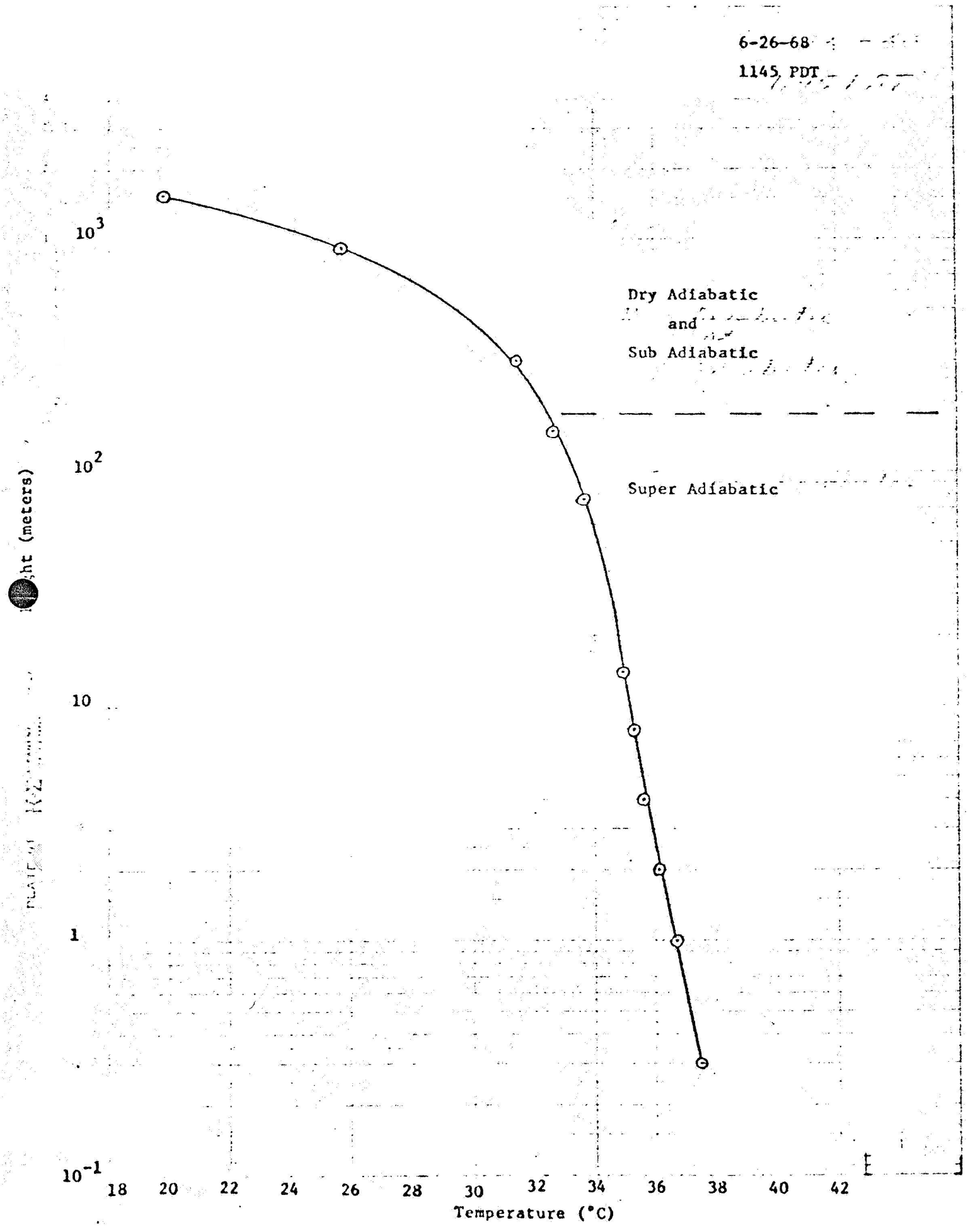
6-26-68
1145 PDT
Dry Adiabatic
and
Sub Adiabatic
Super Adiabatic
10^3
10^2
10
1
10^{-1}
ht (meters)
18
20
22
24
26
28
30
32
34
36
38
40
42
Temperature (°C)

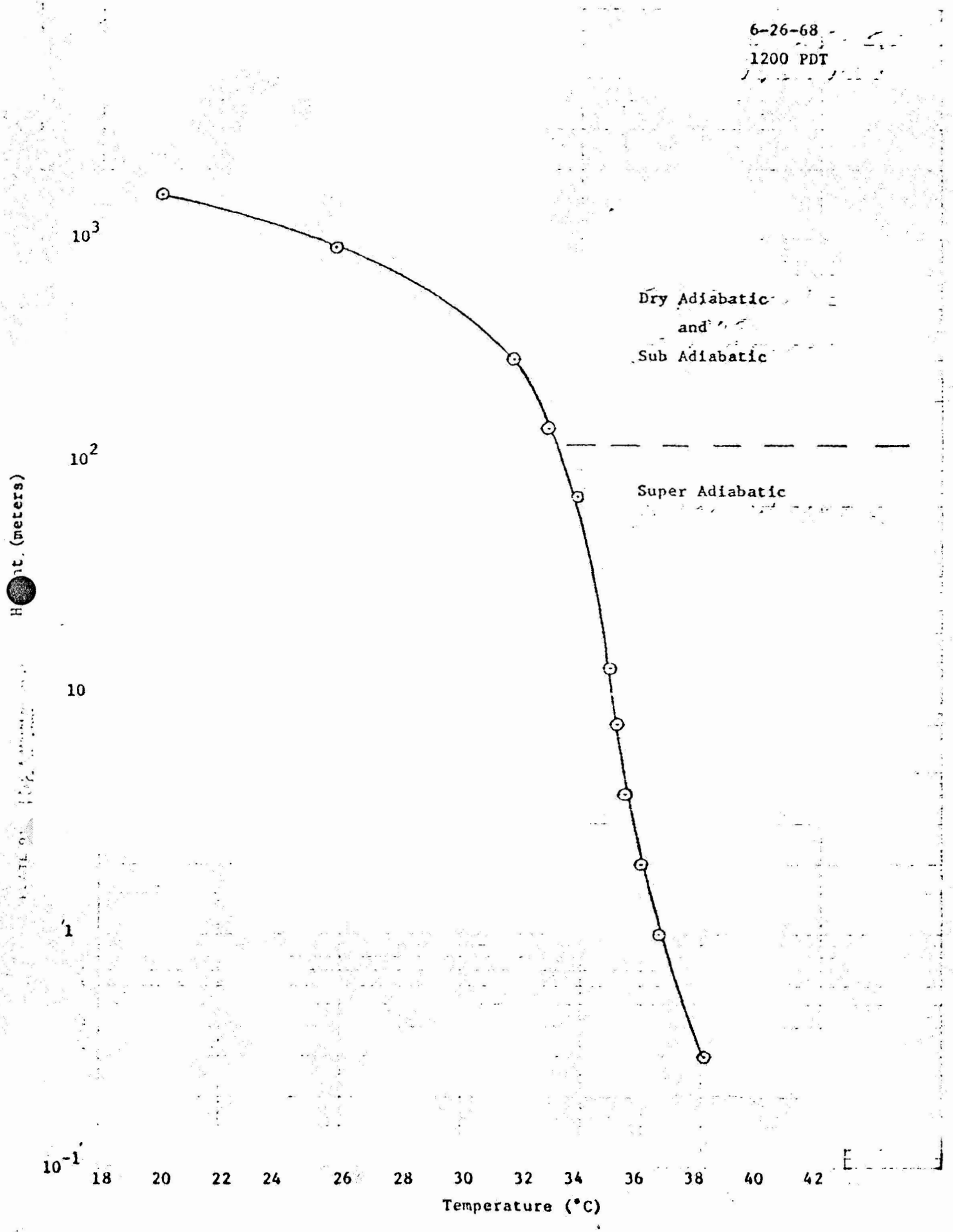
6-26-68
1200 PDT
Dry Adiabatic
and
Sub Adiabatic
Super Adiabatic
10^3
10^2
10
1
10^{-1}
Height (meters)
18
20
22
24
26
28
30
32
34
36
38
40
42
Temperature (°C)

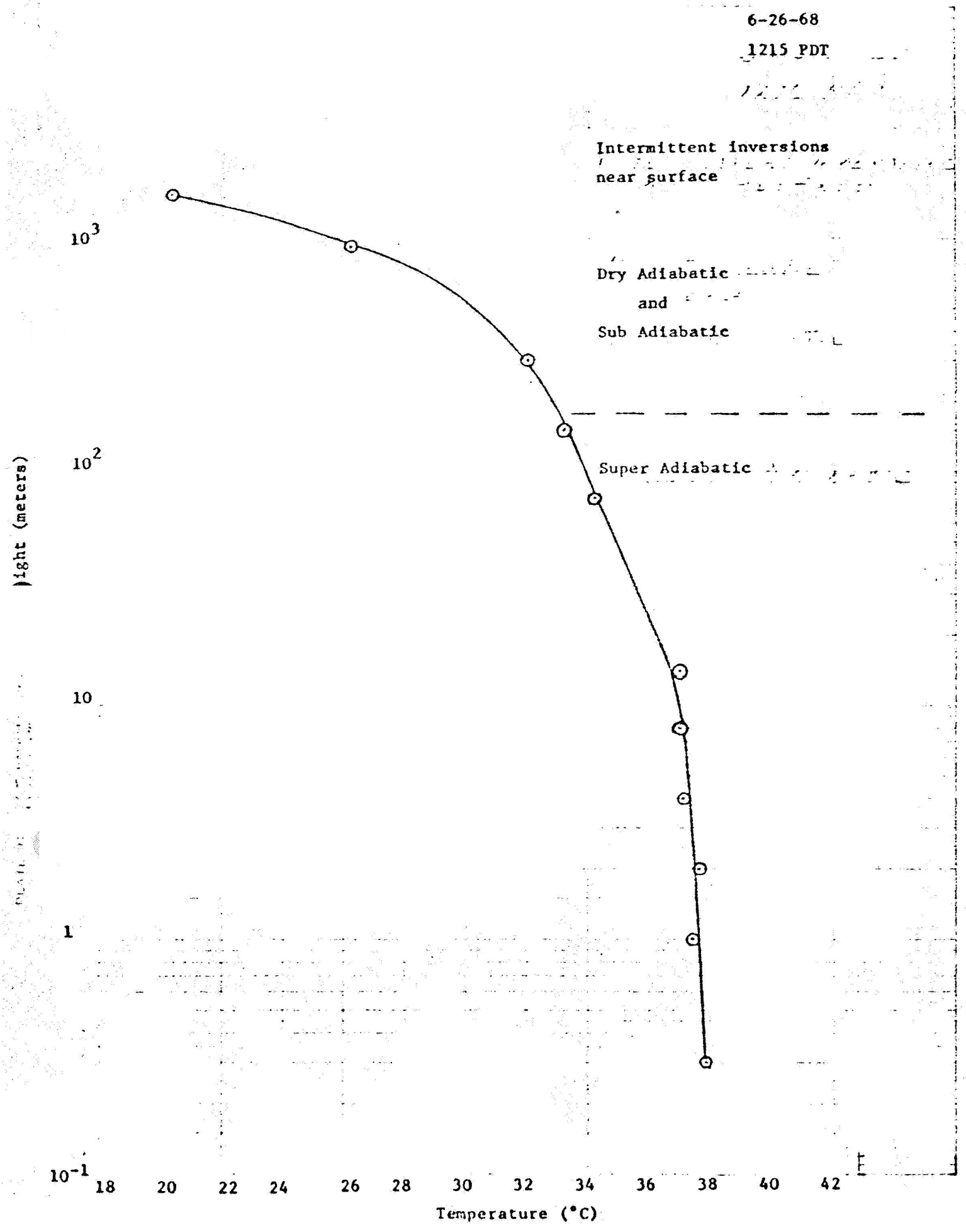
6-26-68
1215 PDT
Intermittent inversions
near surface
Dry Adiabatic
and
Sub Adiabatic
Super Adiabatic
10^3
10^2
10
1
10^{-1}
ight (meters)
18
20
22
24
26
28
30
32
34
36
38
40
42
Temperature (°C)

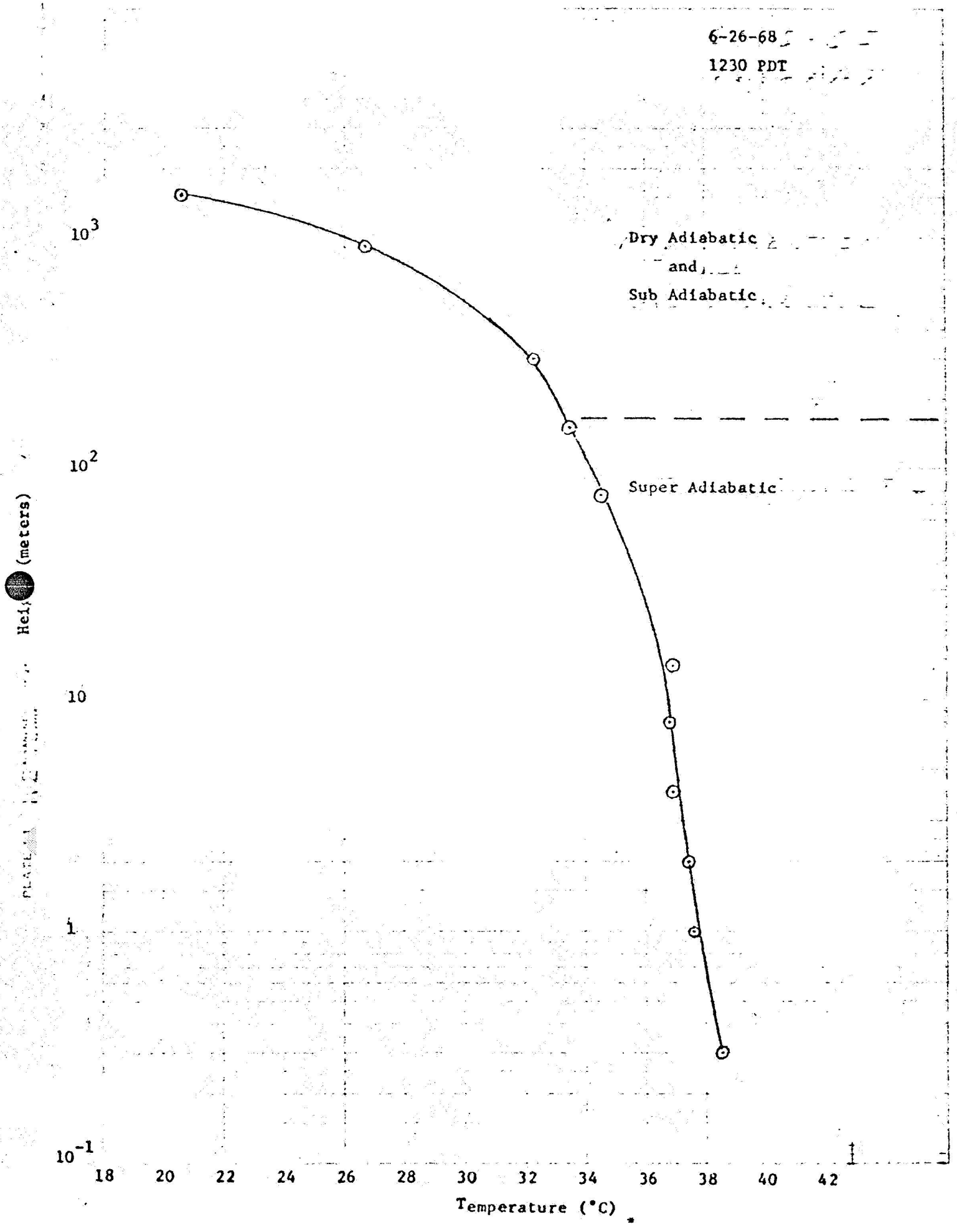
6-26-68
1230 PDT
Dry Adiabatic
and
Sub Adiabatic
Super Adiabatic
10^3
10^2
10
1
10^{-1}
Height (meters)
18
20
22
24
26
28
30
32
34
36
38
40
42
Temperature (°C)

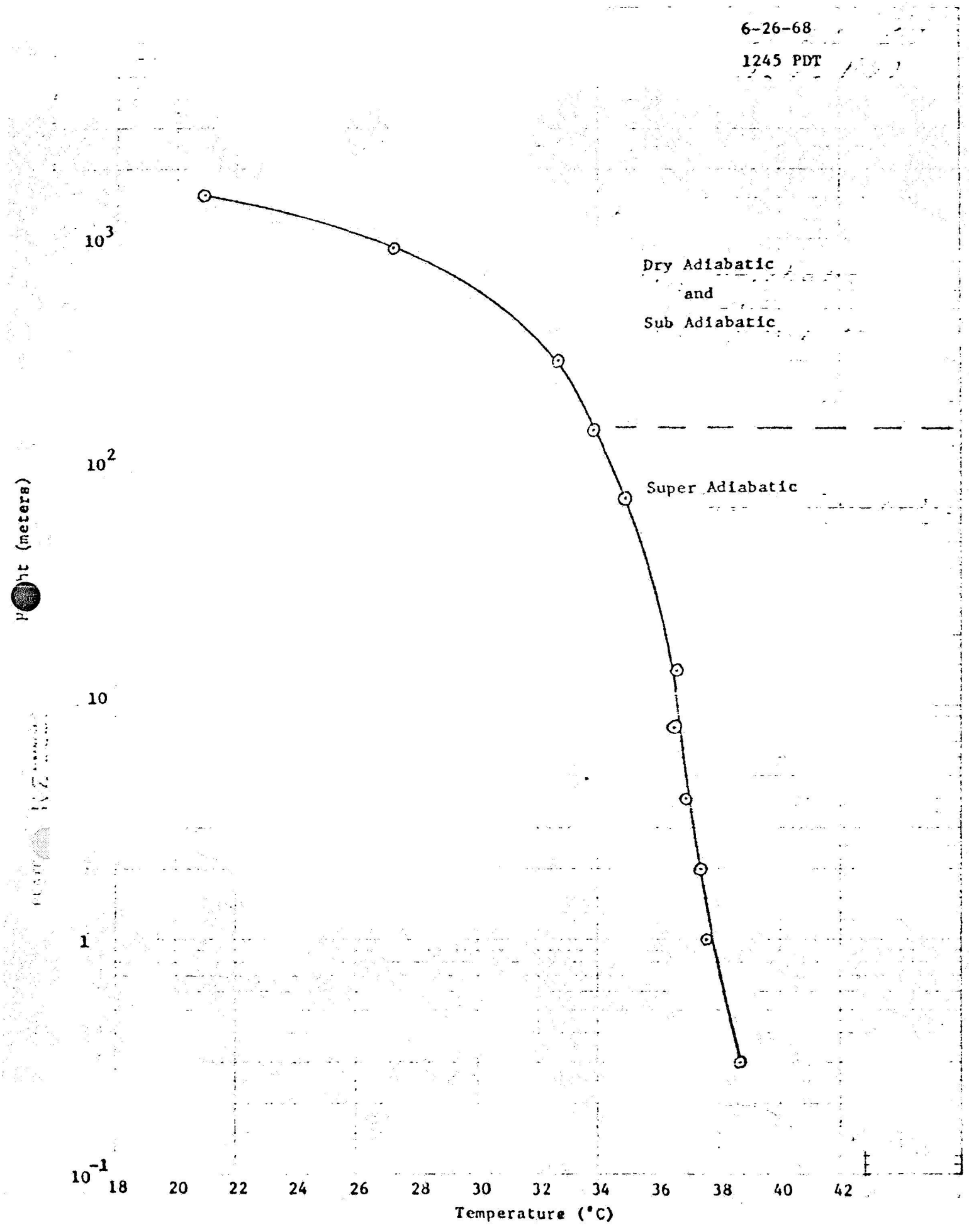
6-26-68
1245 PDT
Dry Adiabatic
and
Sub Adiabatic
Super Adiabatic
10^3
10^2
10
1
10^{-1}
18
20
22
24
26
28
30
32
34
36
38
40
42
Temperature (°C)

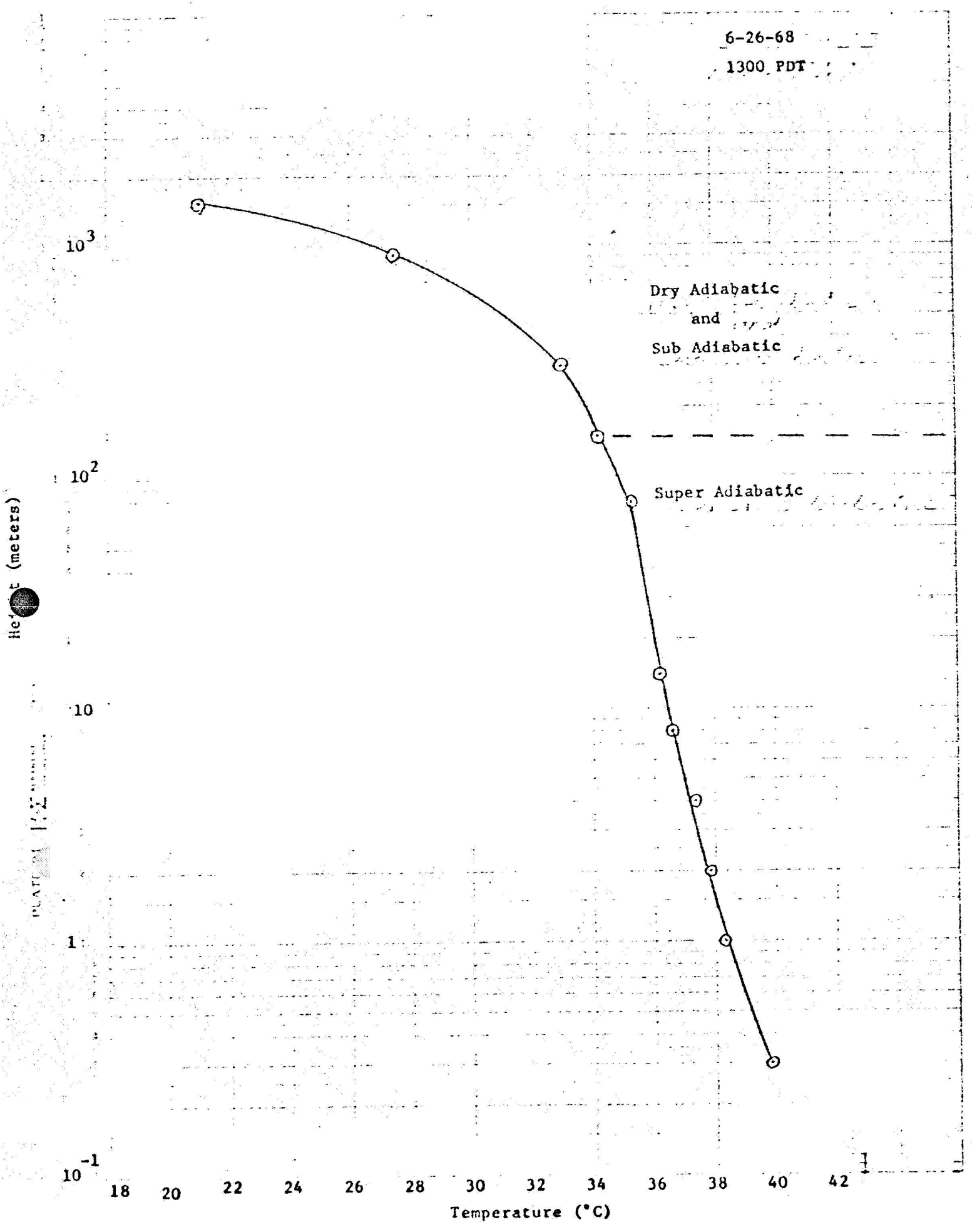
6-26-68
1300 PDT
Dry Adiabatic
and
Sub Adiabatic
Super Adiabatic
Height (meters)
10^3
10^2
10
1
10^{-1}
18
20
22
24
26
28
30
32
34
36
38
40
42
Temperature (°C)

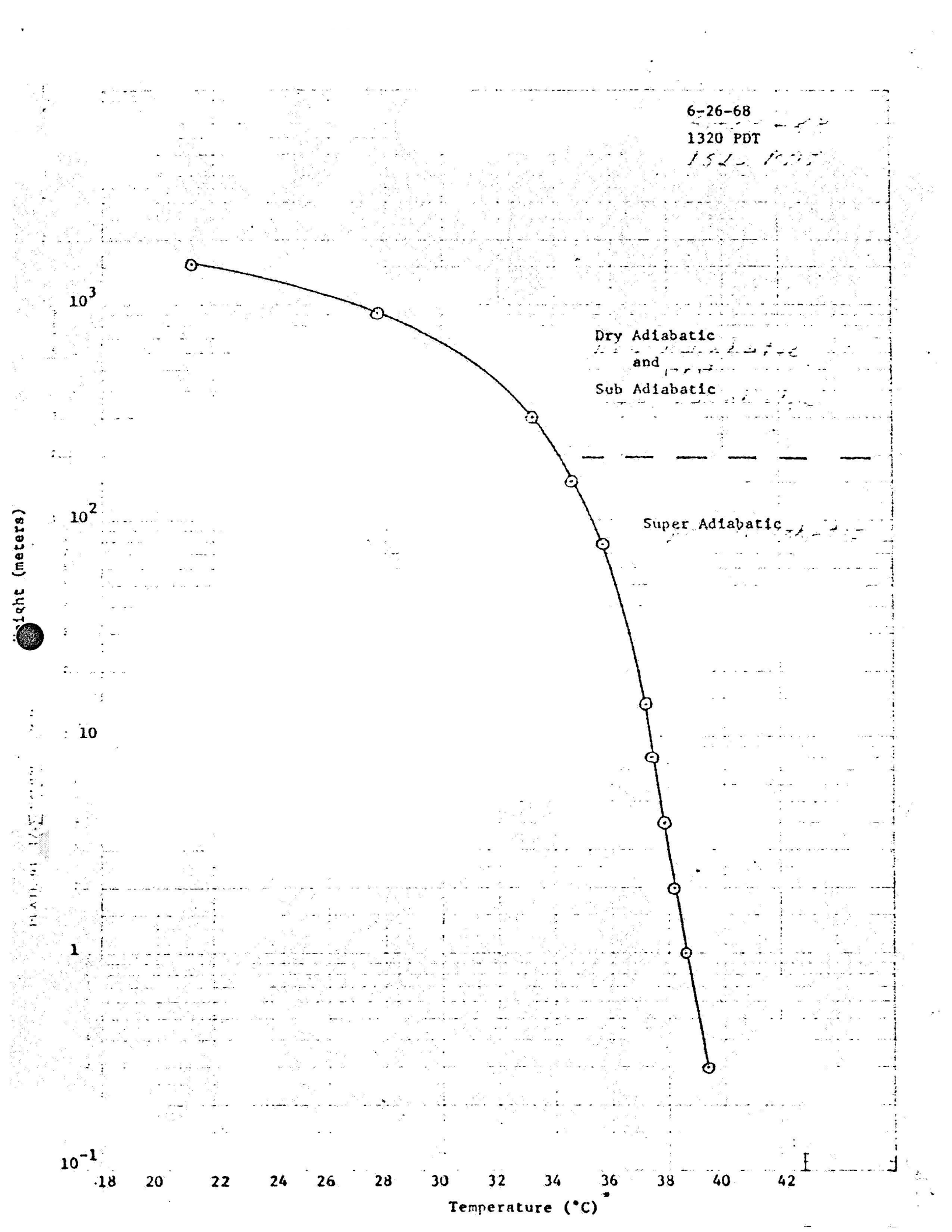
6-26-68
1320 PDT
Dry Adiabatic
and
Sub Adiabatic
Super Adiabatic
10^3
10^2
10
1
10^{-1}
Height (meters)
18
20
22
24
26
28
30
32
34
36
38
40
42
Temperature (°C)

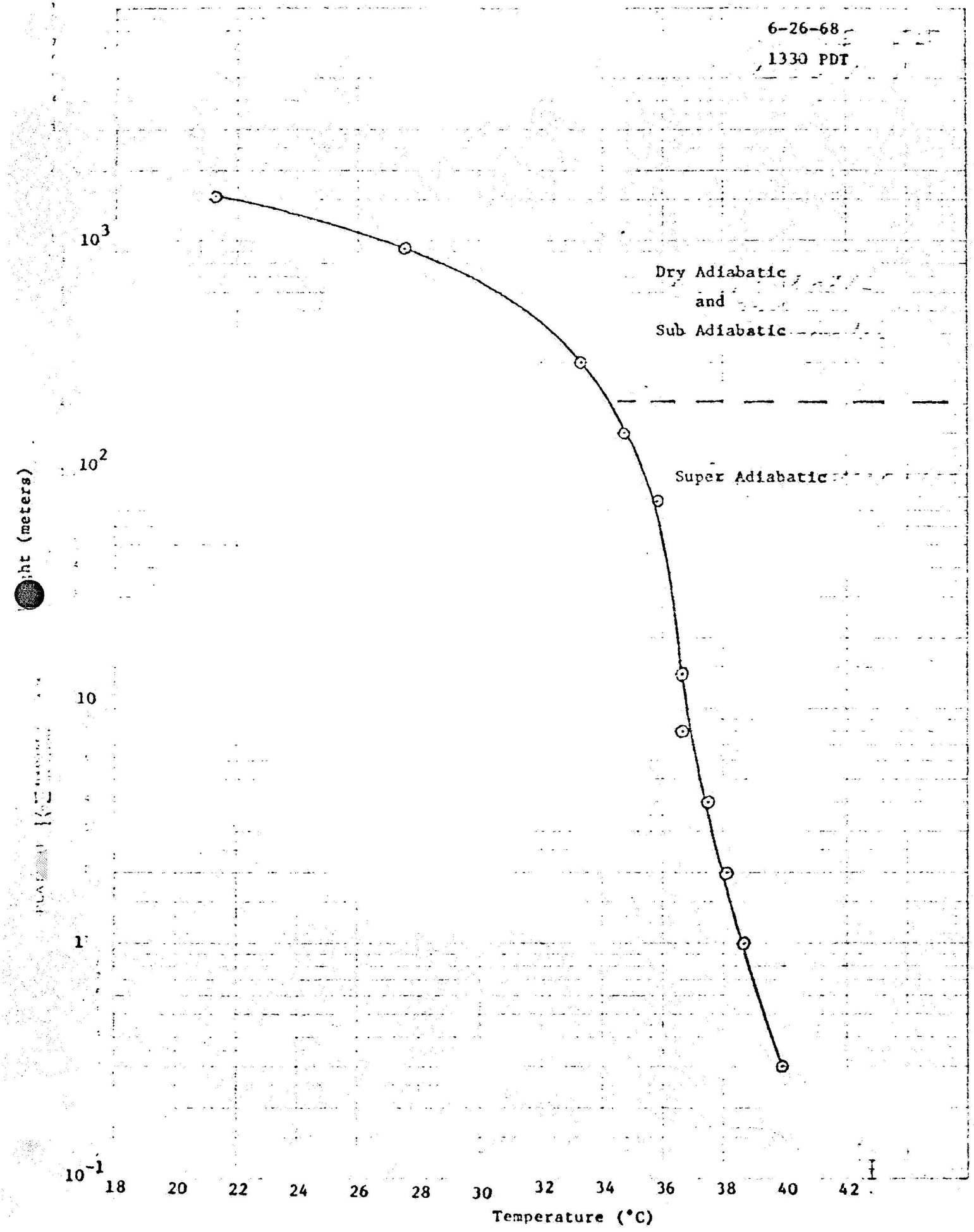
6-26-68
1330 PDT
Dry Adiabatic
and
Sub Adiabatic
Super Adiabatic
10^3
10^2
10
1
10^{-1}
ht (meters)
18
20
22
24
26
28
30
32
34
36
38
40
42
Temperature (°C)

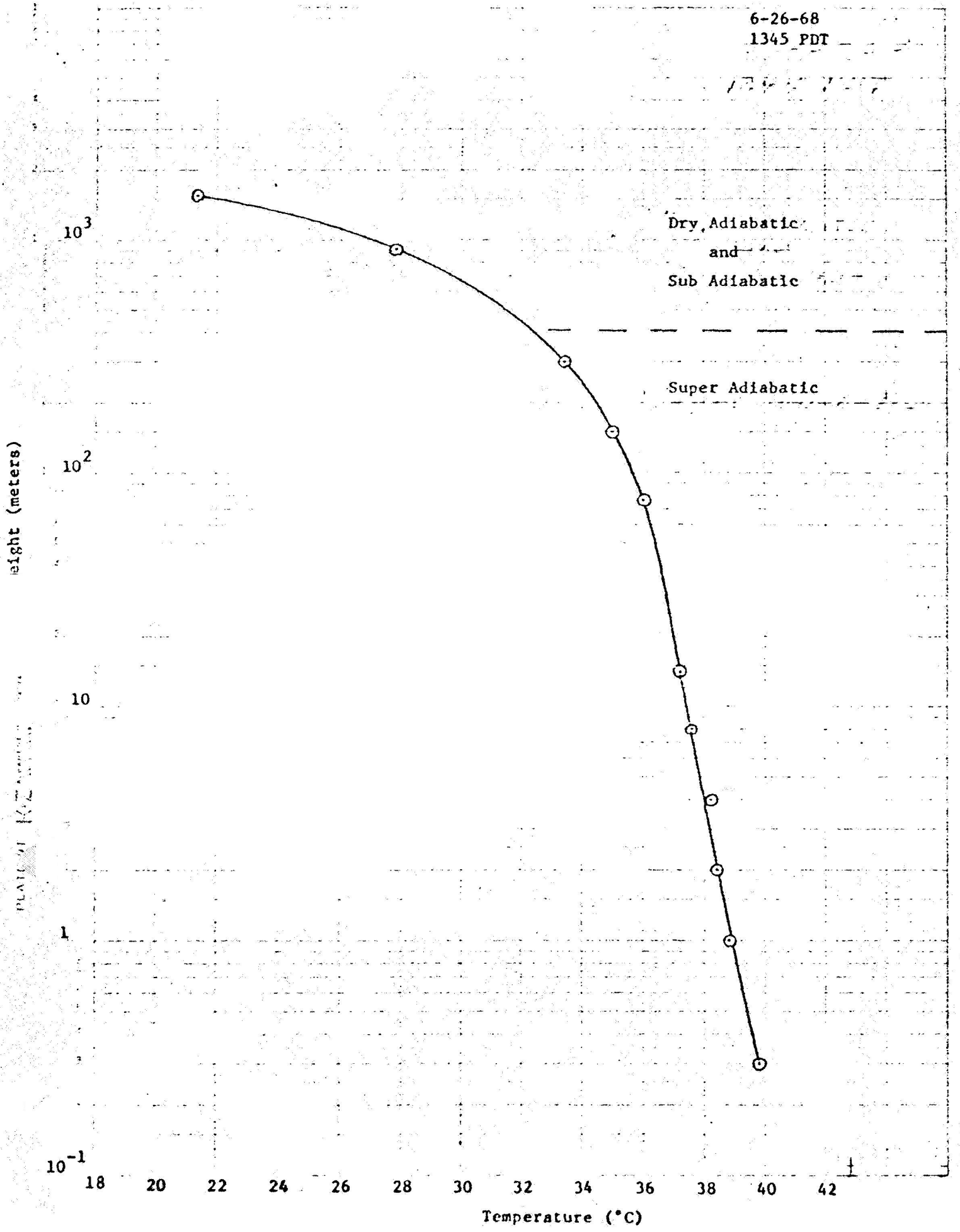
6-26-68
1345 PDT
Dry Adiabatic
and
Sub Adiabatic
Super Adiabatic
10^3
10^2
10
1
10^{-1}
eight (meters)
18
20
22
24
26
28
30
32
34
36
38
40
42
Temperature (°C)

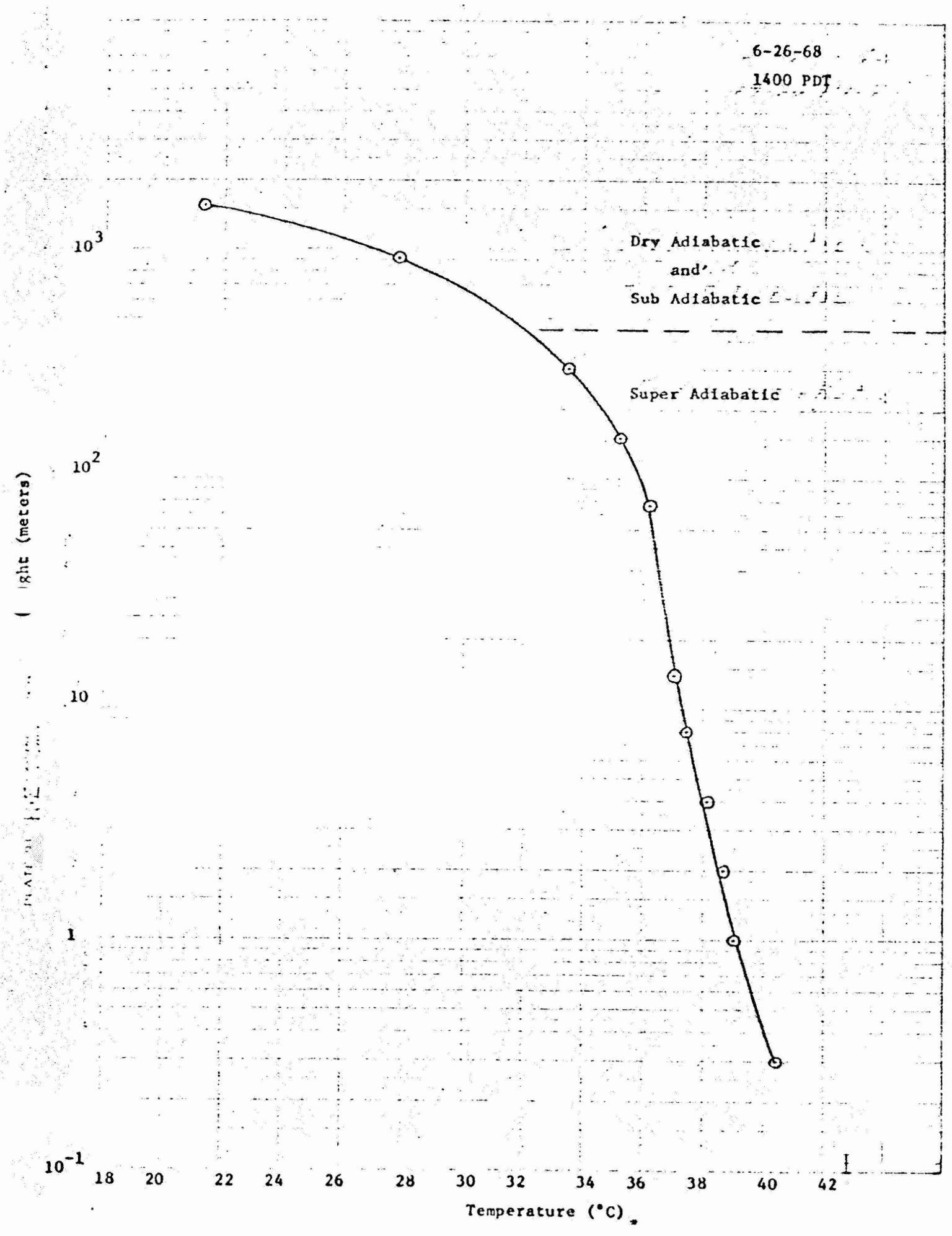
6-26-68
1400 PDT
Dry Adiabatic
and
Sub Adiabatic
Super Adiabatic
10^3
10^2
10
1
10^{-1}
ght (meters)
18
20
22
24
26
28
30
32
34
36
38
40
42
Temperature (°C)

TEMPERATURE DATA FOR JUNE 27, 1968

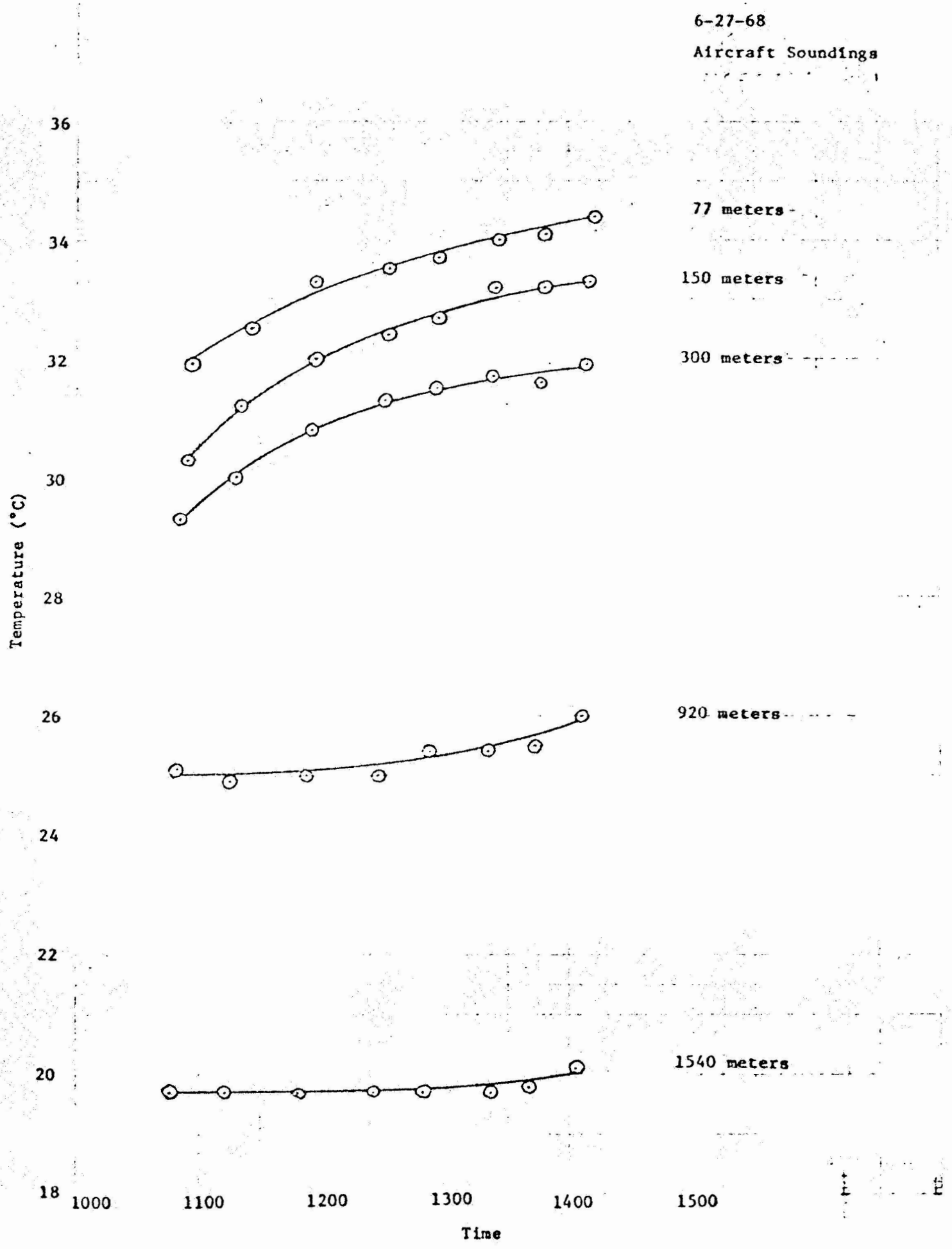
6-27-68
Aircraft Soundings
77 meters
150 meters
300 meters
920 meters
1540 meters
Temperature (°C)
36
34
32
30
28
26
24
22
20
18
1000
1100
1200
1300
1400
1500
Time

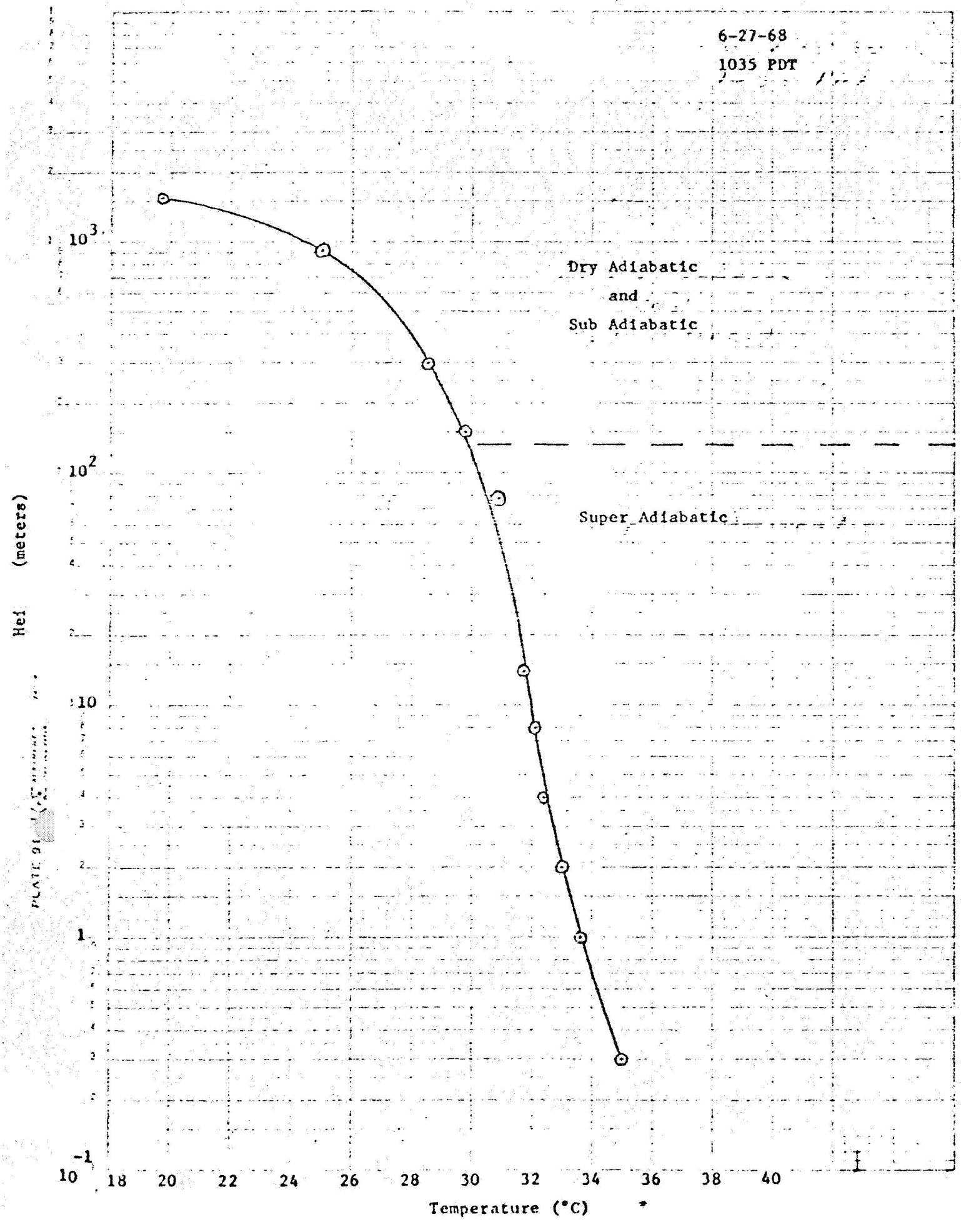
6-27-68
1035 PDT
Dry Adiabatic
and
Sub Adiabatic
Super Adiabatic
Hel (meters)
10^3
10^2
10
1
10^{-1}
18
20
22
24
26
28
30
32
34
36
38
40
Temperature (°C)

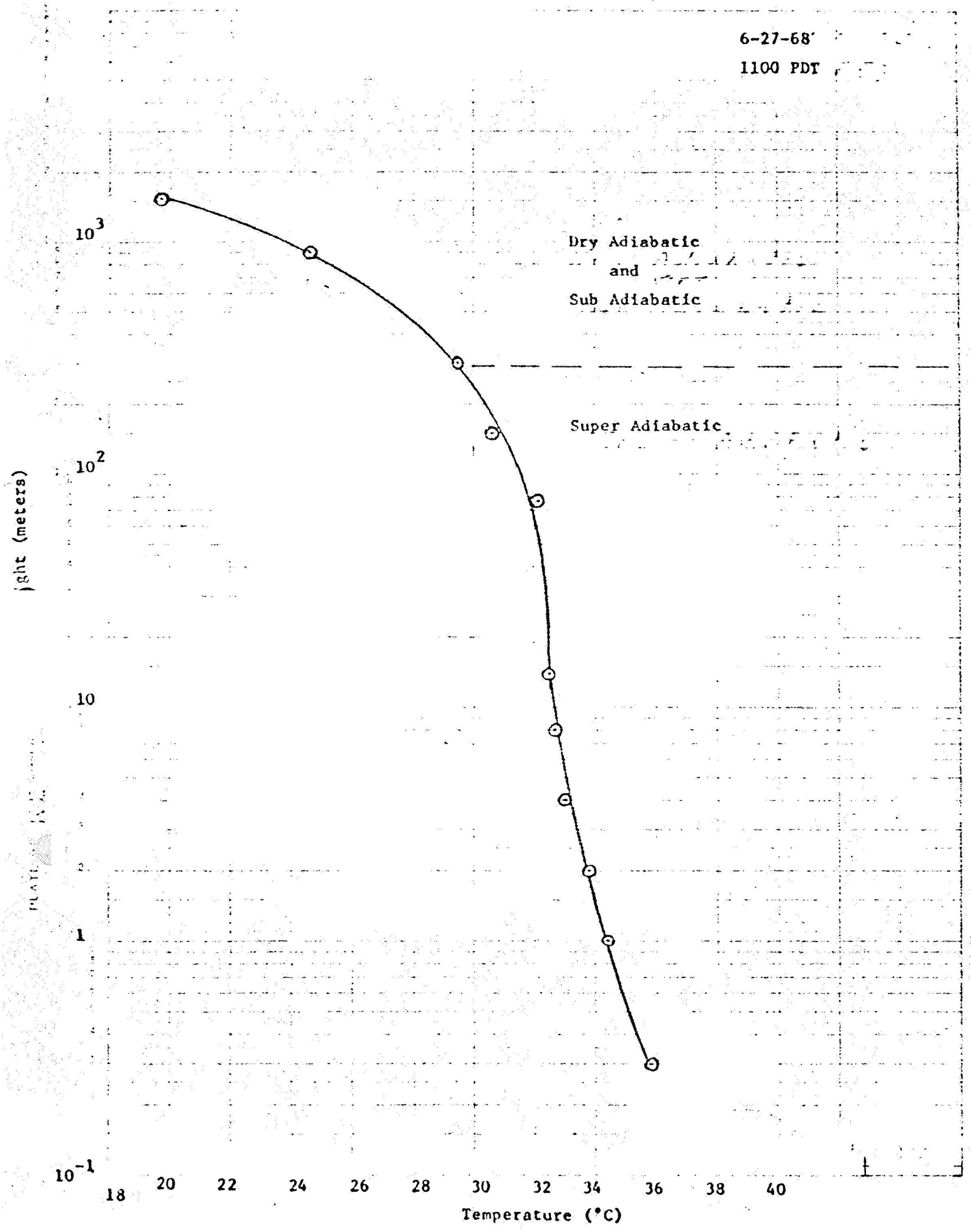
6-27-68
1100 PDT
Dry Adiabatic
and
Sub Adiabatic
Super Adiabatic
10^3
10^2
10
1
10^{-1}
ght (meters)
18
20
22
24
26
28
30
32
34
36
38
40
Temperature (°C)

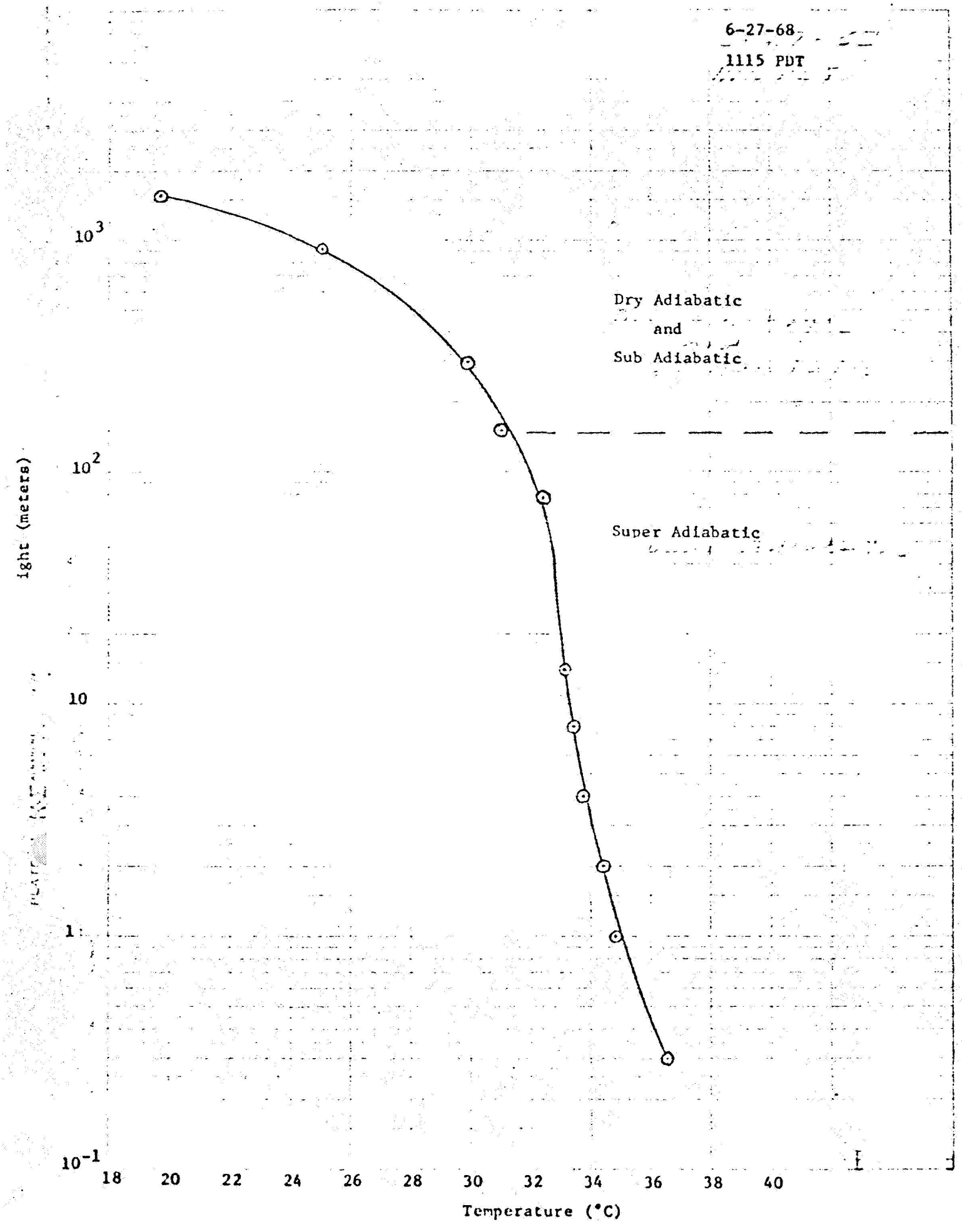
6-27-68
1115 PDT
Dry Adiabatic
and
Sub Adiabatic
Super Adiabatic
ight (meters)
10^3
10^2
10
1
10^{-1}
18
20
22
24
26
28
30
32
34
36
38
40
Temperature (°C)

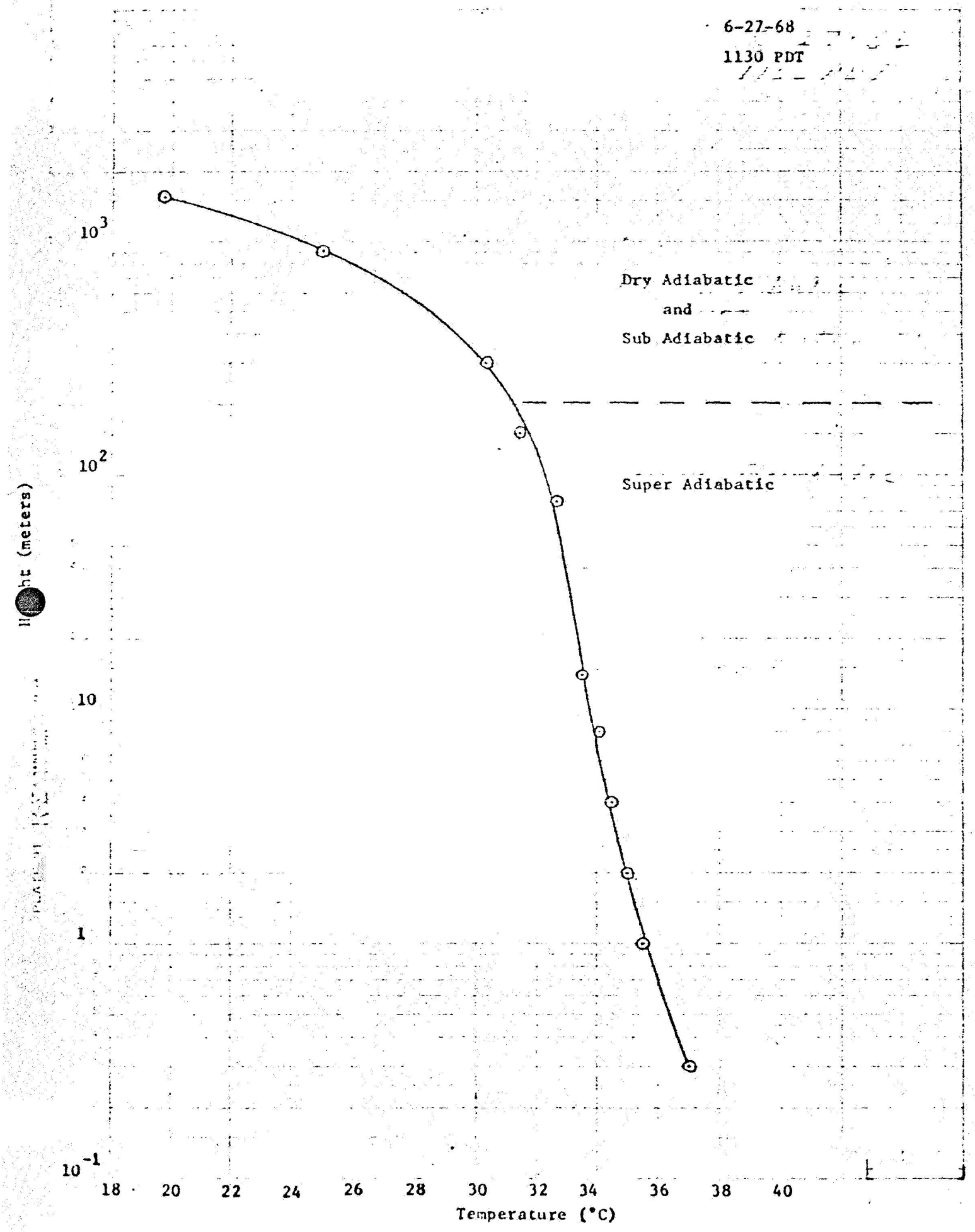
6-27-68
1130 PDT
Dry Adiabatic
and
Sub Adiabatic
Super Adiabatic
10^3
10^2
10
1
10^{-1}
Height (meters)
18
20
22
24
26
28
30
32
34
36
38
40
Temperature (°C)

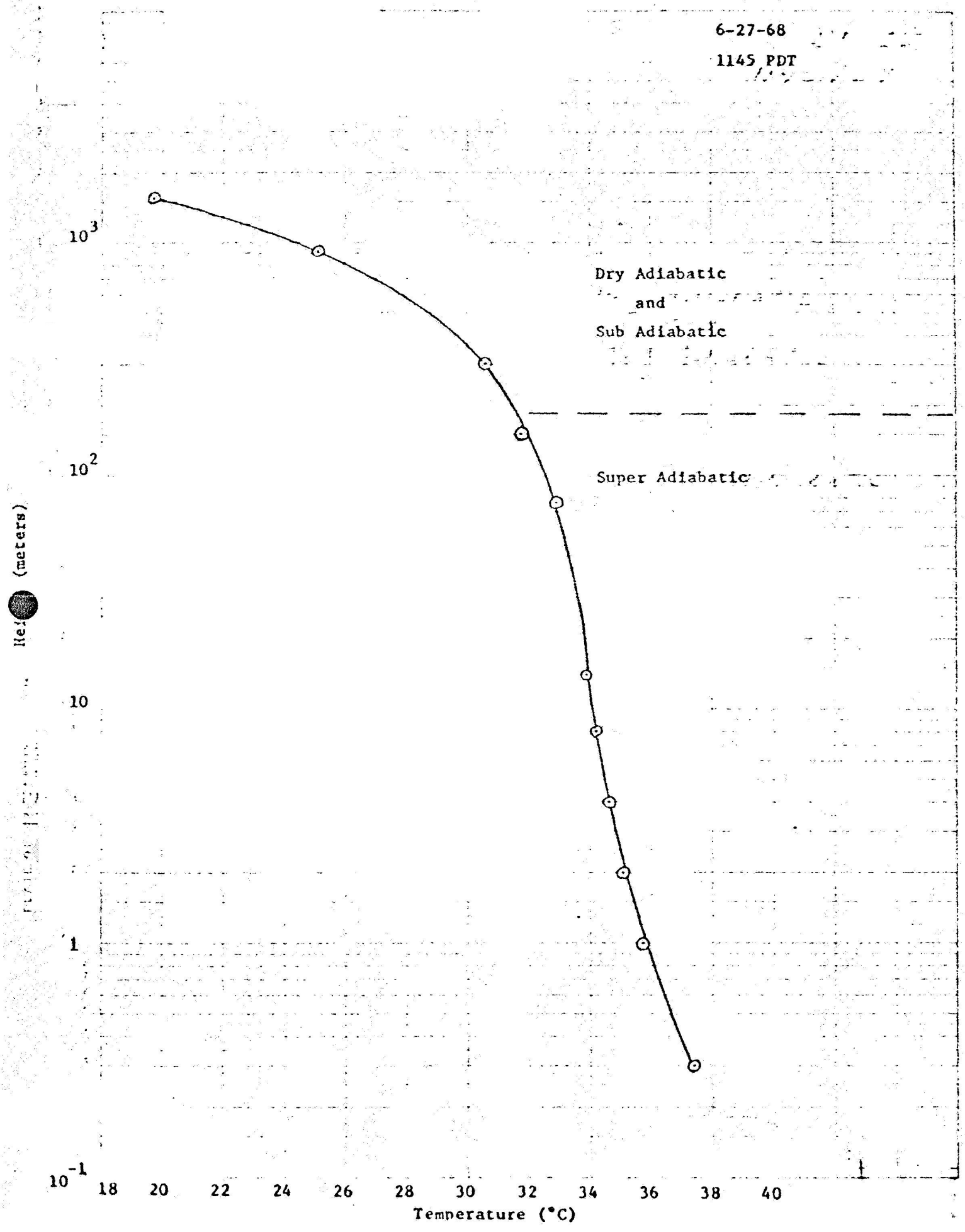
6-27-68
1145 PDT
Dry Adiabatic
and
Sub Adiabatic
Super Adiabatic
10^3
10^2
10
1
10^{-1}
(meters)
18
20
22
24
26
28
30
32
34
36
38
40
Temperature (°C)

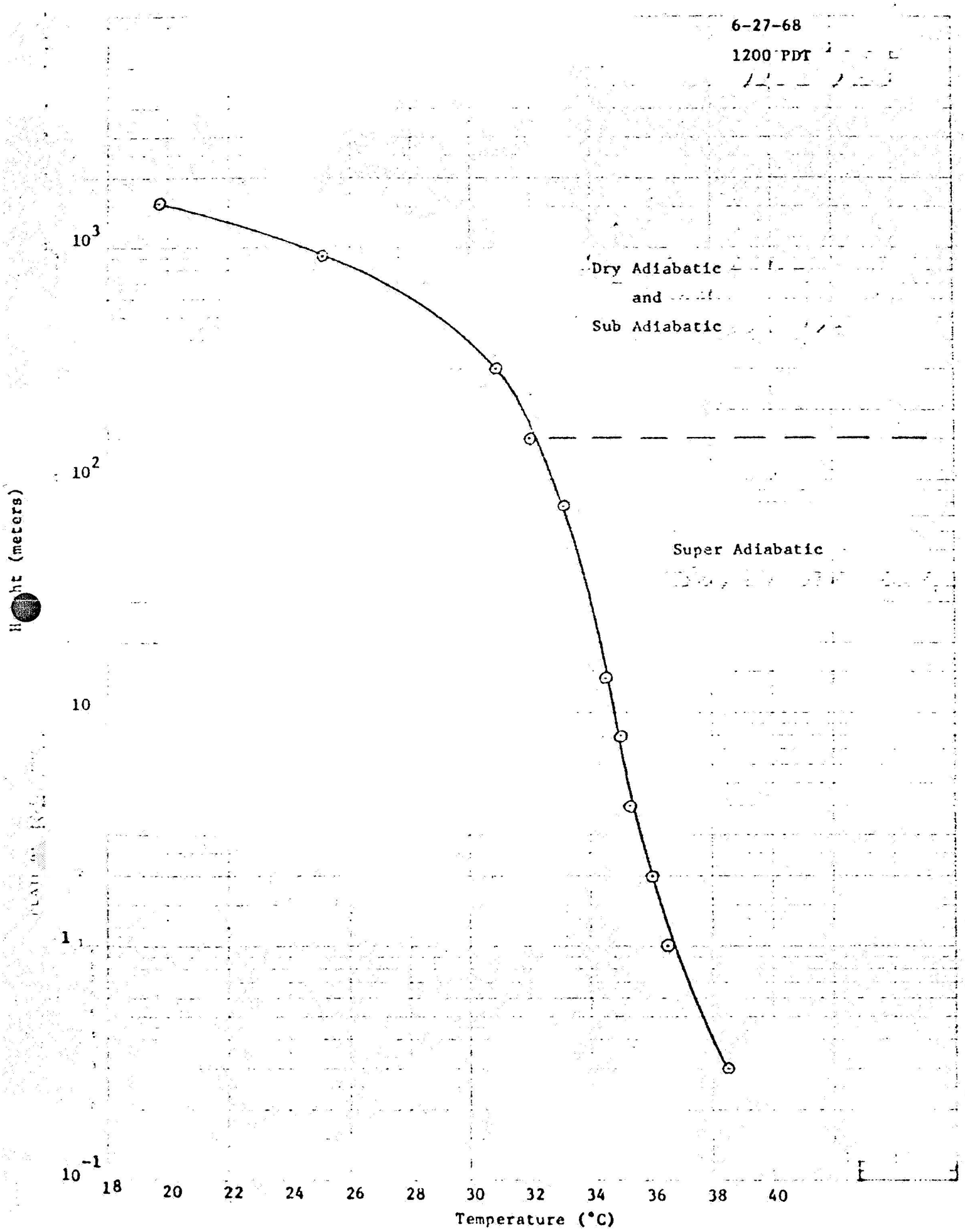
6-27-68
1200 PDT
Dry Adiabatic
and
Sub Adiabatic
Super Adiabatic
10^3
10^2
10
1
10^{-1}
Height (meters)
18
20
22
24
26
28
30
32
34
36
38
40
Temperature (°C)

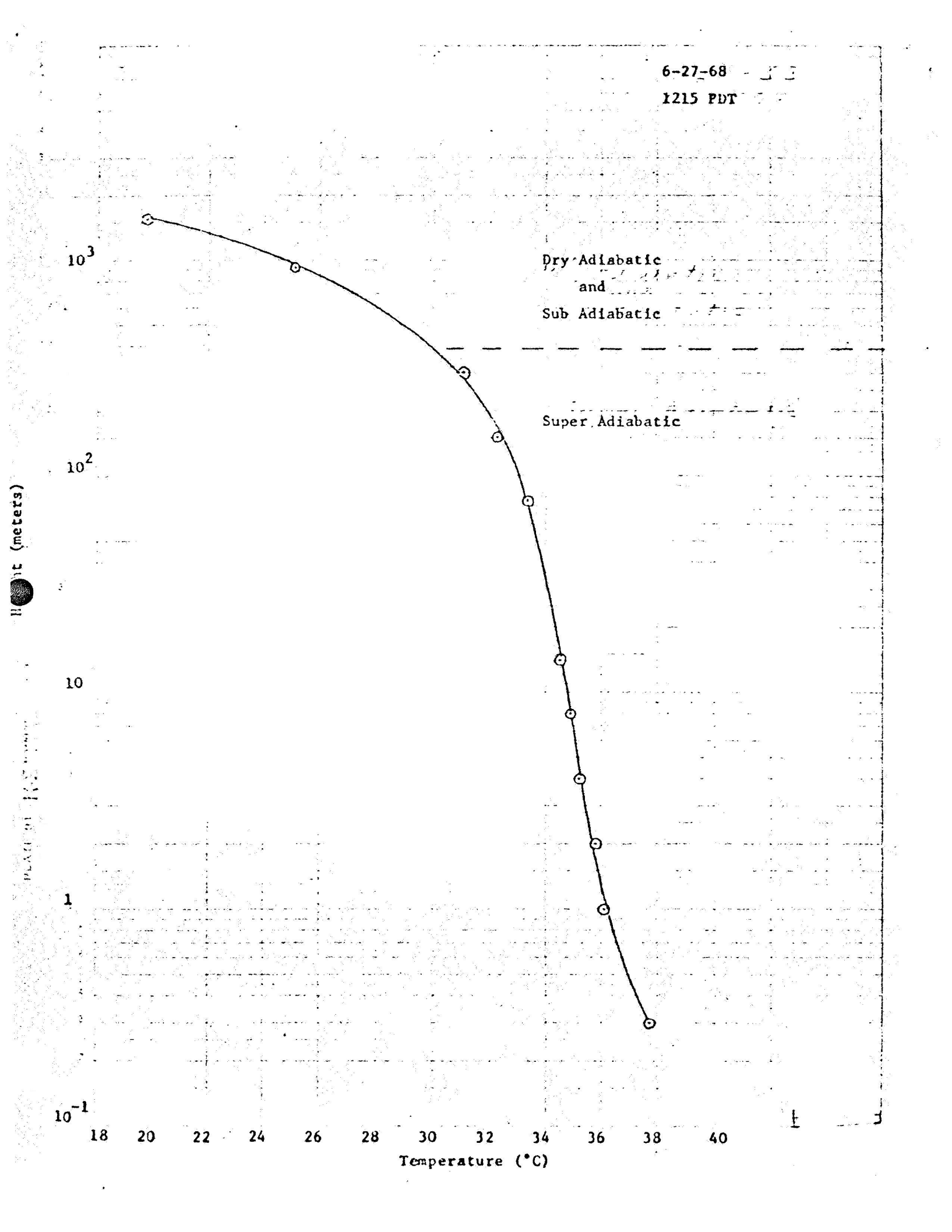
6-27-68
1215 PDT
Dry Adiabatic
and
Sub Adiabatic
Super Adiabatic
10^3
10^2
10
1
10^{-1}
Height (meters)
18
20
22
24
26
28
30
32
34
36
38
40
Temperature (°C)

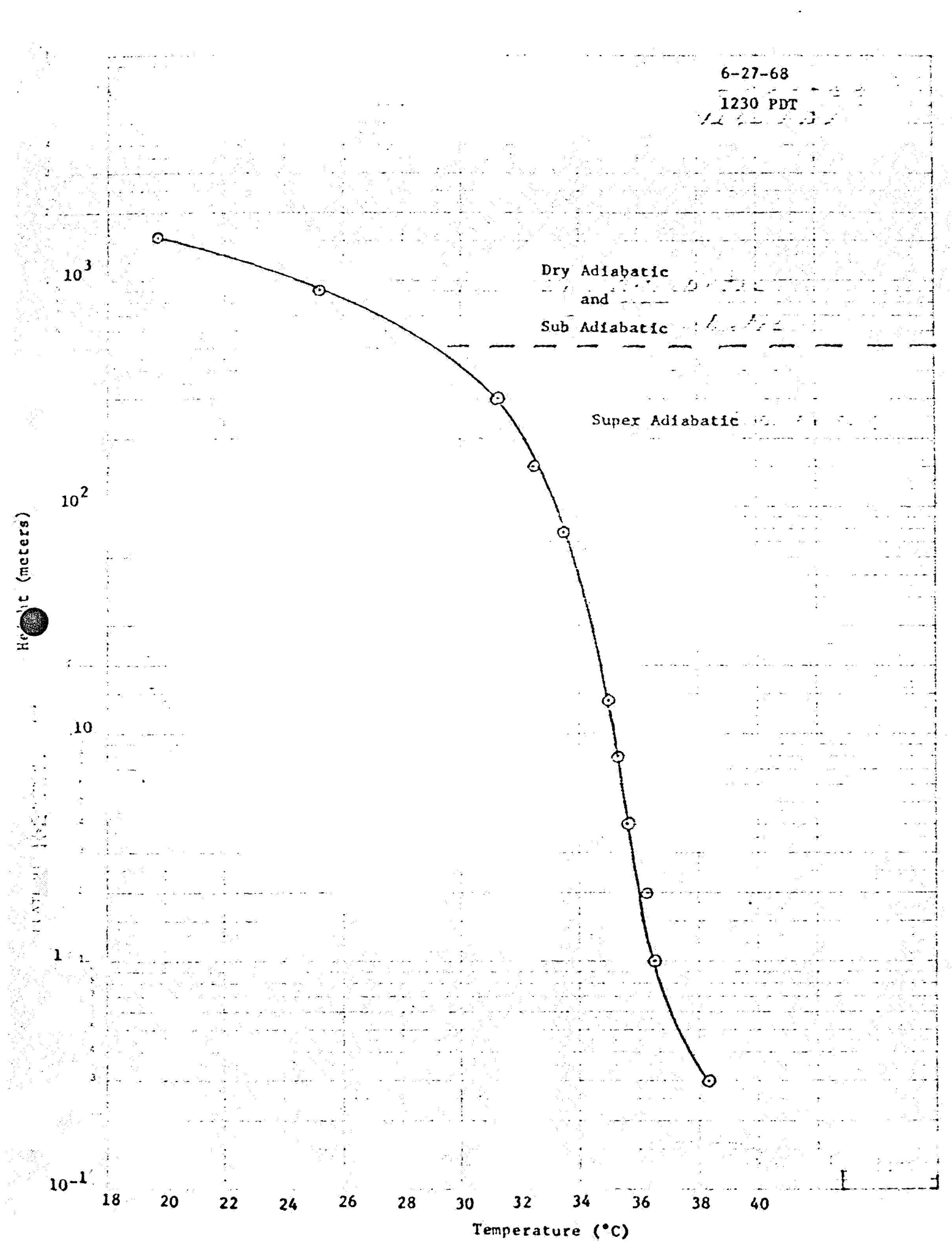
6-27-68
1230 PDT
Dry Adiabatic
and
Sub Adiabatic
Super Adiabatic
10^3
10^2
10
1
10^{-1}
Height (meters)
18
20
22
24
26
28
30
32
34
36
38
40
Temperature (°C)

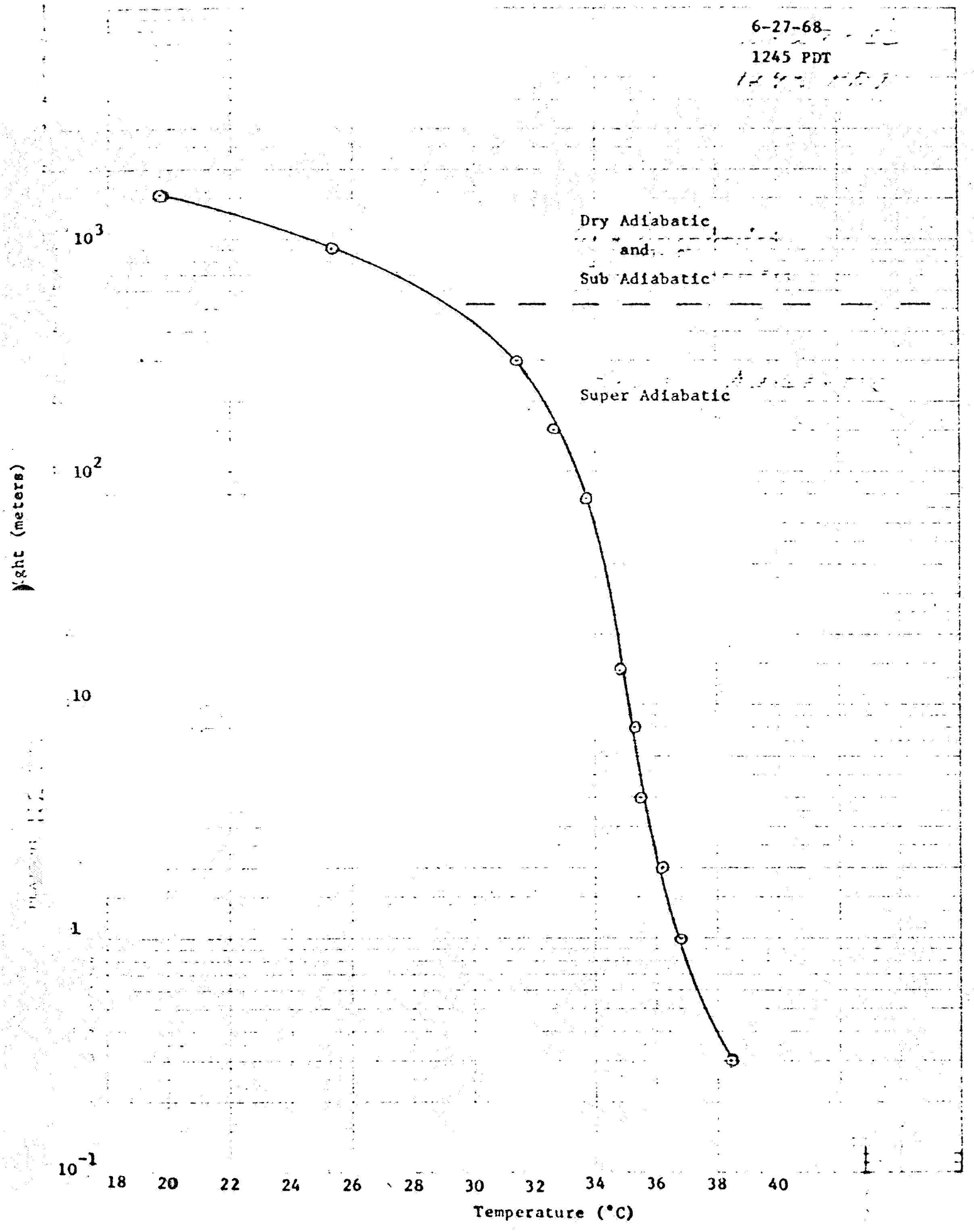
6-27-68
1245 PDT
Dry Adiabatic
and
Sub Adiabatic
Super Adiabatic
10^3
10^2
10
1
10^{-1}
ght (meters)
18
20
22
24
26
28
30
32
34
36
38
40
Temperature (°C)

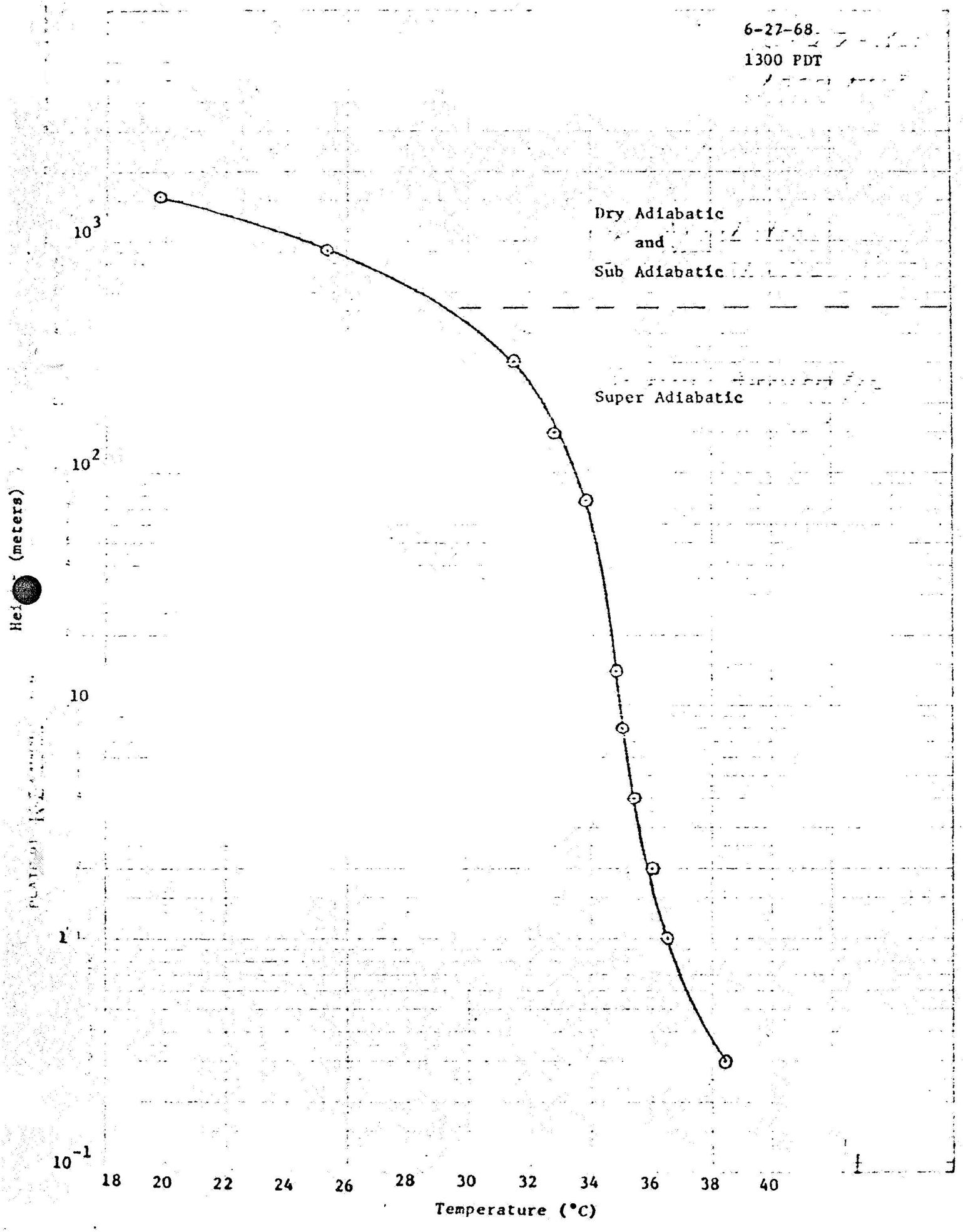
6-27-68
1300 PDT
Dry Adiabatic
and
Sub Adiabatic
Super Adiabatic
10^3
10^2
10
1
10^{-1}
Height (meters)
18
20
22
24
26
28
30
32
34
36
38
40
Temperature (°C)

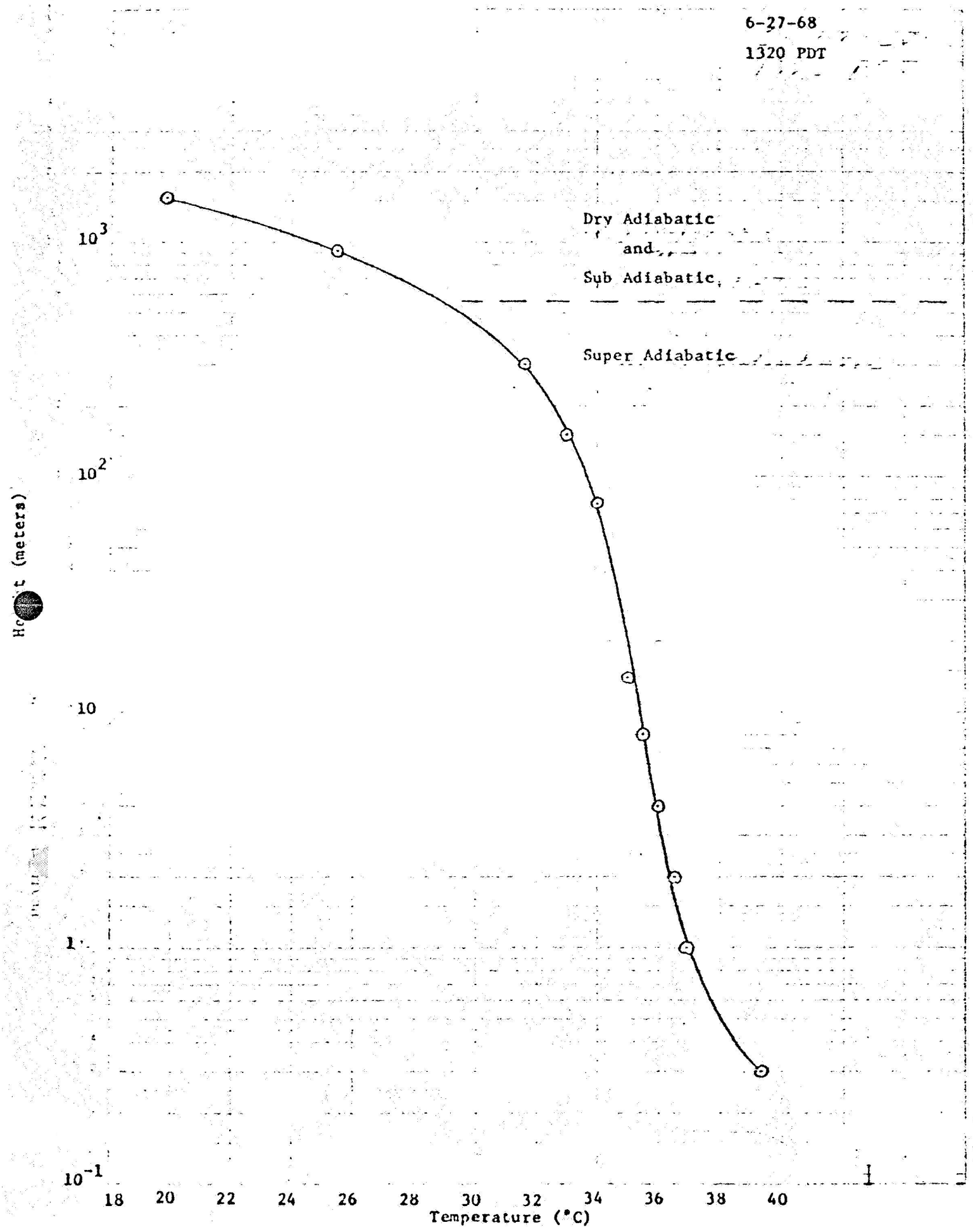
6-27-68
1320 PDT
Dry Adiabatic
and
Sub Adiabatic
Super Adiabatic
10^3
10^2
10
1
10^{-1}
Height (meters)
18
20
22
24
26
28
30
32
34
36
38
40
Temperature (°C)

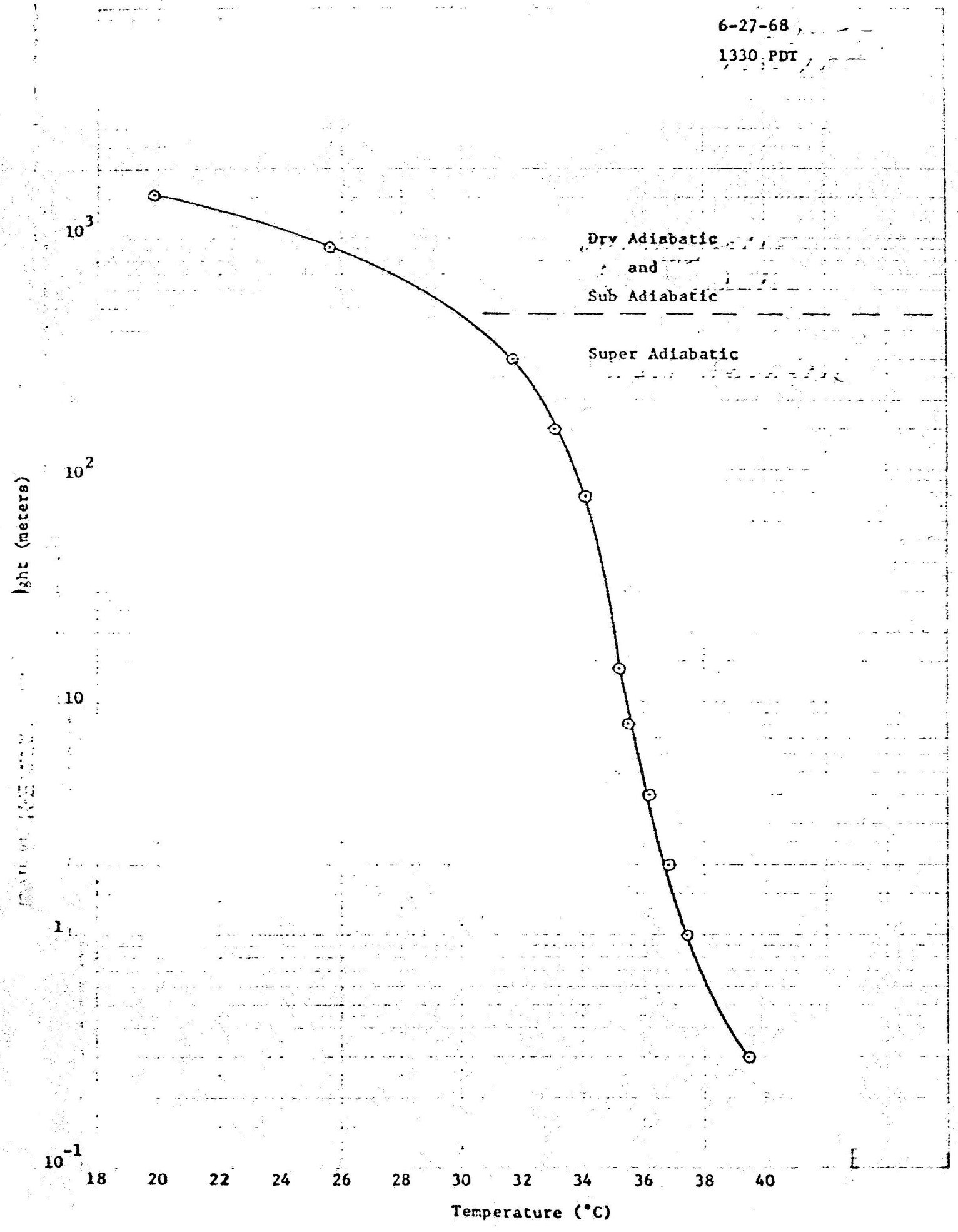
6-27-68
1330 PDT
Dry Adiabatic
and
Sub Adiabatic
Super Adiabatic
10^3
10^2
10
1
10^{-1}
ght (meters)
18
20
22
24
26
28
30
32
34
36
38
40
Temperature (°C)

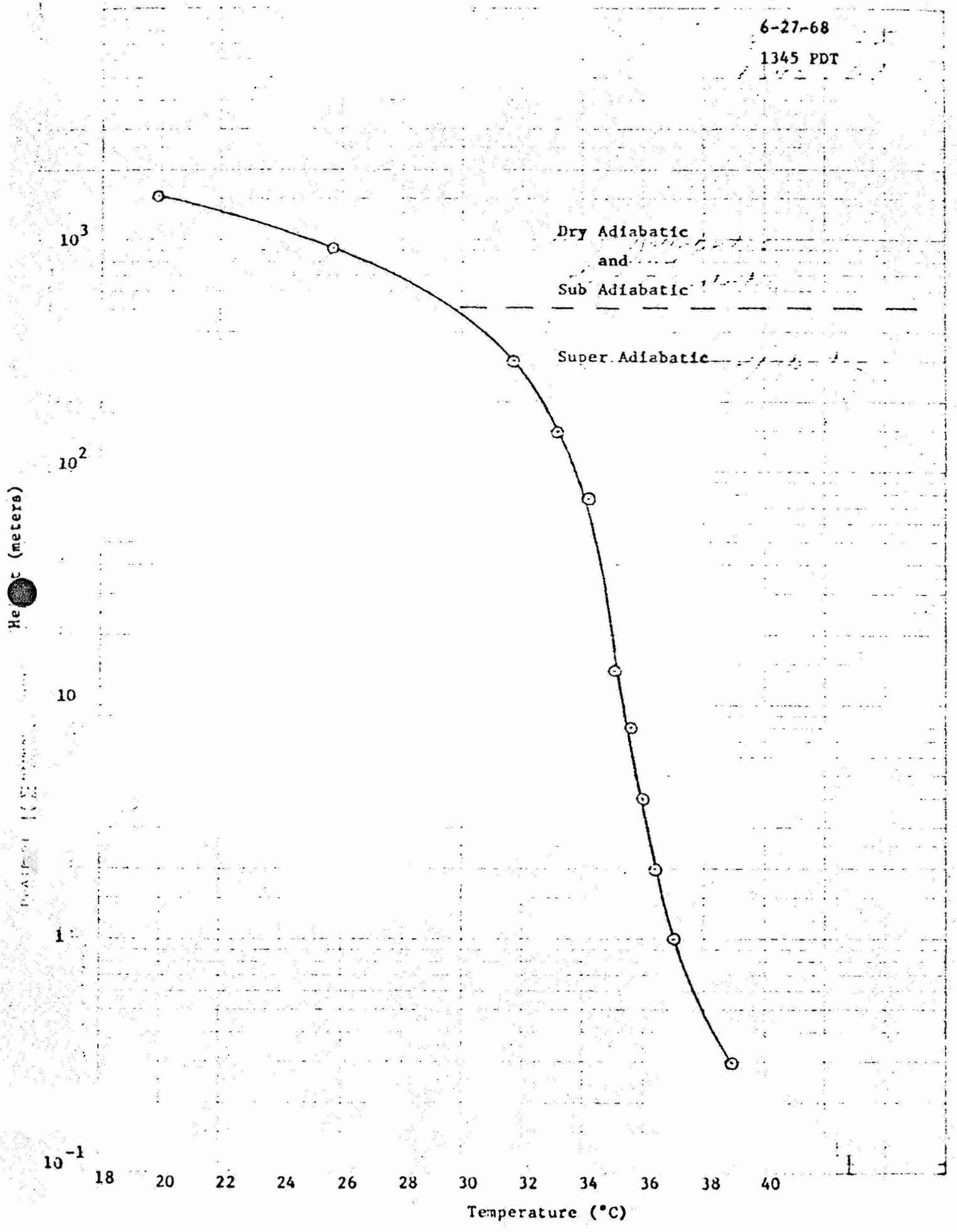
6-27-68
1345 PDT
Dry Adiabatic
and
Sub Adiabatic
Super Adiabatic
10^3
10^2
10
1
10^{-1}
Height (meters)
18
20
22
24
26
28
30
32
34
36
38
40
Temperature (°C)

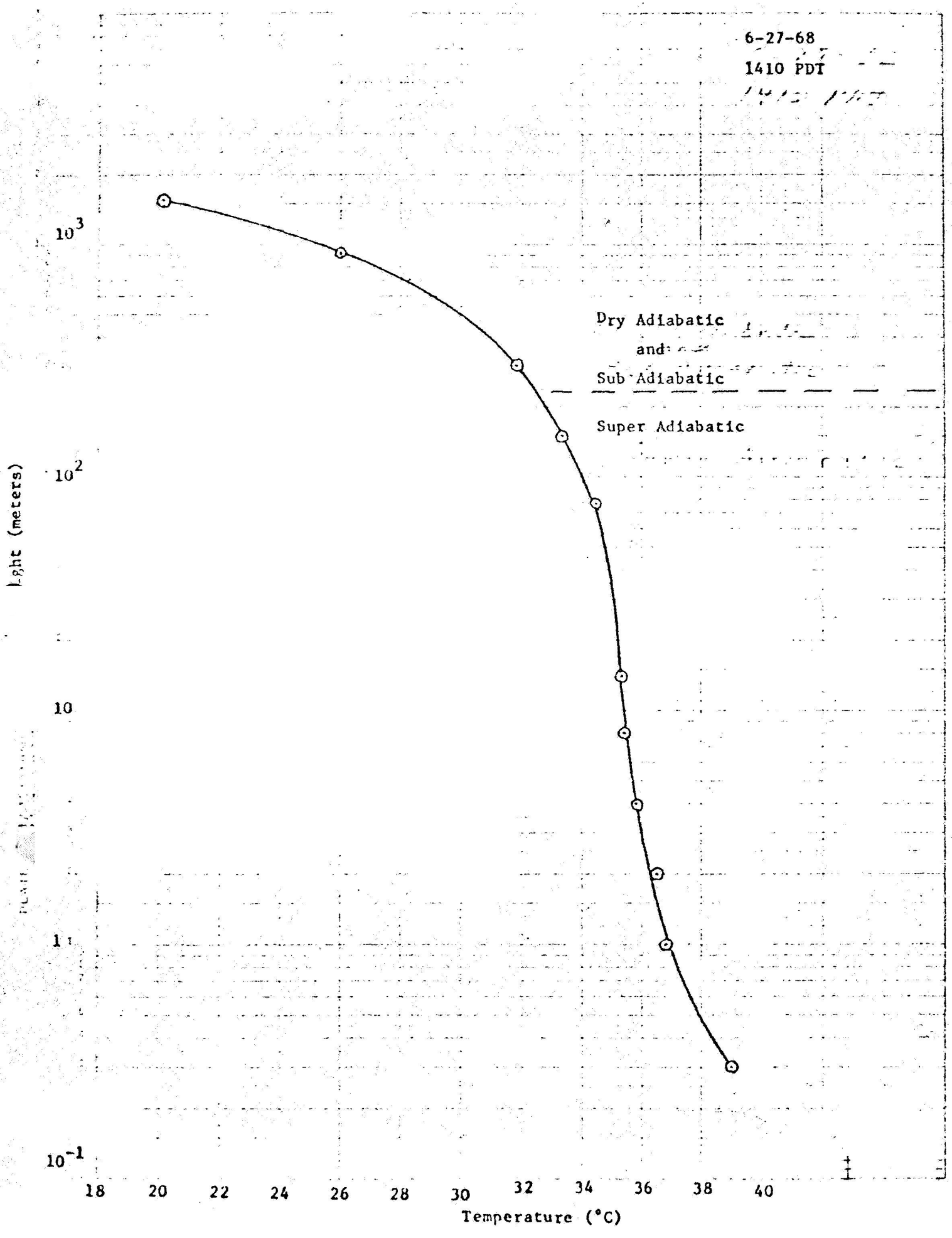
6-27-68
1410 PDT
Dry Adiabatic
and
Sub Adiabatic
Super Adiabatic
10^3
10^2
10
1
10^{-1}
Height (meters)
18
20
22
24
26
28
30
32
34
36
38
40
Temperature (°C)

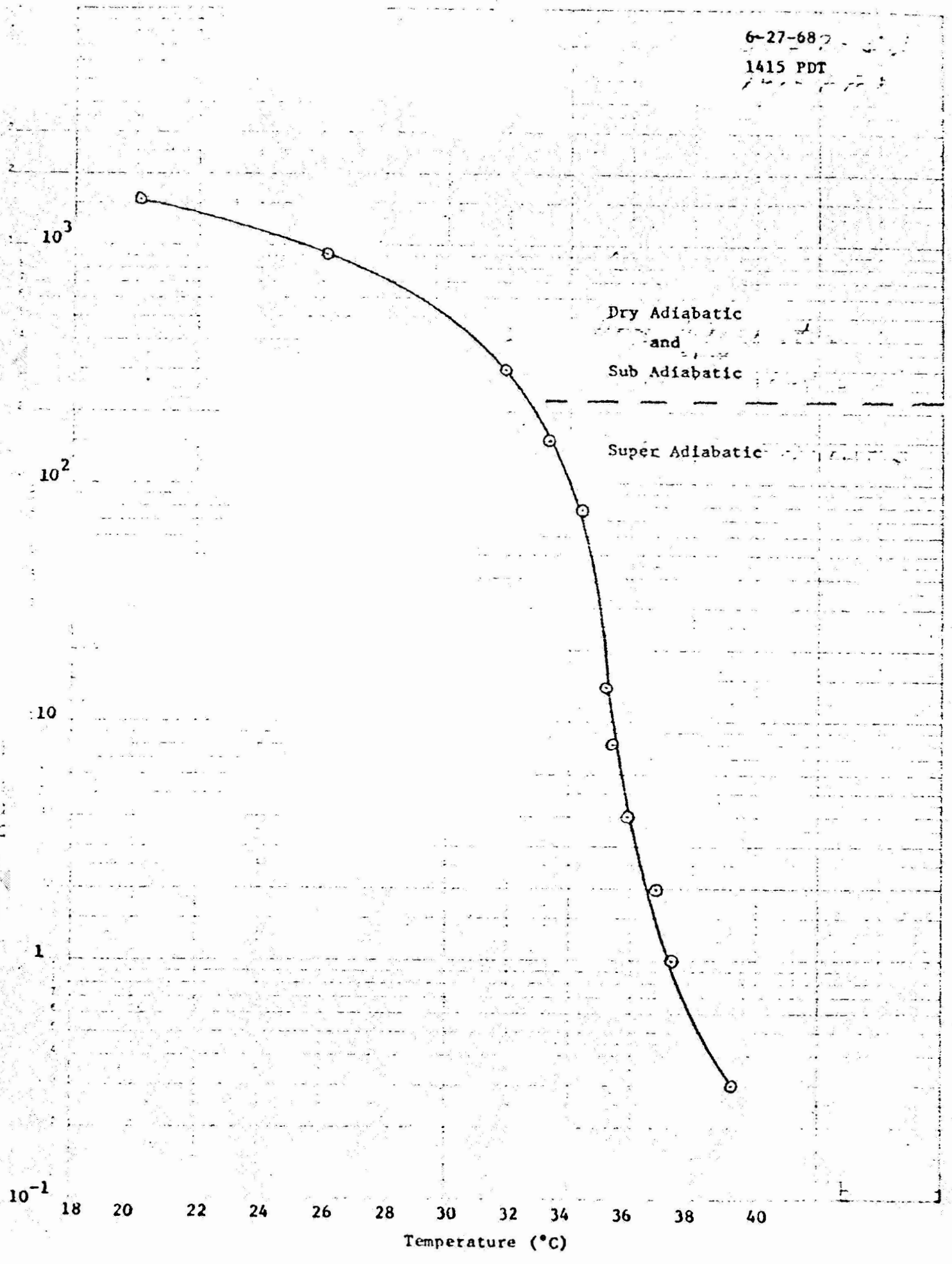
6-27-68
1415 PDT
Dry Adiabatic
and
Sub Adiabatic
Super Adiabatic
10^3
10^2
10
1
10^{-1}
18
20
22
24
26
28
30
32
34
36
38
40
Temperature (°C)